Application of Ag-doped carbon nanotubes for wastewater treatment: antimicrobial and catalytic activity

Leiddi Laura Maria Leal

Dissertation submited to Escola Superior Agrária de Bragança to obtain the Degree of Master in Environmental Technology under the scope of the double diploma with Universidade Tecnológica Federal do Paraná

Supervised by:

Prof. Helder Teixeira Gomes

Profa. Renata Mello Giona

Bragança
2024

ACKNOWLEDGEMENTS

I am grateful to the Universidade Tecnológica Federal do Paraná – Campus Medianeira (UTFPR) for providing me with the opportunity to pursue a double degree and for the enriching educational experience. The dedication of the faculty and the conducive academic environment have significantly contributed to my intellectual growth.

Additionally, I acknowledge the Instituto Politécnico de Bragança (IPB) for their support and resources, which were crucial for the successful completion of this research. The facilities and academic atmosphere at IPB have been pivotal in fostering my academic achievements.

Special thanks go to my supervisor, Professor Dr. Helder Teixeira Gomes (IPB), and my co-supervisor, Professor Dra. Renata Mello Giona (UTFPR), for their support, expert guidance, and valuable insights throughout the research process. Their mentorship has been indispensable in shaping this work and my academic journey.

I extend my sincere appreciation to Adriano da Silva for his invaluable support during this study. His guidance, encouragement, and clear teaching have been instrumental in overcoming challenges and achieving milestones. I am also thankful to my laboratory colleagues, particularly Paloma Lopes, for their collaboration, understanding and friendship.

I sincerely thank my family and friends from Brazil and Portugal, who have provided unwavering support, faith, and motivation throughout my journey. Their encouragement has been a constant source of strength, and I am deeply grateful for their love and belief in me.

I express my heartfelt gratitude to my husband, Gustavo Farias, and my son, Miguel Leal Farias, for their patience, understanding, and encouragement. Their presence has been my anchor, providing me with comfort and motivation to pursue my goals.

Lastly, I thank God for the gift of life and for His unwavering presence. I am deeply grateful for His blessings.

Abstract

An efficient wastewater treatment system provides economic, environmental, and social advantages that positively impact communities. Therefore, this study proposes the application of silver-doped carbon nanotubes obtained by upcycling plastic solid waste for wastewater treatment to evaluate their antimicrobial and catalytic activity. The metallic catalyst used in the chemical vapor deposition of carbon nanotubes was prepared with a composition of 88% alumina phase, 9% nickel oxide phase, and 3% cobalt ferrite phase with a polymer mix (25% low-density polyethylene, 35% high-density polyethylene, and 40% polypropylene). The carbon nanotubes were functionalized with 15.2 M nitric acid and subsequently subjected to two silver doping techniques (0.05 M): one by chemical co-precipitation with 0.05 M sodium borohydride, with 5% and 10% silver and the other by wet impregnation, also with 5% and 10% silver. The results obtained for N_2 adsorption isotherms characterize the materials as Type IV, attributed to mesoporous materials. BET, thermogravimetric, and elemental analyses demonstrated that doping by wet impregnation was more efficient than doping by chemical co-precipitation, resulting in higher surface areas, up to 219 m^2/g, and higher C/H ratios (1546.7) in the 10% silver wet impregnation doping. CWPO experiments demonstrated that the catalysts doped by wet impregnation with 5% and 10% silver were the only ones capable of reducing 100% of the bisphenol-A concentration (100 ppm) after 8 hours of reaction, with the CNT doped by wet impregnation with 5% silver showing the best overall performance. Adsorption and desorption experiments of the materials recovered from the reaction confirmed that the pollutant was mainly oxidized, not adsorbed, and the adsorptions observed were characterized as physisorptions. The CWPO experiment coupled with the disinfection of an *Escherichia coli* bacterial strain at an initial concentration of 0.5 on the McFarland scale over a simulated pollutant matrix showed that hydrogen peroxide (537 ppm), as well as the CWPO reaction using 5% silver wet impregnation doped CNT was able to eliminate 99.99% of the microorganisms, demonstrating a bactericidal effect.

Keywords: Plastic solid waste; Chemical recycling, Organic compounds; CWPO; Disinfection.

Resumo

Um sistema de tratamento de águas residuais eficiente proporciona vantagens económicas, ambientais e sociais que impactam positivamente as comunidades. Portanto, neste trabalho é proposta a aplicação de nanotubos de carbono obtidos de resíduos sólidos plásticos dopados com prata para o tratamento de águas residuais a fim de avaliar a sua atividade antimicrobiana e catalítica. Para isso, o catalisador metálico utilizado na deposição química em fase vapor de produção de nanotubos de carbono foi preparado com uma composição de 88% de fase de óxido de alumínio, 9% de fase de óxido de níquel e 3% de fase de ferrite de cobalto com um MIX de polímeros (25% de polietileno de baixa densidade, 35% de polietileno de alta densidade e 40% de polipropileno). Os nanotubos de carbono foram funcionalizados com ácido nítrico 15,2 M e, posteriormente, submetidos a duas técnicas de dopagem com prata (0,05 M): uma por co-precipitação química com borohidreto de sódio 0,05 M, com 5% e 10% de prata, e outra por impregnação húmida, também com 5% e 10% de prata. Os resultados obtidos para as isotérmicas de adsorção de N_2 caracterizam os materiais como Tipo IV, atribuídos a materiais mesoporosos. As análises BET, termogravimétrica e elementar demonstraram que a dopagem por impregnação húmida foi mais eficiente que a dopagem por co-precipitação química, resultando em maiores áreas superficiais, chegando a 219 m^2/g e maiores relações C/H (1546,7) na dopagem por impregnação húmida a 10%. Os ensaios de CWPO demonstraram que os catalizadores dopados por impregnação húmida com prata a 5 e 10% foram os únicos capazes de reduzir 100% a concentração de bisfenol A (100 ppm) após 8 horas de reação, onde o CNT dopado por impregnação húmida com prata a 5% apresentou o melhor desempenho geral. Os ensaios de adsorção e dessorção dos materiais recuperados da reação confirmaram que o poluente foi principalmente oxidado, e não adsorvido, e as adsorções constatadas foram caracterizadas como fisissorções. O ensaio de CWPO acoplado na desinfecção de uma cepa de bactérias *Escherichia coli* a uma concentração inicial de 0,5 da escala McFarland sobre uma matriz simulada de poluente, mostrou que o peróxido de hidrogénio (537 ppm), assim como a reação CWPO utilizando CNT dopado com prata por impregnação húmida a 5% foi capaz de eliminar 99,99% dos microrganismos, apresentando efeito bactericida.

Palavras chave: Resíduos sólidos plásticos; Reciclagem química; Compostos orgânicos; CWPO; Desinfecção.

TABLE OF CONTENTS

INDEX OF FIGURES ..... **x**
INDEX OF TABLES ..... **xii**
INDEX OF ABBREVIATIONS ..... **xiii**
1 INTRODUCTION **2**
2 OBJECTIVES **4**
2.1.SPECIFIC OBJECTIVES 4
3 STATE OF THE ART **6**
3.1.WASTE GENERATION 6
3.1.1.Global context *6*
3.1.2.European Union *7*
3.1.3.Portugal *8*
3.2.MUNICIPAL SOLID WASTE: What has been done in the literature? 9
3.3.PLASTIC SOLID WASTES 11
3.3.1.Plastic recycling data *12*
3.3.2.Plastic recycling *15*
3.4.LANDFILL LEACHATE 20
3.4.1.Treatment options *21*
3.5.CARBON NANOTUBES 23
3.5.1.From carbon to nanotubes *23*
3.5.2.Synthesis *26*
3.5.3.Ag-doped CNTs for wastewater disinfection *28*
4 MATERIALS AND METHODS **31**
4.1.REACTANTS 31
4.2.PREPARATION OF CNTs 32
4.2.1.Metal catalyst *32*
4.2.2.Synthesis and purification of CNTs *33*

4.2.3.Ag-doped CNTs *34*

4.3.MATERIAL CHARACTERIZATION TECHNIQUES 35

4.3.1.Surface and pore analyser *35*

4.3.2.Thermogravimetric analysis (TGA) *37*

4.3.3.Elemental analysis (EA) *37*

4.3.4.X-ray diffraction (XRD) *37*

4.3.1.Transmission electron microscopy (TEM) and Scanning electron microscopy (SEM) *38*

4.4.MICROBIOLOGICAL CHARACTERIZATION OF LANDFILL LEACHATE 38

4.5.CWPO OF BISPHENOL-A 39

4.6.CWPO AND DISINFECTION 41

4.7.ANALYTICAL TECHNIQUES 43

5 RESULTS AND DISCUSSION 47

5.1.CHARACTERIZATION OF MATERIALS 47

5.1.1.Textural properties and morphology *47*

5.1.2.Thermogravimetric analysis (TGA) *53*

5.1.3.Elemental analysis (EA) *55*

5.1.4.X-ray diffraction (XRD) *56*

5.2.MICROBIOLOGICAL CHARACTERIZATION OF LANDFILL LEACHATE 58

5.3.EXPERIMENTAL REACTIONS 58

5.3.1.Adsorption *58*

5.3.2.H_2O_2 catalytic decomposition *59*

5.3.3.Catalytic wet peroxide oxidation (CWPO) *61*

5.3.4.Coupled disinfection and CWPO *64*

6 CONCLUSIONS AND FUTURE WORK 68

6.1.CONCLUSIONS 68

6.2.FUTURE WORK 69
7 REFERENCES 71

INDEX OF FIGURES

Figure 1. Solid waste generation to the income level of countries [25]. 7
Figure 2. Waste hierarchy according to The Waste Framework Directive of the EU [4]. 8
Figure 3. The 50 most frequent keywords in the works of relevant authors in the WoS addressing MSW. 10
Figure 4. Plastic production (a) Through years in Europe and the World, (b) Distribution of plastic production worldwide (2020 data) [12].....13
Figure 5. European plastics converters - demand by polymer type (2021) [12]. 14
Figure 6. Properties of Carbon atom. 24
Figure 7. Types of carbon nanotubes [87]. 25
Figure 8. Various methods of CNTs preparation, purification, functionalization, and characterization.....26
Figure 9. Experimental method for carboxylation of CNTs using HNO_3. 28
Figure 10. Antimicrobial mechanism of Ag-doped CNTs. 29
Figure 11. One-chamber reactor setup used to synthesize CNTs by CVD. 33
Figure 12. Classification of physisorption isotherms by IUPAC [103].....36
Figure 13. IUPAC classification for hysteresis loop [103]. 36
Figure 14. Representation of experimental stages including CWPO process and microbiological analysis. 43
Figure 15. Calibration curve for H_2O_2 determination.....44
Figure 16. Calibration curve for pollutant leached measurements. 45
Figure 17. Hysteresis loop for (a) NiFe/CoFe@Al_2O_3, (b) CNT, (c) CNT-COOH, (d) CNT-COOH/Ag1-5%, (e) CNT-COOH/Ag1-10%, (f) CNT-COOH/Ag2-5% and (g) CNT-COOH/Ag2-10%. 48
Figure 18. TEM images recorded for (a) CNT sample, (b) Image recorded showing 28 graphene layers, (c) Image recorded showing 17 graphene layers and (d) metals encapsulated on CNTs. 50
Figure 19. SEM images recorded for samples (a) CNT-COOH, (b) CNT-COOH@Ag1-5%, (c) CNT-COOH@Ag1-10%, (d) CNT-COOH@Ag2-5% and (e) CNT-COOH@Ag2-10%.....51

Figure 20. SEM and EDS results for sample (a,b) CNT-COOH/Ag1-5%, (c,d) CNT-COOH/Ag1-10%, and (e,f) CNT-COOH/Ag2-5%, respectively. 52
Figure 21. Mass losses (left Y-axis) and their corresponding derivatives (right Y-axis) of different CNTs. 54
Figure 22. X-ray diffractogram of NiFe/CoFe@Al_2O_3. 57
Figure 23. Plate (a) Growth of bacteria, (b) Growth of yeasts and fungi. 58
Figure 24. Comparison between removal of BPA with adsorption after 8 h and CWPO after 8 h. 59
Figure 25. Catalytic efficiency of synthesized materials for H_2O_2 decomposition. 60
Figure 26. The concentration of (a) BPA and (b) H_2O_2 upon reaction time during CWPO experiences. 61
Figure 27. BPA desorption results obtained using materials recovered from pure adsorption experiments. 64
Figure 28. The concentration of (a) BPA and (b) H_2O_2 upon reaction time during coupled disinfection and CWPO experiences. 65

INDEX OF TABLES

Table 1. 20 most used author's keywords. “F” is the frequency (number of times) with which the authors used the keyword.....10
Table 2. A Summary of commercial applications of different plastics. 11
Table 3. Mechanical recycling studies.....16
Table 4. Chemical recycling studies. 18
Table 5. Landfill leachate treatments in the literature. 22
Table 6. Characteristics of the vertical/horizontal tubular furnace.....34
Table 7. Reagent volume for different dopage percentages. 35
Table 8. S_{BET} from the materials. 49
Table 9. Elemental composition of the different CNTs. 55
Table 10. Results of disinfection experiment. 66

INDEX OF ABBREVIATIONS

MSW	Municipal solid waste
PSW	Plastic solid waste
CE	Circular economy
EU	European Union
AOPs	Advanced Oxidation Processes
CWPO	Catalytic wet peroxide oxidation
CNTs	Carbon nanotubes
MWCNTs	Multi-walled carbon nanotubes
PP	Polypropylene
PE	Polyethylene
HDPE	High-density polyethylene
LDPE	Low-density polyethylene
MR	Mechanical recycling
CR	Chemical recycling
CVD	Chemical vapor deposition
ROS	Reactive oxygen species
Ag-NPs	Silver-nanoparticles
BET	Brunauer-Emmett-Teller method
TGA	Thermogravimetric analysis
EA	Elemental analysis
XRD	X-ray diffraction
TEM	Transmission electron microscopy
SEM	Scanning electron microscopy
UV-VIS	Absorption spectroscopy
HPLC	High-Performance Liquid Chromatography
COD	Chemical Oxygen Demand
TOC	Total Organic Carbon
CFU	Colony Forming Unit
BPA	Bisphenol-A

INTRODUCTION

1 INTRODUCTION

The worldwide population growth and the consequent pursuit of enhanced lifestyles have led to increased consumption of products and energy. This consumption is connected to economic growth, but it also directly leads to a notable increase in waste generation [1]. The global waste production in 2017 was estimated to be around 20 billion tons, with Municipal Solid Waste (MSW) accounting for a portion ranging from 2.29 to 3.13 billion tons annually [2]. In Europe, 1.66 billion metric tons of waste are generated annually, with construction and demolition, of which MSW is the main contributor. In this context, Portugal generated approximately 507 kg of MSW per person in 2022 [1,3].

The European Union (EU) has taken significant steps towards sustainable management of MSW. The Waste Framework Directive [4], focusing on prevention, reuse, recycling, recovery, and landfill disposal, aims to ensure proper waste management. By 2025, EU countries are expected to achieve a minimum rate of 55% for urban waste reuse and recycling, with progressive targets until 2035 [5]. Despite challenges in waste management in Portugal, national strategies aim to prevent excessive generation and promote reuse and recycling. Data from 2022 [6] indicates progress, but there are still improvements in waste management to achieve the proposed goals.

The increasing demand for plastics, driven by their advantages in various industrial applications [7], underscores the importance of effective management of Plastic Packaging Waste (PPW), which accounts for approximately 40% of plastics produced globally [8]. It accounts for 39.9% of the total plastic solid waste (PSW) in the EU [9]. Plastics are derived from non-renewable petrochemicals such as oil and natural gas and include various polymers adaptable in shapes and physical properties [7,10]. The European Commission recognizes the Circular Economy (CE) as a solution to challenges related to plastics [11], and the report “Plastics – The Facts 2022” reveals that, in 2021, the total demand from European plastic transformers was 50.3 million tons, with nearly half composed of polyolefins [12]. In this context, the chemical recycling of PSW stands out, with approaches such as fluid catalytic cracking, hydrocracking, gasification, and pyrolysis as essential components for sustainable advancements in managing these wastes [13].

The final disposal of plastic waste in landfills remains a prevalent method for plastic

elimination. However, this approach causes significant environmental harm, such as groundwater contamination and ecosystem degradation [14]. This issue extends to the complex management of landfill leachate, known for its diverse composition and high concentration of contaminants [15], including organic compounds. The composition and concentration of these compounds in landfill leachates vary widely, influenced by landfill phases and waste management practices. They can encompass various substances like organic acids, phenols, nitrogenous compounds, and sulfur compounds. Additionally, microplastics have been detected in landfill leachates, known for their refractory nature and resistance to conventional treatments. Therefore, the management and treatment of landfill leachates pose a considerable challenge, as biological pretreatment systems are often deemed ineffective [16].

For leachate treatment options, various conventional, physical, biological, and chemical approaches are explored, including advanced oxidation processes (AOPs) like catalytic wet peroxide oxidation (CWPO), where the application of carbon nanotubes (CNTs) shows promise [17]. CNTs are often recovered in the chemical upcycling of polyolefins such as polypropylene (PP) and polyethylene (PE) through pyrolysis, followed by chemical vapor deposition [18]. Inorganic nanomaterials such as silver nanoparticles and carboxylated multi-walled carbon nanotubes (MWCNTs) are used to enhance polymeric membranes due to their antibacterial, antifouling, and stability properties [19].

The research addressed the challenge of improving the performance of solid catalysts used in wastewater treatment systems. Therefore, the main objective of this work is to explore the effect of silver (Ag) doping on CNTs produced from PE and PP, concerning their pronounced activity in removing organic pollutants, like organic compounds, through CWPO. Additionally, tests were conducted to assess the antimicrobial activity of the prepared materials. This study is based on the hypothesis that incorporating antimicrobial properties into catalysts used in CWPO processes can enhance their efficiency in removing organic pollutants and microorganisms from wastewater, resulting in a more effective and comprehensive treatment. The most relevant and updated literature will be shown in the present dissertation.

2 OBJECTIVES

Explore the catalytic and antimicrobial activity of Ag-doped CNTs towards the removal of organic pollutants by catalytic wet peroxide oxidation (CWPO) and bacteria from wastewater.

2.1. SPECIFIC OBJECTIVES

- Synthesize carbon nanotubes using plastics as a carbon source.
- Synthesize silver-doped carbon nanotubes using different doping techniques.
- Characterize the prepared materials regarding their morphological properties, crystalline structure, and chemical composition.
- Evaluate the performance of each material in terms of efficiency in removing organic pollutants and microorganisms in wastewater through CWPO tests.
- Compare the results obtained with each material to identify the most effective and comprehensive catalyst for wastewater treatment.

STATE OF THE ART

3 STATE OF THE ART

3.1. WASTE GENERATION

3.1.1. Global context

The report entitled "What a Waste 2.0: A Global Snapshot of Solid Waste Management to 2050" by The World Bank thoroughly examines worldwide solid waste generation. In 2016, this production reached 2.01 billion tons, with alarming projections indicating a possible increase to 3.40 billion tons by 2050 [20]. According to the same report, nations in East Asia, the Pacific, Europe, and Central Asia contribute 43% of the total worldwide waste. On the other hand, the Middle East, North Africa, and Sub-Saharan Africa regions produce the least amount of waste, together representing 15% of the global total. In absolute terms, it is estimated that East Asia and the Pacific generated the highest amount, totalizing approximately 468 million tons in 2016, while the Middle East and North Africa region produced the least amount, approximately 129 million tons.

Over time, the growth in waste production reflects an increase in consumption and the evolution of lifestyles and production methods in modern societies [21,22]. Detailed studies have emphasized the close connection between the amount of generated waste and variables such as urbanization, gross national income (GNI), and economic development [20]. As urban areas expand, demands for products and services increase, driving consumption and waste production. Simultaneously, economic development is often associated with changes in consumption habits, leading to a higher generation of waste, particularly in packaging and disposable products [23,24].

The global analysis of these wastes categorizes countries into groups according to their GNI - high-income countries (HICs), upper-middle-income (UMICs), lower-middle-income (LMICs), and low-income (LICs). The regions revealed significant disparities in urban solid waste generation in 2016, with substantial projections for 2025 and 2050, as shown in Figure 1. It’s essential to highlight the directly proportional correlation between waste generation levels and the urbanization process. In 2018, the urban population represented a significant portion of the population composition in different country groups: 32.2% in LICs, 40.6% in LMICs, 66.6% in UMICs, and 81.5% in HICs. This correlation becomes evident when we consider the contribution to solid waste generation by country in 2016: 5% for LICs, 29% for LMICs, 32% for UMICs and

34% for HICs.

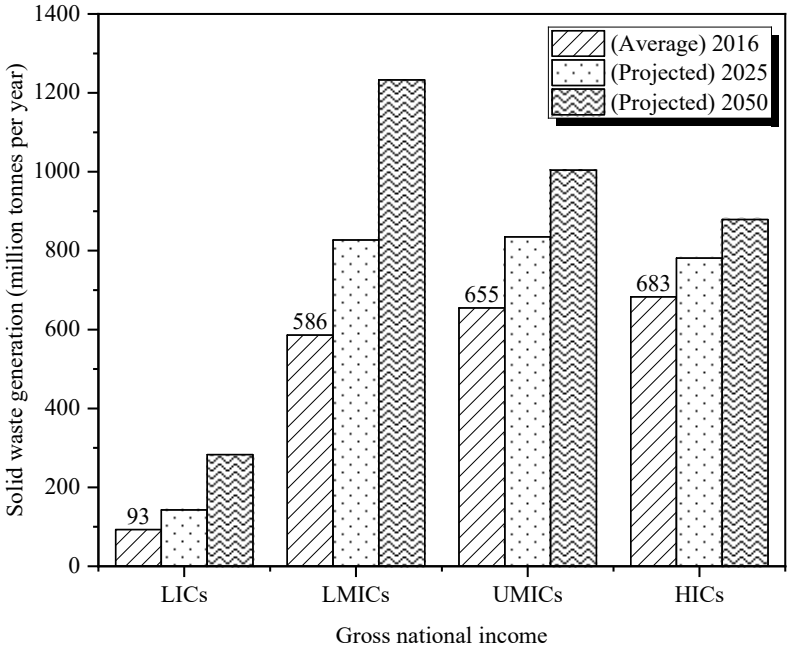

Figure 1. Solid waste generation to the income level of countries [23].

The data presented in Figure 1 shows that LMICs project higher generations than HICs for 2050 despite generating lower volumes of MSW in 2016. This is due to the rapid urbanization in these areas, and the high population growth predicted for the coming decades. According to the United Nations (UN), global population growth is mainly driven by Asia and Africa, a trend expected to continue in the coming decades. Projections indicate that in the second half of this century, Sub-Saharan Africa will emerge as the most populous region on the planet. Simultaneously, there will be a decrease in the number of inhabitants in regions where fertility is declining, and the population is aging, such as some Eastern European countries [20].

3.1.2. European Union

The EU implemented laws and policies to promote a circular economy, aiming to achieve these recycling targets and adapting its guidelines to consider factors such as per capita gross domestic product (GDP), time of EU accession, resource productivity, and investments in Investigation and Development (I&D). Recent legislative changes, including the CE Package of 2018, established more robust objectives for waste recycling,

aiming to align member countries to meet these goals [25]. According to the European Commission, in 2020, the EU developed a new action plan to advance in this transition. The Waste Framework Directive has become a cornerstone in EU legislation for waste treatment and management, establishing a specific hierarchy for its management: prevention, reuse, recycling, recovery, and landfill disposal, with waste prevention being the preferred option. This hierarchy is illustrated in Figure 2 below, which highlights the priority steps in waste management according to the Directive [4].

Figure 2. Waste hierarchy according to The Waste Framework Directive of the EU [4].

This directive aims to ensure waste management without risks to human health or the environment, addressing the transformation of waste into secondary raw materials, distinguishing between waste and by-products, introducing the polluter-pays principle, and extending producer responsibility. By 2025, EU countries are expected to increase the reuse and recycling of urban waste to a minimum of 55%. This rate should progressively increase, reaching 60% by 2030 and 65% by 2035, following this gradual progression [5]. Eurostat data shows that in 2022, the recycling rate of urban waste in the EU+27 was 48.6% [26], with Germany, Austria, and Slovenia having already achieved or surpassed the 60% target.

3.1.3. Portugal

According to the Agência Portuguesa do Ambiente (APA), Portugal generated approximately 5.323 million tons of MSW in 2022 [3]. In mainland Portugal, MSW production reached about 5 million tons during the same period, resulting in an annual

average of 507 kg per inhabitant, equivalent to approximately 1.39 kg of MSW per person daily. This value is below the European average, estimated at 527 kg per inhabitant per year for 27 countries, according to Eurostat data in 2021 [27]. Regarding the management, it was observed that in the year 2022, the final destination of MSW in Continental Portugal was distributed as follows: approximately 57% were sent to landfill; 16% were directed for recycling; 15% underwent energy recovery; 8% were destined for composting/anaerobic digestion, and the remaining 2% received other forms of valorisation.

In Portugal, plans regarding waste materialize the national waste policy, shaping the objectives of waste prevention and its utilization as a resource, ensuring the efficient use of natural resources, and returning materials and energy to the economy. Thus, the plans define guidelines, objectives, actions, and goals at the national level, which are translated into action plans at the municipal level. Portugal has set three national targets for waste management as outlined in Decree-Law No. 102-D/2020 of December 10. These targets include Waste Generation Prevention, Waste Preparation for Reuse and Recycling, and Waste Landfill Disposal. In 2022, the country generated 513 kg of waste per capita per year, with a target of reducing this by 5% by 2025 and 15% by 2030 compared to 2019. Regarding Waste Preparation for Reuse and Recycling, Portugal achieved a rate of 33% in 2022, with targets set to increase to 55% by 2025, 60% by 2030, and 65% by 2035. Regarding Waste Landfill Disposal, Portugal disposed of 55% of waste in landfills in 2022, aiming to reduce this to 10% by 2035.

3.2. MUNICIPAL SOLID WASTE: What has been done in the literature?

The previous section made clear the importance of solid waste in different contexts. This demonstration highlights the need to address municipal solid waste specifically in the next phase of the study, considering its multifaceted relevance and significant impact on economic, social, and environmental areas. A literature search was carried out using the term “Municipal Solid Waste” to understand trends in the literature, targeting scientific documents that included this expression in keywords, abstracts, and titles. This resulted in identifying 29,404 documents in the Web of Science (WoS) since 1968 when the first study on the topic was published in this database. Through an analysis using the

bibliometrix R package, the 20 most relevant keywords used by the authors were identified, along with their frequencies, as shown in Table 1 below.

Table 1. 20 most used author's keywords. "F" is the frequency (number of times) with which the authors used the keyword.

Position	Keyword	F*	Position	Keyword	F*
1	Anaerobic Digestion	1500	11	Incineration	577
2	Landfill	1094	12	Circular Economy	517
3	Waste Management	1069	13	Food Waste	516
4	Heavy Metals	821	14	Life Cycle Assessment	498
5	Biogas	814	15	Fly Ash	494
6	Recycling	722	16	Pyrolysis	480
7	Composting	643	17	Gasification	469
8	Leachate	620	18	Biomass	449
9	Solid Waste	613	19	Waste-to-Energy	400
10	Sewage Sludge	578	20	Sustainability	379

Additionally, the Biblioshiny tool from the Bibliometrix R package was used to explore the content of the collected database. The analysis of the 50 most significant author keywords resulted in the images in Figure 3. A list of synonyms was employed after reviewing the initial keyword results to ensure accurate analysis. This approach aimed to avoid misinterpretations of terms. For instance, the term "landfill" emerged as a relevant keyword in the WoS, and "landfills" was also considered relevant, but in reality, both represent the same keyword. This systematic strategy was consistently applied in all subsequent analyses discussed. In this representation, the size of the word is directly proportional to the number of times this term was found as the author's keyword.

Figure 3. The 50 most frequent keywords in the works of relevant authors in the WoS addressing MSW.

The authors address various stages of the life cycle of urban solid waste, focusing on treatment methods and expressing particular concern regarding landfills. Efficient waste management, including collection, transportation, and recycling, is a central concern. Additionally, topics like food waste, pollution, and specific environmental issues like leachate and biomass are explored. Strategies related to the circular economy are also discussed.

3.3. PLASTIC SOLID WASTES

Plastics derived from non-renewable petrochemicals such as oil, natural gas, and coal consist of synthetic polymers formed by covalent bonds of monomers. These materials, including polyethylene terephthalate (PET), high-density polyethylene (HDPE), low-density polyethylene (LDPE), linear low-density polyethylene (LLDPE), polyvinyl chloride (PVC), polypropylene (PP) and polystyrene (PS), are highly developed and adaptable in terms of shapes and physical properties through techniques such as rotation, injection, extrusion, and thermoforming. These polymers are customized to meet specific requirements, including strength, permeability, opacity, and colour. Polyolefins like HDPE and LDPE, known for their chemical and biological inertness, are durable and less prone to degradation by environmental elements like light, water, and microbial enzymes [7,10,28]. Information about the use of these polymers is shown in Table 2.

Table 2. A Summary of commercial applications of different plastics.

Plastic Type/ Recycling Code	Chemical Formula	Major Products
PET/1	$(C_{10}H_8O_4)n$	Single-use drink bottles, peanut butter containers, salad, dressing and vegetable oil containers.
HDPE/2	$(C_2H_4)n$	Milk jugs, juice bottles, bleach, detergent, cleaner bottles, shampoo bottles and motor oil bottles.
PVC/3	$(C_2H_3Cl)n$	Plumbing pipes and fitting, wire jacketing, blister packaging, cooking oil bottles, teething rings.
LDPE/4	$(C_2H_4)n$	Sheeting, squeezable bottles, shopping bags, furniture, heavy-duty sacks, general packaging.
PP/5	$(C_3H_6)n$	Straws, wrapping, caps, syrup and medicine bottles, potato chip bags, packing tape and rope.
PS/6	$(C_8H_8)n$	Disposable plates and cups, meat trays, egg carton.
Others/7	-	Electronic devices, pipes, children's toys, personal protective equipment, footwear industry.

The recycling code, established by the American Society for Testing and Materials (ASTM) International, is adopted to categorize different types of plastics. This coding is based on physical and biodegradable properties to identify and classify plastics in a standardized way, making the recycling process more accessible for the industry. Recycling code 1 refers to materials made of PET, a thermoplastic polymer from the polyester family with high tensile strength. Code 2 is assigned to materials made of HDPE, with linear polymeric chains and few branches, resulting in stronger intermolecular bonds, giving it greater rigidity compared to LDPE. Recycling code 3 is assigned to materials from PVC, a polymer with aliphatic carbon atoms in its main chain, offering greater rigidity and hardness. Recycling code 4 refers to LDPE materials with lower specific resistance and temperature than HDPE. This is due to its long, flexible, and linear polyethylene chain, which is more adaptable to external forces. PP is assigned recycling code 5, a material composed of lightweight fibres. Code 6 refers to materials made of PS, including general-purpose PS, expanded PS, high-impact PS, and syndiotactic PS. Expanded PS and high-impact PS have exceptional mechanical and insulation properties. Finally, recycling code 7 refers to materials made of Acrylonitrile butadiene styrene (ABS), Ethylene vinyl acetate (EVA), Polyurethane (PU), and Polycarbonate (PC) [28].

Each ton of recycled mixed plastic is estimated to save approximately seven barrels of oil, highlighting the significant energy-saving potential with the effective implementation of recycling [29]. Recycling plays an important role in addressing plastic pollution, reducing environmental impacts, and alleviating economic and geopolitical concerns associated with our continued dependence on oil and natural gas. Adopting sustainable strategies in plastic waste management is crucial, as is avoiding incineration, which contributes to greenhouse gas emissions, while not creating solid waste problems. Prioritizing increased recycling and reuse is critical to addressing global plastic challenges with technologies that can efficiently extend its lifespan. Recycling reduces the need for new materials and minimizes waste accumulation in landfills, preserving the environment and generating local employment opportunities [7,30].

3.3.1. Plastic recycling data

Frequent discussions about global warming, pollution, and climate change have

influenced consumer choices, leading to a visible shift toward more sustainable practices [31]. Plastics are essential in modern life and are used in various areas, from construction materials to packaging, medical devices, and food protection. This industry employs over 1.5 million people across the European Union [12]. These materials not only enhance the quality of life for many people due to their durability and lightness, contributing to reducing the weight of vehicles, packaging, and pipes, but they are also versatile, serving various purposes. Additionally, they can be of utmost importance for the global green transition [32]. Figure 4 illustrates the evolution of plastic production in recent years, covering both the global and European scenarios and highlighting the distribution of plastic production worldwide. This information was detailed in the "Plastics – The Facts 2022" report [12].

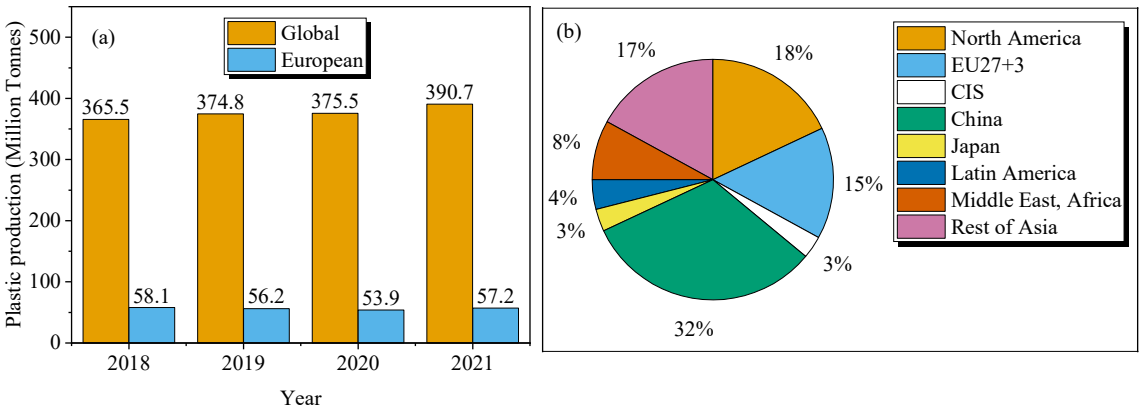

Figure 4. Plastic production (a) Through years in Europe and the World, (b) Distribution of plastic production worldwide (2020 data) [12].

In 2020, due to the Covid-19 pandemic, there was a stagnation in global plastic production. However, in 2021, this production increased to 390.7 million tons, with 90.2% coming from fossil fuels. Plastics recycled after use and those of biological origin represented 8.3% and 1.5% of global production, respectively, with circular plastics reaching about 9.8% of the total production. In Europe, after a reduction in 2020 due to the pandemic, production increased to 57.2 million tons in 2021, with 87.6% originating from fossil fuels. Recycled plastics after use and those of biological origin represented 10.1% and 2.3% of European production, respectively, while circular plastics reached approximately 12.4% of the total production [12]. Additionally, in 2021, the plastics sector in Europe recorded a trade surplus of 14.4 billion euros.

The European Commission identifies CE as a comprehensive solution to address the complex challenges of plastics. This includes plastic pollution, reliance on non-renewable resources in conventional production, improper waste management, and the need for more sustainable alternatives. The concept of CE, in this context, aims to close the plastic cycle, resulting in economic benefits for suppliers and users while bringing environmental advantages such as reducing raw material extraction, decreasing waste generation, and reducing associated emissions [11]. Therefore, ensuring proper management of plastic waste to move towards CE is essential [33], and understanding the composition of plastic solid waste is crucial to seeking recycling solutions as it is directly linked to the demand for specific polymer types. In this context, the demand for plastics in Europe, categorized by polymer type, is presented in Figure 5 [12].

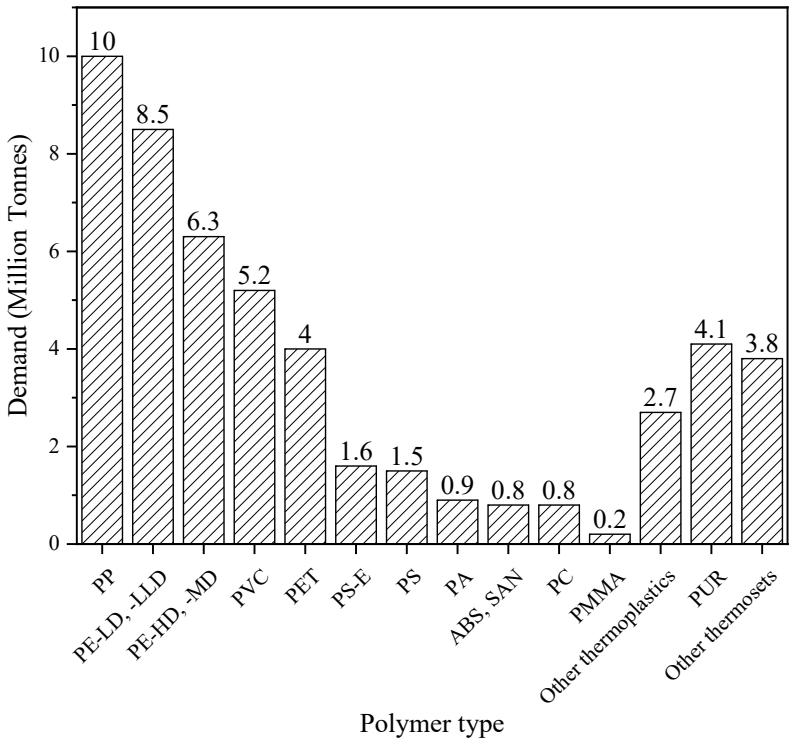

Figure 5. European plastics converters - demand by polymer type (2021) [12].

In other words, in 2021, the total demand from European plastics converters reached 50.3 million tons, of which almost half of the converted plastics demand consisted of polyolefins. The report also notes that in the same year, European converters' use of post-consumer recycled plastics reached 5.5 million tons, representing a recycled content of 9.9%, indicating an increase of about 20% compared to 2020. In 2020, 29.5 million tons

of post-consumer plastic waste were collected in the EU27+3, where 42% was directed to energy recovery, 23% to landfills, and 35% to recycling. It was also observed that plastic waste recycling rates were 13 times higher when collected separately than in mixed waste collection schemes. Furthermore, regarding the evolution of waste treatment, it was noted that from 2006 to 2020, the allocation to energy recovery increased by 77%, recycling increased by 117%, and landfill disposal decreased by 47% [12]. These data highlight how recycling policies are essential to eliminate the practices of disposing of plastic waste in landfills.

3.3.2. Plastic recycling

Effective use of plastics after their initial use is essential to establish a CE for plastics, alleviate the demand for natural resources and prevent waste from leaking into ecosystems [34]. Finding the best method to deal with domestic plastic waste is challenging, considering both effectiveness and environmental impact, however, is challenging to recycle due to its complex composition [35]. Currently, most plastics undergo mechanical recycling (MR), while chemical recycling (CR) is emerging as a technology. MR faces challenges in preserving the technical quality of the material and may have limitations in the market due to regulations that prevent applications such as food packaging. This is because of the heterogeneous composition of plastics, including inorganic and organic contaminants, and polymer degradation during their lifespan and reprocessing [36]. Therefore, CR is an interesting technological route to reduce waste and drive CE [37]. The following sections will address the latest publications and strategies for recycling solid plastic waste.

3.3.2.1. Mechanical Recycling (MR)

MR transforms plastic waste into new products, including downcycling recycled polymers into low-value items and upcycling them into high-value ones. It involves sorting, crushing, and separating plastics from other materials, followed by decontamination and transformation into new pieces or sheets through crushing and extrusion. More detailed studies available in the literature are presented in Table 3.

Table 3. Mechanical recycling studies.

Reference	Focus	Results
Ragaert et al., 2020 [38]	Apply the MDD method (Design from Recycling) to develop a product named 'Greentile', using the waste fraction known as the "sink fraction", including removing non-ferrous metals and PVC.	Development of a new product with this material called Greentile.
Luu et al., 2022 [39]	Evaluating the technical feasibility of mechanically recycling post-use bioprocessing plastic containers.	Recycled plastics from single-use assemblies used in bioprocessing can find new applications if suitable sorting and mass-processing solutions are implemented.
Yu et al., 2019 [40]	Analysis of the mechanical properties, thermal stability, and long-term durability of recycled polysulfone (PSU) through mechanical recycling.	The recycled polysulfone plastic exhibits similar tensile properties with lower impact strength than virgin PSU plastic.
Lase et al., 2022 [41]	Material flow analysis and recycling performance of an enhanced mechanical recycling process for post-consumer flexible plastics.	Although yields do not increase significantly, extra sorting and recycling produce better granulates.
Bashirgonbadi et al., 2022 [42]	Quality evaluation and economic assessment of an improved mechanical recycling process for post-consumer flexible plastics.	It is shown that the economic value can be increased by 5-38% through this improved recycling process.
Mulakkal et al., 2021 [43]	Enhance the mechanical recycling of post-consumer flexible plastic waste (PCFP) through additional sorting, hot washing and improved extrusion.	Material modelling like this has the potential to significantly reduce trial-and-error approaches, accelerating the optimization of material properties for specific applications.
Bustos Seibert et al., 2022 [44]	Production of a filament from recycled PET material for Material Extrusion (MEX).	The extrusion of the used PET into a filament and the subsequent printing with the MEX process offers a viable recycling process for the discarded material.
Ramos-Hernández et al., 2023 [45]	Evaluate the reprocessing of high melt flow index (MFI) PLA, examining the effects of accelerated weathering on PLA properties during additional extrusion cycles.	Mechanical recycling of PLA is effective unless exposed to severe weathering, requiring a chain extender for acceptable properties.
Park & Kim, 2020 [46]	To investigate whether plastics from the oceans could be used to manufacture cement-based materials.	The use of recycled plastic fibres improved the tensile strength of cement-based materials.
M. Y. Khalid et al., 2022 [47]	Examine mechanical recycling's impact on composite mechanical properties, emphasizing tensile strength, and explore its viability for automotive industry reuse.	The recycled composites exhibited superior mechanical properties compared to the unreinforced matrix material.

Recycled plastics like PET, PS, nylon 6, and HDPE are used in construction to enhance the strength of cementitious products, replacing conventional aggregates. MR also efficiently recycles metal matrix composites, especially fibre-reinforced plastics, by

disintegrating fibres through crushing, grinding, and pulverizing, turning them into fine powder for use as secondary reinforcements or fillers in new composites [48,49].

3.3.2.2. Chemical Recycling (CR)

CR represents a promising approach to dealing with heterogeneous plastic waste, especially when mechanical recycling is not technically or economically viable. This method breaks down polymer chains by chemical or thermochemical processes, resulting in monomers or petrochemical raw materials. From a technical, economic, practical, and sustainable standpoint, advanced strategies for the valorisation of MSW based on green chemical technologies are preferable, as they allow diversification in forming multiple products from a single source using sustainable technologies. These strategies can be categorized according to the desired end products, such as technologies for energy or value-added products [50,51].

CR, also known as tertiary recycling or chemolysis, promotes the recovery of virgin monomers to regenerate new plastics, even from highly damaged and contaminated raw materials. With its high recycling rate, PET can be recycled through various chemolysis methods such as glycolysis, alcoholysis and hydrolysis. Hydrolysis uses aqueous solutions with acid, alkaline or neutral catalysts, while glycolysis and alcoholysis use glycols or alcohols. Other approaches, such as aminolysis and ammonolysis, employ aqueous solutions of amines or ammonia, although they are rarely considered due to a lack of product applications [52,53].

Thermochemical methods, such as incineration, gasification, pyrolysis, torrefaction, and hydrothermal carbonization, are MSW treatment methods capable of generating thermal energy, gas, or fuel oil. Although they require intense operational conditions, they exhibit a higher conversion rate than biochemical methods [50]. The sustainable management of the organic fraction of MSW involves biological conversion into biofuels and value-added chemicals. Biological methods, such as pretreatment followed by anaerobic digestion, enzymatic hydrolysis with fermentation, or hydrothermal carbonization, offer significant potential for producing value-added products from organic MSW [54]. Literature provides various approaches to the chemical recycling of PSW, including fluid catalytic cracking, hydrocracking, gasification, and pyrolysis [13]. Table 4 presents some of these studies, highlighting their objectives and

results in this specific area.

Table 4. Chemical recycling studies.

Reference	Focus	Results
Mark et al., 2020 [13]	To explore the potential of heterogeneous catalysis in the chemical valorisation of plastic waste, focusing on the thermal and catalytic conversion of these materials into value-added products.	Heterogeneous catalysis can potentially convert plastic waste into valuable products, such as fuels and chemicals.
Al-Salem et al., 2021 [55]	Investigates recovered PSW from an active landfill to comprehend its thermal profile and degradation behaviour for potential utilization in thermochemical conversion processes.	The degradation mechanism, analysed by the Criado method, indicates that the Avarami-Erofeve model best represents the degradation of PSW.
Weiland et al., 2021 [56]	Chemical recycling of plastic waste through high-temperature oxygen gasification, comparing two complex plastic waste combustion and gasification processes.	Gasification efficiencies of around 80% for plastic reject (PR) and 60% for automotive shredder residue (ASR).
González-Arias et al., 2024 [57]	Thermochemical recycling, particularly steam gasification, to recover carbon from single-use medical items.	At 700°C, the recovery rates were approximately 79% for face masks, 82% for plastic syringes, 38% for nitrile gloves and 76% for non-woven gowns.
Zeller et al., 2021 [58]	Chemical recycling of complex plastic waste through intermediate pyrolysis.	Pyrolysis is suitable for recovering chemical feedstock from complex mixed plastic wastes.
Musivand et al., 2023 [59]	Chemically recycle polystyrene through pyrolysis and hydrothermal liquefaction, investigating the effects of temperature and reaction time on optimizing the production of valuable compounds.	The effective hydrothermal liquefaction at 360 °C for 4 hours converts polystyrene into oil (83%) and water-soluble compounds (10%), rich in aromatics. Pyrolysis at 500 °C produces gas (45%) and oil (55%), notable for recovering 40% styrene.
H. Jiang et al., 2020 [60]	To use high-temperature microwave-assisted pyrolysis to convert a mixture of plastic waste and vegetable oil into ethylene, propylene and other valuable chemical compounds.	The process converted plastic waste into ethylene, propylene and other valuable chemicals without costly sorting and pre-treatment.
Almeida Streitwieser et al., 2023 [61]	Chemical recycling of used motor oil through catalytic cracking.	The metal doping improved the catalyst's performance, resulting in higher conversion rates.
Tito et al., 2023 [62]	Chemical recycling of multi-material layered plastic films using a two-stage hydrothermal liquefaction (HTL) process.	It enabled the recovery of PET monomers and the production of paraffinic oil and hydrocarbon-rich gas as potential raw materials for the chemical industry.
Akhmetova et al., 2021 [63]	Hydrocracking of recycled plastic into high-quality liquid fuel using various catalysts based on natural zeolite deposits.	The 2% Mo/Taizhuzgen catalyst achieved the highest yield of liquid products, reaching 61.56%.

HDPE, in its various usage forms, is discarded in considerable volumes in the

environment, and only about one-third of this material is recycled or reused each year. Sani et al. [52] conducted a study on the dielectric performance of post-consumer recycled HDPE mixed with virgin HDPE, aiming for its application as an insulator for wires and electrical cables. Using thermal and chemical methods such as Thermogravimetric Analysis (TGA), Differential Scanning Calorimetry (DSC), and Energy-Dispersive X-ray Spectroscopy (EDX) to investigate the presence of impurities in the recycled material, they observed a significant amount of inorganic impurities, varying according to the melt filtration process. Recycled HDPE showed higher dielectric loss and dielectric constant values than virgin HDPE. The short-circuit resistance of recycled HDPE was slightly lower. Adding virgin HDPE to the recycled material was effective, resulting in a reduction of almost 50% in dielectric losses and improving short-circuit resistance.

LDPE exhibits high recyclability, but overcoming challenges such as the low economic value of recycled LDPE and its limitations in producing new packaging poses an obstacle to improving recycling rates for this material. Chemical recycling has proven effective for LDPE, generating fuels and low-molecular-weight products. Methods such as hydrothermal decomposition and pyrolysis have been studied, as well as catalytic cracking, where catalysts like zeolites have the potential to reduce temperature and influence the fragmentation reaction [53]. The study carried out by Santagata et al., (2020) [64] proposed the production of LDPE from mixed plastic waste, using high-temperature gasification to generate syngas, which was integrated into a process involving fermentation, ethanol production, and polymerization. Chemical analysis demonstrated the efficiency of gasification in producing syngas with a high content of CO and H_2. Thermal and material balances were performed to optimize the process, and cost analyses showed economic viability, considering revenues from waste. From an environmental perspective, chemical recycling was highlighted as a sustainable alternative, avoiding incineration.

Gorre et al., (2020) [65] focused on selecting solvents and nonsolvents for CR of PE and PP metalized films. The methodology involved selecting solvents based on Hansen solubility parameters and predicting polymer solubility through the Hansen sphere model. The results showed that using p-cymene as a solvent and acetone as a nonsolvent led to the successful recovery of PE and PP with average recovery yields of 78.43% and 93.92%, respectively. Fourier Transform Infrared Spectroscopy identified

the recovered polymers as PE and PP, and the analysis of differential scanning calorimetry showed that the melting temperature and percent crystallinity of the recovered polymers were comparable to virgin PE and PP films.

3.4. LANDFILL LEACHATE

The disposal in landfills represents the least favourable option for plastic treatment in the context of CE; however, it is still a widespread practice in the United States and Europe. Additionally, landfilling results in secondary damages such as contamination of the groundwater and ecosystem degradation [14]. Although landfill disposal is one of the most widely used methods for solid waste elimination, managing leachate from landfills is challenging due to its complex composition and high concentration of contaminants [15]. Various elements, including physical, chemical, and biochemical interactions, the high moisture content in the waste, precipitation water percolation, and contact of water with solid waste, contribute to the formation of landfill leachate. This wastewater combines pollutants such as ammonia, organic and inorganic compounds, natural and synthetic binders, xenobiotics, xenophobic organic substances, biological organisms, toxic compounds, and heavy metals. However, its specific composition varies according to the landfill hydrology, type and composition of waste, climatic conditions, and the age of the landfill [66].

A study conducted by Adaryani et al., (2022) [67] assessed the presence of CECs in leachates from four landfills in North Carolina, USA, between 2019 and 2020. This study identified 13 pharmaceuticals (7 detected) and 3 plasticizers (2 detected). Carbamazepine and ibuprofen were consistently found, with higher concentrations in open cells than those closed for over 13 years. Other substances, such as 17 alpha-ethinylestradiol, acetaminophen, bisphenol-A, doxycycline and metformin, were also detected in various concentrations. Carbamazepine was associated with older leachate, while acetaminophen, doxycycline and bisphenol-S were found in lower concentrations. Thus, it was observed that leachate remains a source of CECs many years after the landfill closure, suggesting the persistent transport of these contaminants with leachate if this effluent is produced.

In addition to the liquid percolating through the waste mass within the landfill cell,

the composting technique is another factor contributing to leachate generation [68]. Composting in landfills is a degradation process in which organic matter in the waste is decomposed through a bio-oxidative process. During composting, compost leachate is generated due to the high moisture content of the compost, and some essential nutrients such as nitrogen (N), phosphorus (P), potassium (K) and micronutrients may leach from the compost. This leachate can be recovered and used as an organic liquid fertilizer to promote plant growth. Typically, compost leachate is discharged into the local wastewater treatment system [69].

3.4.1. Treatment options

The treatment of landfill leachate is an essential phase in waste management, where various approaches are employed to deal with its complex composition. A common approach is biological treatment, where leachates are decomposed by living microorganisms such as bacteria, using aerobic (with oxygen) or anaerobic (without oxygen) techniques or a combination of both. Examples of biological treatment include activated sludge processes, upflow anaerobic sludge blanket reactors (UASB), aerated lagoons, biofilters and moving bed biofilm reactors (MBBR). Additionally, other treatment options, such as chemical and physical procedures are also utilized. These include air stripping, adsorption, chemical oxidation, coagulation/flocculation, chemical precipitation, and sedimentation/flotation.

Membrane technologies, such as membrane bioreactors, microfiltration, ultrafiltration, nanofiltration, and reverse osmosis, are used to separate and purify leachates. AOPs, such as photocatalysis, electrocatalysis, the Fenton process, and persulfate oxidation, can generate active species to degrade refractory organic compounds present in leachate [16,70,71]. In addition to refractoriness, another important parameter to assess the biodegradability of landfill leachate is the recalcitrance of organic matter, indicated by the BOD_5/COD ratio, as a low ratio indicates that the leachate is difficult to biodegrade, which can complicate treatment by biological processes [72]. Since more recalcitrant compounds require advanced techniques, chemical treatment can be applied for leachate purification [73], considering that pollutant concentrations reduce microbial activity and the effectiveness of biological treatment due to the presence of nitrogen and

refractory organics with high molecular weight and complex structures [68]. Table 5 summarizes some studies focusing on landfill leachate treatment.

Table 5. Landfill leachate treatments in the literature.

Reference	Focus	Results
Kabir et al., 2023 [74]	Remediation of microplastics in landfill leachate.	The treatment techniques for removal include bio-flocculation, filtration, coagulation-flocculation, oxidation and disinfection.
Samsudin et al., 2022 [75]	Utilization of biomass-based adsorbents to replace the currently employed activated carbon in landfills.	COD, ammoniacal nitrogen, and total nitrogen were removed at 73%, 70%, and 97%, respectively, along with a reduction in heavy metals.
Nalladiyil et al., 2023 [76]	Assessment of the potential of fungi and fungal-derived enzymes in landfill leachate treatment.	Membrane reactors based on fungi reduce membrane fouling and extend the lifespan.
Kanmani & Dileepan, 2023 [77]	Removal of recalcitrant organic pollutants from landfill leachate through advanced oxidation processes based on photocatalysis.	Photocatalysis using TiO_2 and ZnO is a promising approach for removing recalcitrant inorganic and organic pollutants from landfill leachate.
Guo et al., 2022 [78]	Application of aerobic granular sludge (AGS) in landfill leachate treatment.	AGS has the potential to withstand high carbon and nitrogen loads in the treatment of landfill leachate without significantly impairing removal efficiencies and biomass sedimentation.
V. E. Silva et al., 2022 [79]	Landfill leachate treatment through nitrogen removal techniques.	The nitrogen removal efficiency of the anaerobic ammonium oxidation (ANAMMOX) technology can exceed 99%.
Li et al., 2021 [80]	Landfill leachate treatment through AOPs based on ultrasound (US).	Effective degradation of conventional organic pollutants and emerging contaminants (ECs) in leachate, with a fast mass transfer rate and no secondary pollution.
Lei et al., 2023 [81]	Treatment of landfill leachate using the electroflotation system with designed titanium electrodes.	Electroflotation can be an effective pre-treatment technique, achieving significant COD, colour, and NH_3-N removals under optimized conditions.
Shadi et al., 2021 [82]	Use of reverse osmosis for landfill leachate treatment.	The alga *Desmodesmus subspicatus* was the most tolerant to leachate toxicity, achieving reductions of up to 100% in iron and 83% in ammonia nitrogen.
Zineb et al., 2020 [83]	Treatment of landfill leachate through coupling a Membrane Electrochemical Reactor (MER) with the Fenton oxidation process.	Can mitigate the ineffective removal of ammonia, high demand for acid and chemical reagents, and significant sludge generation associated with Fenton oxidation.

Within CWPO, CNTs have shown promise as materials for removing organic pollutants, employing adsorption mechanisms involving surface diffusion, pore diffusion,

and adsorption reaction. CNTs are produced from the chemical recycling of polyolefins such as polyethylene and polypropylene in a two-step catalytic process. Polyolefins undergo pyrolysis to generate an intermediate gas containing paraffin and hydrogen. This gas is then used as a precursor for the selective growth of single-walled or few-walled CNTs at high temperatures with an appropriate catalyst, resulting in CNTs with small external diameters and few walls. This innovative approach allows for the valorisation of plastic waste in producing high-value CNTs [18]. Additionally, materials based on CNTs can be applied in AOPs for wastewater treatment, possessing the ability to catalyse various oxidants such as hydrogen peroxide (H_2O_2), persulfates (PMS/PDS), ozone (O_3), and ferrate/permanganate (Fe^{6+}/Mn^{7+}).

Several strategies for landfill leachate treatment incorporate a biological phase based on denitrification and nitrification processes, responding to the high concentration of organic matter assessed through parameters such as BOD_5, COD and nitrogen in landfill leachate [84]. Although advanced oxidation methods effectively degrade organic pollutants in landfill leachate, biotreatment processes are necessary to eliminate biodegradable organic matter, turbidity, nitrogen and phosphorus nutrients [85].

The complexity of the microbial composition of these leachates, subject to variations influenced by the present waste, landfill operational conditions and cell decomposition dynamics, highlights the need to pay attention to the biological composition of leachate before and after treatment to assess the effectiveness of technologies aimed at eliminating the persistent microbial load [86]. In this context, research focused on developing technologies incorporating antimicrobial activity in the final stage of treatment, along with catalytic activity in AOP systems emerges as a promising and worthy area of investigation.

3.5. CARBON NANOTUBES

3.5.1. From carbon to nanotubes

To understand CNTs, it is essential to comprehend the structure and forms of carbon, as these nanomaterials are predominantly composed of carbon. Carbon is a non-metallic chemical element found in group IV and period II of the periodic table, with atomic number 6 and symbol “C” (Figure 6). Recognized for its remarkable versatility,

carbon can form bonds with various elements. Its atoms, comprising 6 electrons distributed among the 1s, 2s, and 2p orbitals, actively participate in chemical bonds, influencing the structure and properties of the molecules formed. These properties are determined by the number and nature of bonds, which can vary widely. Carbon can form bonds in different ways, resulting in a variety of allotropic forms, such as diamond, graphite, and CNTs, each with unique characteristics. These allotropic forms vary in physical properties, such as hardness and malleability. Carbon's hybridization determines its three-dimensional structure and can result in different arrangements, from planar structures like graphene to more complex forms like diamond [87].

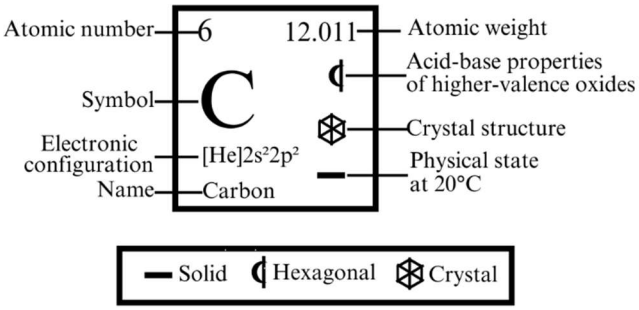

Figure 6. Properties of Carbon atom.

A CNT consists of a cylindrical arrangement composed of a single layer of carbon atoms, and its interconnections at the nanoscale offer advantages such as stability under extreme conditions, resistance to aggressive chemicals, and operation at high temperatures. With a melting temperature of 3550 °C and a boiling temperature of 4027 °C, CNTs possess a symmetrical, one-dimensional structure that allows charge carriers to move along the tube without dispersion. The individual resistivity of CNTs is on the order of 10−8 Ωm due to the absence of dispersion, resulting in electrical conductivity ranging from 10^6 to 10^7 S/m. Additionally, the density of CNT wire ranges from 0.0014 g/mm^3 to 0.00226 g/mm^3, making them lighter than copper and aluminium. With their tubular shape and adjustable electrical properties, CNTs exhibit characteristics such as low density, minimal skin effect, ballistic electron transport, high mechanical strength, high thermal conductivity, and greater stiffness compared to metals [88].

CNTs are classified into four main types - single-walled (SWCNTs), double-walled (DWCNTs), triple-walled (TWCNTs), and multi-walled (MWCNTs) - depending on the diameter, length, and number of walls (Figure 7) [89]. Furthermore, the properties of

CNTs, such as tensile strength, electrical conductivity, and thermal conductivity, are influenced by factors such as diameter-length ratio, number of layers, temperature, and length. At 25°C, SWCNTs and MWCNTs have average free paths of 103 nm and 104 nm, and thermal conductivity of 1.5-5 W/mK and 3 W/mK, respectively [88]. Over the past twenty years, research on SWCNTs has been an active area in both experimental and theoretical domains. However, DWCNTs, TWCNTs, and MWCNTs have only recently gained attention. DWCNTs are composed of two concentric SWCNTs, primarily stabilized by weak van der Waals forces, with a spacing between the walls ranging from 3.3 to 4.2 Å. The practical advantages of DWCNTs and MWCNTs over SWCNTs lie in the fact that, while SWCNTs are in direct contact with the environment, which can alter their properties, the presence of outer tubes in DWCNTs and MWCNTs protects the inner tubes from any external influences. Additionally, due to the weak forces between the tubes in a DWCNT/MWCNT, they can roll, rotate, and slide amongst each other [90].

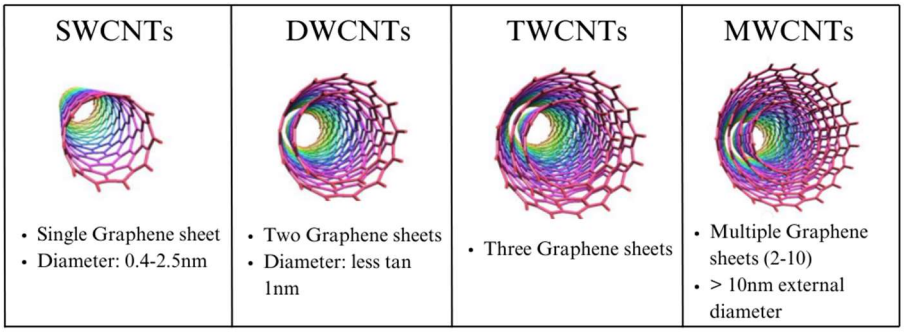

Figure 7. Types of carbon nanotubes [89].

CNTs are also classified into different structure types - chiral, armchair, and zigzag - each with unique properties that affect their physical and thermal characteristics. Chiral CNTs have a helical structure, whereas armchair CNTs feature edges with carbon atoms arranged at right angles, and zigzag CNTs have edges composed of carbon atoms arranged in straight lines. The distinction between these structures is crucial for selecting the most suitable CNT for a specific application, considering its desired properties and characteristics. This consideration is paramount in the design of CNT-based materials, as it directly influences the performance and properties of the final product, optimizing it to meet the specific needs of each application [91].

3.5.2. Synthesis

Various techniques are utilized in synthesizing CNTs, and their properties can differ based on the method applied [89]. Figure 8 illustrates the diverse methods used in the synthesis, purification, functionalization, and characterization stages of CNTs.

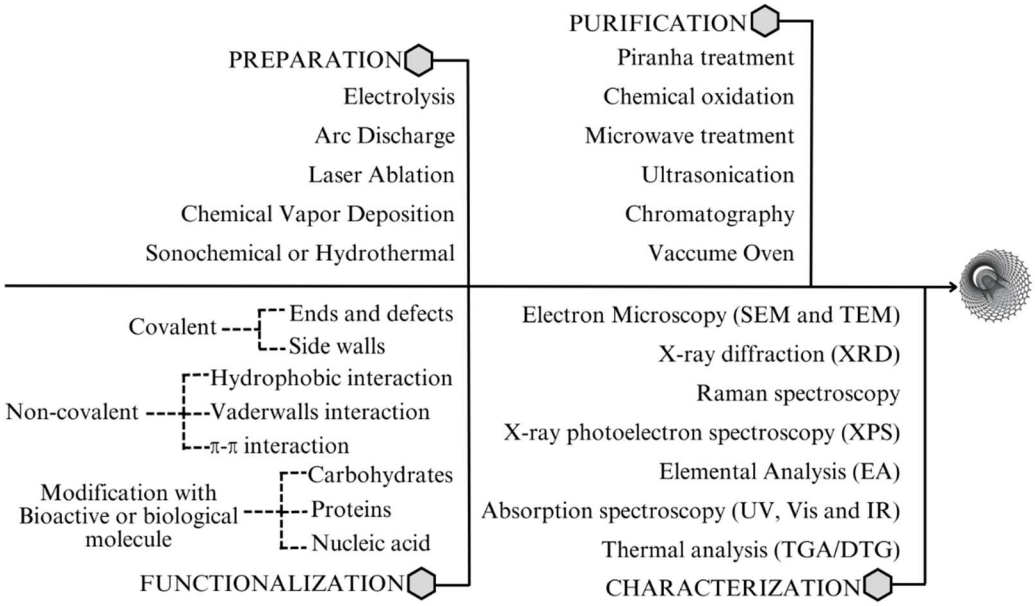

Figure 8. Various methods of CNTs preparation, purification, functionalization, and characterization.

There are several techniques for preparing CNTs, with chemical vapor deposition (CVD) being one of the most common. Thermal CVD and microwave plasma CVD are often used for this purpose, especially in industrial settings. With the use of transition metal catalysts, CVD enables the catalytic decomposition of hydrocarbons or carbon monoxide, resulting in high-purity carbon nanotubes on a large scale. Another common method is electric arc discharge, where an inert atmosphere is created between two graphite electrodes to generate CNTs. Additionally, laser ablation is a powerful technique in CNT production, although nanotubes synthesized by this method typically contain impurities in significant proportions. Although the approaches to CNT preparation vary, they all essentially involve inducing the cracking of the carbon source at high temperatures, depositing carbon atoms on catalysts, and consequently, the growth of CNTs [92,93].

A wide range of purification methods have been described in the literature. Typically, these methods involve various processing steps that may include oxidation in

either the gas or liquid phase, as well as physical separation processes such as filtration, centrifugation, chromatography, or selective functionalization methods. Oxidative steps are widely used in CNT purification protocols to remove both unwanted metallic particles and undesired carbon forms. Commonly employed methods for this purpose include heating in an oxidizing atmosphere to eliminate amorphous structures and non-tubular forms of carbon, refluxing in strong inorganic acids such as HNO_3, H_2SO_4, $HClO_4$, or mixtures of $KMnO_4/H_2SO_4$, $H_2O_2/KMnO_4$ mixtures, gas-phase purification based on halogens, microwave irradiation, hydrogen treatment, gas-phase oxidation in air, ozone, H_2S, and CO_2 [94].

Options for purifying SWNTs include a combination of air and microwave treatment, demonstrating effective metal removal in a shorter period compared to acid reflux methods. Another alternative involves a two-step process, starting with microwave treatment followed by gas-phase chlorination. Piranha mixtures, both acidic (H_2SO_4/H_2O_2) and alkaline (NH_4OH/H_2O_2), are commonly used in wet oxidation. Additionally, purifying CNTs using nitric acid has proven effective in removing amorphous carbon and metallic catalysts by unfolding the tube wall [95].

Functionalizing CNTs is essential to expand their applications, as they face challenges such as insolubility in solvents and limited dispersion. This process can occur in two main ways: covalently, involving direct or indirect chemical bonds, and non-covalently, utilizing physical interactions. Various chemical methods, such as amidation, oxidation, and halogenation, can be employed in covalent functionalization, resulting in structural alterations of CNTs. Conversely, non-covalent binding may involve hydrogen, van der Waals, and electrostatic interactions, promoting solubility and dispersion of CNTs, albeit with limitations in drug delivery due to weak van der Waals forces. Additionally, modification with biological molecules like nucleic acids and proteins is also being investigated to enhance the properties of CNTs [89].

The application of nitric acid (HNO_3) is a common oxidation technique for purifying CNTs. This effectively removes metallic catalyst particles from the nanotubes and generates small carboxylated carbonaceous fragments that coat them [96]. The carboxylic acid groups introduced by nitric acid oxidation can serve as precursors for further covalent functionalization of the CNT surface, such as salinization, esterification, thiolation, etc. The carboxylic groups help increase the affinity of the CNT surface to

various solvents and polymer matrices, improving their dispersibility and compatibility [97]. Figure 9 illustrates an experimental method demonstrating the carboxylation of CNTs using HNO_3.

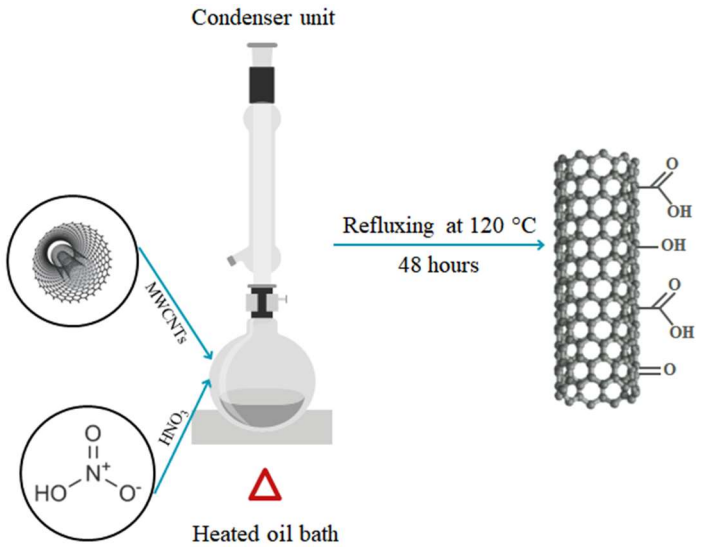

Figure 9. Experimental method for carboxylation of CNTs using HNO_3.

3.5.3. Ag-doped CNTs for wastewater disinfection

Nanotechnology, especially functionalized nanomaterials, is emerging as an effective solution to environmental pollution at a global scale [98]. A promising field of research is the use of metal-doped nanoparticles for wastewater disinfection. These nanoparticles exhibit antibacterial properties due to their ability to generate Reactive Oxygen Species (ROS), which are effective in destroying pathogens. Additionally, they can bind to the surface of microorganisms, causing damage to their cells and genetic material. The effectiveness of these nanoparticles can be enhanced by modifying the particle surface to increase contact time with pathogens, and metal doping is a viable strategy for designing nanoparticles with specific properties that improve their interaction with pathogens, thereby increasing their disinfection efficacy. Silver nanoparticles (Ag-NPs) are particularly known for their strong toxicity against a variety of microorganisms, demonstrating efficacy against both Gram-negative and Gram-positive bacteria, with lower production of residues during the process [99].

On the other hand, the use of silver nanoparticles Ag-NPs still raises concerns due to their increased toxicity in water compared to other silver-based materials. A promising

way to address post-disinfection water contamination issues with Ag-NPs is to use them as dopants. This approach allows for leveraging the antimicrobial characteristics of Ag-NPs without concern for post-treatment implications. For example, this strategy has already been successfully applied to Ag-NPs doped into other materials, such as CNTs, which are recognized as promising nanomaterials due to their bactericidal properties, antifouling, and unique structure, making them an ideal choice for stabilizing Ag-NPs, as it enhances their antimicrobial effectiveness without concerns associated with post-treatment toxicity [99,100]. Figure 10 illustrates an example of an antimicrobial mechanism.

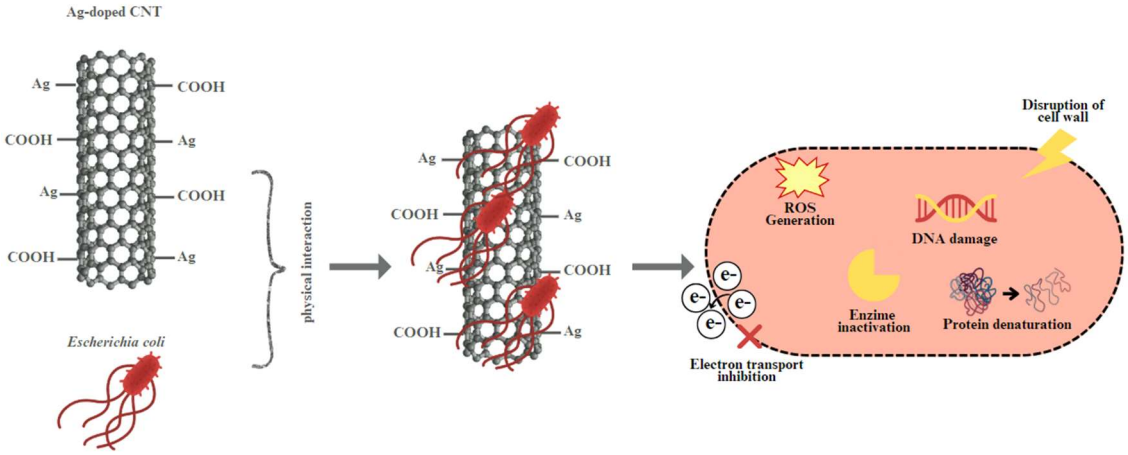

Figure 10. Antimicrobial mechanism of Ag-doped CNTs.

In this mechanism, CNTs adhere to the microbial cell surface to facilitate electron transfer across the membrane, inducing damage to the cell wall and membrane. Additionally, protein dysfunction and DNA damage occur when CNTs penetrate bacterial cells and produce secondary products such as reactive oxygen species (ROS) [101]. Furthermore, various hypotheses can interpret these mechanisms: bacterial cells were encompassed by the silver-CNT nanocomposite, augmenting the pores and gaps in the cell's outer membrane. The Ag-CNTs can significantly bind to sulfur molecules on the membrane and within the microbial cell, leading to metabolic process interruption, protein denaturation, and cellular damage. Additionally, they may interact with other phosphorus-based macromolecules, such as RNA and DNA, resulting in metabolism suppression, bacterial growth inhibition, and cell death [100].

MATERIALS AND METHODS

4 MATERIALS AND METHODS

4.1. REACTANTS

The reactants used in this work are given below, separated by the application for which they were used.

Synthesis of metal catalyst for carbon nanotubes preparation

- Cobalt (II) chloride hexahydrate (99%). Fisher Chemical; Formula: $CoCl_2.6H_2O$
- Nickel (II) chloride hexahydrate (99%). Fisher Chemical; Formula: $NiCl_2.6H_2O$
- Ethanol absolute (99.8%). Fisher Scientific; Formula: C_2H_5OH
- Iron (III) chloride hexahydrate (99%). Merck; Formula: $FeCl_3.6H_2O$
- Ethanediol (99%). Fisher Scientific; Formula: $C_2H_6O_2$
- Aluminium oxide (99.7%). ThermoScientific; Formula: Al_2O_3

Synthesis and purification of CNTs

- Polyethylene low density, average Mw 35000 by GPC, average Mn 7700 by GPC LDPE. Sigma-Aldrich; Formula: $(C_2H_4)n$
- Polyethylene high density, melt index 2.2 g/10 min (190 °C/2.16kg) HDPE. Sigma-Aldrich; Formula: $(C_2H_4)n$
- Polypropylene isotactic, average Mw 250000, average Mn 67000. Sigma-Aldrich; Formula: $(C_3H_6)n$
- Nitrogen gas (>99.99%). Lindt; Formula: N_2

Doping of CNTs

- Nitric acid (65%). Fisher Scientific; Formula: HNO_3
- Deionized water
- Silver nitrate (99.8%). AppliChem Panreac; Formula: $AgNO_3$
- Sodium borohydride (≥98%). VWR; Formula: $NaBH_4$

- Ethanol absolute (99.8%). Fisher Scientific; Formula: C_2H_5OH
- Nitrogen gas (>99.99%). Lindt; Formula: N_2

Application of the materials for the degradation of pollutants

- Bisphenol A (≥99%). Merck; Formula: $C_{15}H_{16}O_2$
- Deionized water
- Sulfuric acid (95-98%). Labkem; Formula: H_2SO_4
- Hydrogen Peroxide (30%). Fisher Scientific; Formula: H_2O_2
- Titanium (IV) oxysulfate solution (1.9-2.1%). Sigma-Aldrich; Formula: $TiOSO_4$
- Sodium sulfite (≥98%). Sigma-Aldrich; Formula: Na_2SO_3

Landfill leachate characterization

- Yeast Extract Agar. VWR Chemicals
- Cycloheximide (98%). Panreac. Formula: $C_{15}H_{23}NO_4$
- Rose Bengal Chloramphenicol Agar. Liofilchem
- Sodium chloride (99.5%). Honeywell. Formula: NaCl

Coupled disinfection and CWPO

- Sodium chloride (99.5%). Honeywell. Formula: NaCl
- Nutrient Broth. Liofilchem
- Nutrient Agar ISO 16266. Liofilchem
- Deionized water

4.2. PREPARATION OF CNTs

4.2.1. Metal catalyst

The metal catalysts were prepared to maintain a 1:2 ratio (M^{2+}:M^{3+}), achieved by preparing a solution of 4 mmol of M^{2+}, containing 30% $CoCl_2.6H_2O$ and 70% $NiCl_2.4H_2O$

dissolved in 10 mL of C_2H_5OH. This solution was heated under stirring in a round-bottom flask until reaching the boiling point, followed by cooling to room temperature. Next, a solution containing 8 mmol of M^{3+} from $FeCl_3.6H_2O$ in 20 mL of $C_2H_6O_2$ was prepared, heated for 5 minutes at 60 °C, and allowed to cool to room temperature. Both solutions were then transferred to a flask previously loaded with 5.67 g of Al_2O_3, and the mixture was heated under stirring for 2 hours at 60 °C, another 2 hours at 120 °C, and finally at 189 °C until solid formation. This final solid was transferred to a crucible for thermal treatment in an oxidative atmosphere for 6 hours at 600 °C.

4.2.2. Synthesis and purification of CNTs

The CNTs were synthesized via chemical vapor deposition (CVD) using the reactor setup shown in Figure 11.

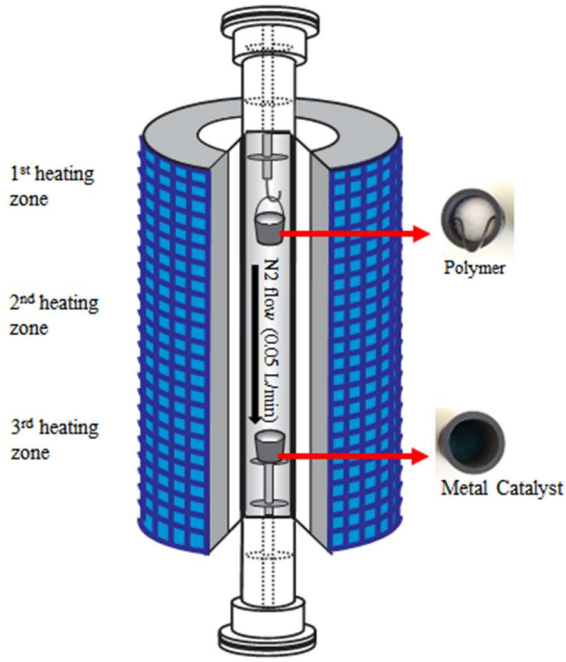

Figure 11. One-chamber reactor setup used to synthesize CNTs by CVD.

In the reactor, the lower crucible was loaded with 1 g of metallic catalyst. Simultaneously, the upper crucible was loaded with MIX polymers, a polymeric composition simulating real plastic solid wastes, consisting of 1.25 g LDPE, 1.75 g HDPE and 2 g PP. The Nitrogen flow was then turned on at a rate of 30 NL min^{-1} and left running

for 2 hours to ensure an inert atmosphere within the reactor. Once confirmed, the reactor was heated to 850 °C in the third and lowest heating zone, while the upper heating zone reached 450 °C. After 1 hour and 30 minutes, the reactor was turned off and, in the next day, the material was recovered from the reactor [102]. The reactor used in this procedure was the vertical/horizontal tubular furnace supplied by TERMOLAB. The company ensures that these furnaces have been designed and built according to technical standards and legal provisions related to machine safety (Machinery Directive 98/37/CE) [103]. The detailed specifications of the furnace are presented in Table 6.

Table 6. Characteristics of the vertical/horizontal tubular furnace.

Designation	Value	Unit
	DIMENSIONS	
Internal tube diameter	50	mm
Length of the hot zone	500	mm
	GENERAL	
Electric potential	230	V
Frequency	50	Hz
Power	4.5	kW
Maximum temperature	1200	ºC
Cooling water flow	1 to 2	L/min

4.2.3. Ag-doped CNTs

To perform silver doping, initially carboxylated CNTs (CNT-COOH) were prepared [104]. This was done by dispersing 1 g of CNT in 75 mL of 15.2 M HNO_3 solution, with sonication for 30 minutes in a round-bottom flask with two necks. Subsequently, the flask was placed under vigorous stirring and reflux condenser at 120 °C for 48 hours. Afterward, the CNT-COOH was recovered and washed with deionized water until the rinsing water reached a neutral pH. For doping, two different methodologies were evaluated: one based on the co-precipitation of Ag nanoparticles in the CNTs and the other based on the wet impregnation of Ag nanoparticles in the CNTs.

In the co-precipitation (methodology 1) [104], two Erlenmeyer flasks were prepared, and in each of them, 1 g of CNT-COOH was added to 100 mL of deionized water and subjected to sonication for 30 minutes. Then, a solution of 0.05 M $AgNO_3$ was added to both mixtures, which were sonicated for another 30 minutes, followed by stirring at room temperature for an additional 30 minutes to obtain Ag-CNT complexes. Subsequently, a freshly prepared solution of 0.05 M $NaBH_4$ was added, and the resulting

mixtures were stirred for 12 hours. The volumes of the $AgNO_3$ and $NaBH_4$ solutions added dropwise through a peristaltic pump into the two mixtures, are described in Table 7.

Table 7. Reagent volume for different dopage percentages.

Ag percentage	V in mL ($AgNO_3$ 0.05 M and $NaBH_4$ 0.05 M
5%	9.28
10%	18.56

For the wet impregnation (methodology 2) [19], two Erlenmeyer flasks were prepared. In each, 1 g of CNT-COOH was added to 63.5 mL of C_2H_5OH and sonicated for 30 minutes. Then, in the first flask, a solution of 9.28 mL of 0.05 M $AgNO_3$ in C_2H_5OH was added for doping with 5% Ag, while in the other flask, a solution of 18.56 mL of 0.05 M $AgNO_3$ in C_2H_5OH was added for doping with 10% Ag. The solutions were dispersed drop by drop using a peristaltic pump, and then the flasks were subjected to sonication for another 30 minutes. After sonication, the mixtures were dried in an air oven at 70 °C overnight. The following day, the thermal treatment was conducted in an inert atmosphere inside a tubular furnace at 450 °C for 3 hours.

The materials were designated according to different synthesis stages and doping techniques, namely: metal catalyst for CVD ($NiFe/CoFe@Al_2O_3$), pure carbon nanotubes (CNT), carboxylated CNTs (CNT-COOH), carboxylated and silver-doped CNTs at 5% using methodology 1 (CNT-COOH/Ag1-5%), carboxylated and silver-doped CNTs at 10% using methodology 1 (CNT-COOH/Ag1-10%), carboxylated and silver-doped CNTs at 5% using methodology 2 (CNT-COOH/Ag2-5%) and carboxylated and silver-doped CNTs at 10% using methodology 2 (CNT-COOH/Ag2-10%).

4.3. MATERIAL CHARACTERIZATION TECHNIQUES

4.3.1. Surface and pore analyser

The textural properties of the materials were determined from N_2 adsorption-desorption isotherms at -196.15 °C, obtained using a Quantachrome NOVA TOUCH LX^4 instrument with long cells featuring a bulb and an outer diameter of 9 mm. The classification proposed by IUPAC is shown in Figure 12.

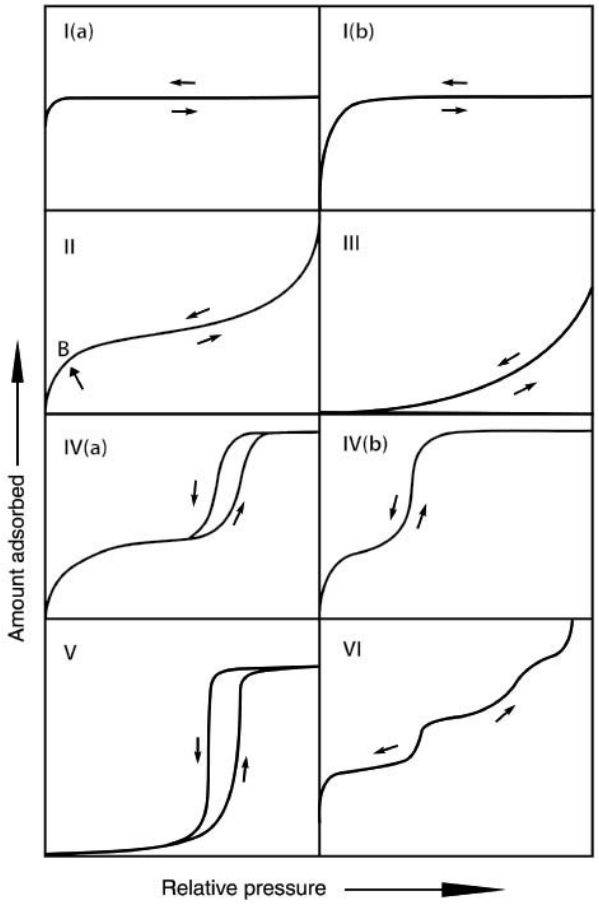

Figure 12. Classification of physisorption isotherms by IUPAC [105].

IUPAC also provides a classification for the hysteresis loop, which is represented in Figure 13.

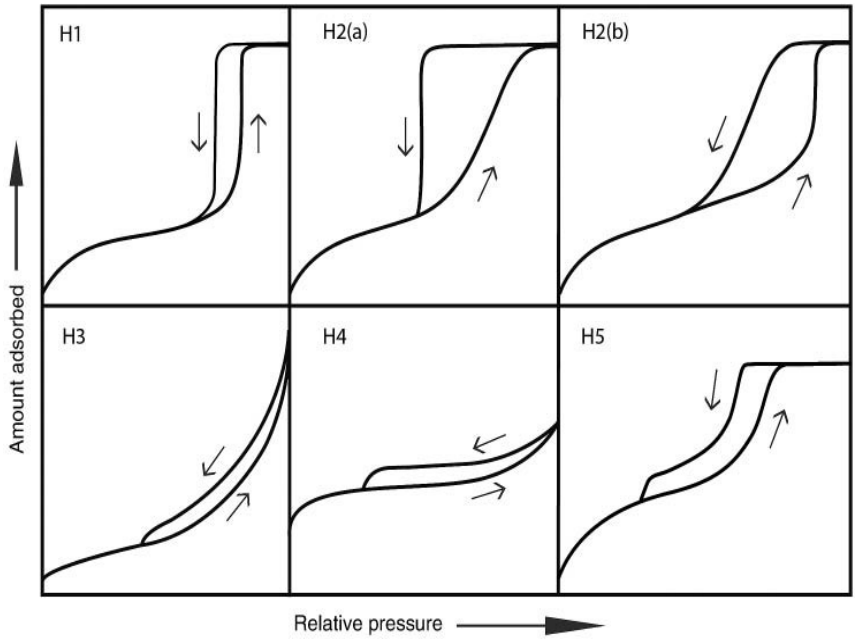

Figure 13. IUPAC classification for hysteresis loop [105].

With these classifications of the isotherms and corresponding hysteresis loop obtained it is possible to characterize the catalysts in terms of the type of material. The specific surface area (S_{BET}) was calculated using the BET method with Quantachrome TouchWin software within the range of p/p_0 0.05 – 0.35. The total pore volume (V_T) was determined at p/p0 = 0.98. The outgassing process was conducted at 120 °C over 16 hours, following the time recommended by IUPAC.

4.3.2. Thermogravimetric analysis (TGA)

The sample was homogenized to ensure a uniform distribution before being weighed and placed in a sample pan, which was then positioned inside the TGA equipment, the NETZSCH TG 209F3. Throughout the experiment, the temperature ranged from 30 to 930 °C at a heating rate of 10 °C per minute. As the temperature varied, the sample mass was continuously monitored by the precision balance. This variation in sample mass was recorded as a function of temperature or time. Additionally, a controlled atmosphere (synthetic air) was maintained inside the TGA equipment to prevent undesired reactions or external interferences. The remaining weight of the samples after TG analysis was used to determine the ash content [102].

4.3.3. Elemental analysis (EA)

The elemental analysis (CHNS-O) was carried out in a Flash 2000 analyzer (Thermo Fisher Scientific, Waltham, MA, USA) provided with a thermal conductivity detector (TCD) to quantify the chemical composition of CNTs, including the presence and amount of impurities [106].

4.3.4. X-ray diffraction (XRD)

The X-ray diffraction technique was employed to characterize the crystallinity and structural properties of the metallic CVD catalysts. Analyses were conducted at room temperature using a PANalytical X'Pert Pro diffractometer equipped with an X'Celerator detector and a secondary monochromator in Bragg-Brentano θ/2θ geometry. Measurements were performed using 40 kV and 30 mA, CuKα radiation (λα1 = 1.54060

Å and λα2 = 1.54443 Å), 0.017°/step, 100 s/step, over a 2θ angular range of 10-80°. Data processing was carried out using X'Pert HighScore Plus software with reference cards from the Crystallography Open Database [107].

4.3.1. Transmission electron microscopy (TEM) and Scanning electron microscopy (SEM)

JEOL 2100 high-resolution transmission electron microscope (HR-TEM) with LaB6 filament operating at 200 kV was used to obtain the microphotographs of the CNTs. For nanoscale powder samples such as CNTs, in scanning electron microscopy (SEM), the sample is dispersed in a solvent and applied to the surface of a metallic CVD catalysts, resulting in a well-dispersed and flat mesoscopic-scale sample while ensuring sample conductivity. In this study, this methodology was employed to characterize carbon nanotubes, obtaining high-quality secondary electron images. Secondary electron (SE) images obtained by SEM provide detailed information on surface topography, as well as sample dimensions and size distribution. Additionally, atomic number-sensitive backscattered electron (BSE) images are useful for distinguishing samples with different chemical compositions, such as contamination particles. The elemental composition of the samples can be determined using SEM equipped with an energy-dispersive X-ray spectrometer (EDS), and elemental mapping by EDS provides valuable information on the distribution of elements [108].

4.4. MICROBIOLOGICAL CHARACTERIZATION OF LANDFILL LEACHATE

An experiment was conducted using two culture media for the microbiological characterization of landfill leachate. The first, called Yeast Extract Agar, was prepared for bacterial counting, with the addition of 200 mg/L of cycloheximide to inhibit the growth of yeasts and fungi, and Rose Bengal Chloramphenicol Agar for yeast and fungi counting, where chloramphenicol acts to inhibit bacterial growth. In test tubes, decimal dilutions were prepared from the initial leachate sample in a series of 10^{-1}, 10^{-2}, 10^{-3}, 10^{-4}, 10^{-5}, and 10^{-6} in a NaCl solution (0.85% w/v). Then, 100 µL of each dilution were inoculated in duplicate onto Petri dishes containing the respective culture media. Plates inoculated with Yeast Extract Agar were incubated at 37 °C for 24 hours, and plates

inoculated with Rose Bengal Chloramphenicol Agar were incubated at 22 °C for 72 hours. After incubation, microbial counts were performed on the plates.

To determine the concentration of microorganisms in samples based on the number of colonies observed on Petri dishes after incubation, Equation (1) was applied, according to ISO 7218:2007/Amd.1:2013(E) [109], where CFU is the "Colony Forming Unit", measure of the concentration of the live, viable bacterial cells capable of reproducing when grown on a Petri plate in cells per millilitre (cells/mL); C is the media of the number of colonies on each selected plate for counting; v is the volume inoculated on each plate, and d is the dilution factor retained for counting.

$$\frac{\mathrm{CFU}}{\mathrm{mL}} = \frac{\overline{\mathrm{C}}}{\mathrm{v}\times\mathrm{d}} \tag{1}$$

For colony counting, it was considered that a countable plate has between 30 and 300 colonies, as in the presence of too many colonies on the plate, colonies may merge and become indistinguishable as individual colonies. In this case, the plate is referred to as confluent or too numerous to count, and fewer than 30 colonies are too small a sample size to represent the original sample accurately.

4.5. CWPO OF BISPHENOL-A

This stage involved the application of materials for pollutant degradation experiments. For this purpose, a simulated matrix containing bisphenol-A (model microplastic) was used. Batch oxidation runs were performed using the stoichiometric amount of hydrogen peroxide needed for the complete mineralization of bisphenol-A, according to the chemical equation shown in Equation (2).

$$\mathrm{C_{15}H_{16}O_2} + 36\mathrm{H_2O_2} \rightarrow 15\mathrm{CO_2} + 44\mathrm{H_2O} \tag{2}$$

Considering 100 mL of bisphenol-A solution with a concentration of 100 mg/L, the amount of hydrogen peroxide needed to proceed with the experiment was found to be equal to 179 µL (stoichiometric) of a 30% weight/volume hydrogen peroxide solution. The oxidation reactions were carried out in a well-stirred 250 mL round-bottom flask

reactor (600 rpm) equipped with a condenser and a temperature measurement thermocouple. The reactor was loaded with 100 mL of 100 ppm bisphenol-A solution to simulate landfill leachates, previously acidified to pH 3.5 with H_2SO_4. The system was heated by immersion in an oil bath monitored by a temperature controller to 80 °C, which was the temperature used in the oxidation runs. When the temperature stabilized, the stoichiometric amount of hydrogen peroxide was added to the reaction system. After complete mixing of the reactants, the amount of catalyst necessary to reach 2.5 g/L was added to the reactor. This moment was then considered the start of the CWPO run (t0 = 0 min).

Samples for analysis were periodically withdrawn at selected times: 0, 5, 15, 30, 60, 120, 240, 360 and 480 minutes. At each time point, a 2 mL sample of solution was collected and stored in Eppendorf tubes for the different catalysts. Subsequently, the samples were centrifuged to separate the catalyst from the liquid solution. Then, 200 µL of solution from each Eppendorf were transferred to 5 mL volumetric flasks previously prepared with 1 mL of H_2SO_4 (0.5 M) and 0.1 mL of $TiOSO_4$ in deionized water for further analysis using UV-VIS. After the sample collection, approximately 0.02 g of Na_2SO_3 was added to stop the reaction, and then the catalyst was separated by filtration, the liquid medium was stored for analysis using HPLC, and the catalyst was washed with distilled water and dried in an oven at 60 °C overnight.

For the adsorption tests, 50 mL of the same bisphenol-A solution used in the CWPO runs (100 mg/L) was added to a reactor containing 0.125 g of adsorbent (2.5 g/L adsorbent concentration). The adsorption experiments were conducted under the same conditions described for the CWPO runs but without the addition of H_2O_2. After collection and subsequent filtration, the samples were analysed in the HPLC to assess the concentration of bisphenol-A. The percentage of bisphenol-A adsorbed was calculated by the difference between the initial and final concentrations.

For the catalytic decomposition tests of H_2O_2, 100 mL of water acidified with H_2SO_4 to a pH of 3.5 were added to a reactor containing 0.250 g of catalyst (catalyst concentration of 2.5 g/L) and 179 µL (stoichiometric) of a 30% weight/volume hydrogen peroxide solution. The experiments were conducted under the same conditions described for the CWPO runs, but the pollutant solution was replaced with acidified water. From the volumes collected at each point, 200 µL of the collected solution was transferred to 5

mL volumetric flasks previously prepared with 1 mL of H_2SO_4 (0.5 M) and 0.1 mL of $TiOSO_4$ in deionized water. These samples were analysed using UV-VIS to determine the absorbance at a wavelength of 405 nm.

The desorption of BPA was carried out using materials recovered from adsorption and CWPO experiments. Under these conditions, desorption involved utilizing a methanol/acetic acid mixture (4:1 v/v) with a material dose of 0.5 g/L. The process ran for 48 hours at 25 °C. Following the completion of the operation time, the supernatant was separated and subjected to analysis via HPLC. The amount of BPA desorbed from the materials was determined using Equation (3).

$$\mathrm{BPA_{des}} = \frac{[\mathrm{BPA}]\times \mathrm{V}}{\mathrm{m_{des}}} \quad (3)$$

In which [BPA] represents the BPA concentration (mg/L) determined using HPLC, V is the volume (L) of the aqueous extractant solution used for the experiment and m_{ads} is the mass (g) of adsorbent used in the experiment.

4.6. CWPO AND DISINFECTION

The experiment was conducted in triplicate, subjected to three distinct control conditions: one composed solely of bisphenol-A and *Escherichia coli* bacteria (Sample 1), another containing only hydrogen peroxide and *Escherichia coli* bacteria (Sample 2), and the last simulating the CWPO process with hydrogen peroxide catalysed by CNT-COOH/Ag2-5%, including *Escherichia coli* bacteria and bisphenol-A (Sample 3). This catalyst was selected for exhibiting the best response in the advanced oxidation runs conducted in the previous stage of the experiment. This formulation was developed to evaluate the interaction of the materials with the microorganisms, aiming to identify any interference from both the pollutant and the hydrogen peroxide in isolation.

Initially, the three solutions were prepared for the different samples. For Sample 1, a solution containing bisphenol-A at a concentration of 100 ppm was prepared in deionized water, with the pH adjusted to 5 using acetic acid. For Sample 2, a solution of hydrogen peroxide at a concentration of 537 ppm in deionized water was prepared. Finally, for Sample 3, a solution containing bisphenol-A at a concentration of 100 ppm

and with the pH adjusted to 5 using acetic acid was prepared in deionized water, supplemented with 895 μL of hydrogen peroxide (in stoichiometric quantity, with a concentration of 30% w/v). The three solutions were pasteurized in a water bath at 70 °C for 3 hours to eliminate microorganisms.

To prepare the *Escherichia coli* inoculum from a pure culture, two colonies were collected and transferred to a 250 mL Erlenmeyer flask containing Nutrient Broth (NB). The solution was then incubated at 37 °C for 24 hours. After this period, the concentration of microorganisms was adjusted to 0.5 on the McFarland scale using a densitometer (DEN-1B, Biosan). All experiments involving microorganisms were conducted in a laminar flow hood, and all materials used in this experiment, including test tubes, Eppendorf tubes, pipette tips, Petri dishes, spreaders, Erlenmeyer flasks, and culture media, were previously sterilized in an autoclave at 120 °C for 1.5 hours.

The next step involved inoculating the microorganisms into the three established control conditions. For this purpose, 10 mL of the prepared inoculum was added to each Erlenmeyer flask, along with 90 mL of each corresponding solution. At the initial time (0 minutes), 100 μL of the sample was withdrawn, and decimal dilutions were performed in series of 10^{-1}, 10^{-2}, 10^{-3}, 10^{-4}, 10^{-5}, 10^{-6} and 10^{-7} was performed in test tubes, using NaCl (0.85 w/v.%) as a diluent. After each dilution, the solutions were properly homogenized on a vortex shaker. Subsequently, 100 μL of each sample was inoculated onto Petri dishes containing Nutrient Agar (NA), and the material was evenly spread using the spread plate method. The plates were then incubated in a 37 °C oven for 24 hours for subsequent bacterial counting.

Simultaneously, in Sample 3, 20 mg of CNT-COOH/Ag2-5% were added to each Erlenmeyer flask, corresponding to the CWPO triplicate. The first collection of the reaction was performed at the initial time (0 minutes). All samples, including the triplicates of Samples 1, 2, and 3, were placed on an orbital shaker and subjected to constant agitation at 200 rpm at 45 °C. Collection of the CWPO reactions was performed at times 0, 15, 30, 60, 120, 240, 360 and 480 minutes, as well as after 24 hours of reaction.

For the microbiological analysis, a new collection was performed at the end of the 24-hour reaction period. The samples were withdrawn and incubated following the same methodology applied at the beginning of the experiment. After the 24-hour incubation at 37 °C, the samples were counted to determine the number of bacteria present, following

the same methodology adopted in the microbiological characterization step, as represented by Equation (1) described earlier, and the percentage of *Escherichia coli* reduction was calculated by the difference between the initial and final concentrations (CFU/mL).

For the CWPO analysis, 2 mL of sample were collected and filtered through 0.45 µm PTFE filters to remove bacteria and particulate matter and placed in Eppendorf tubes at each defined time point. From these samples, 200 µL were transferred to 5 mL volumetric flasks previously prepared with 100 µL of $TiOSO_4$ and 1 mL of H_2SO_4 (0.5 M) in deionized water for subsequent analysis using UV-VIS spectroscopy to determine the absorbance at a wavelength of 405 nm. The remaining volume was then treated with approximately 0.02 g of Na_2SO_3 to halt the reaction, and the material was subsequently analysed by HPLC. A representation of the stages, including the CWPO experiment and the microbiological analysis, is presented in Figure 14.

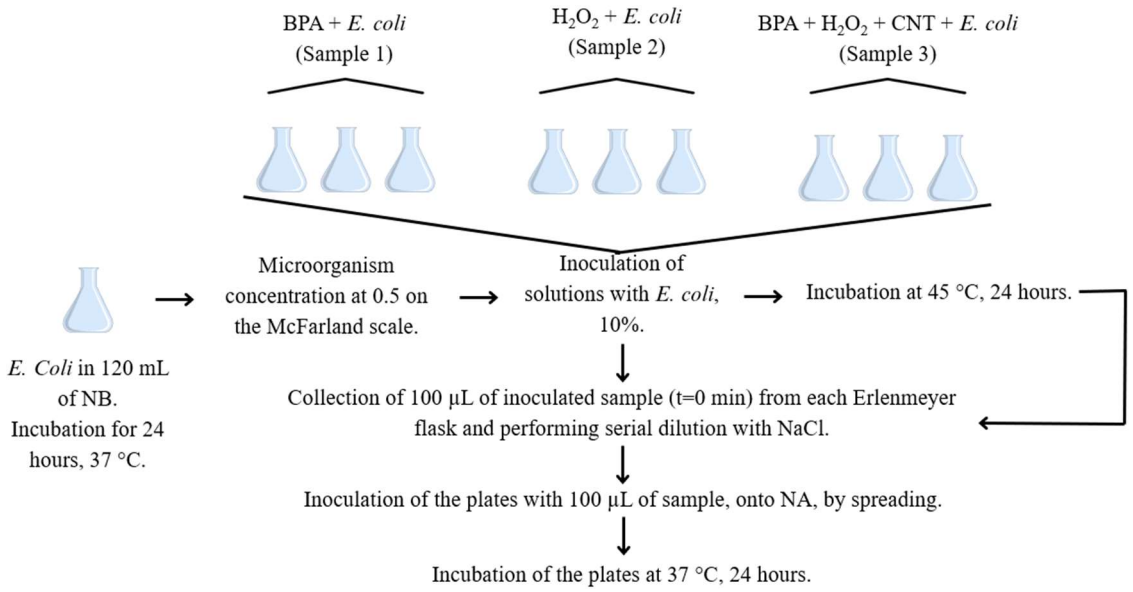

Figure 14. Representation of experimental stages including CWPO process and microbiological analysis.

4.7. ANALYTICAL TECHNIQUES

The determination of hydrogen peroxide concentration was carried out using a colorimetric method. To monitor the H_2O_2 concentration, it was necessary to construct a calibration curve covering a concentration range from 1 to 200 mg/L. For this purpose, 1 mL of different H_2O_2 solutions was added to a 5 mL volumetric flask containing H_2SO_4

solution (1 mL/0.5 M) and $TiOSO_4$ (0.1 mL), then diluted again with distilled water. The samples were subsequently analyzed by UV-VIS spectrophotometry using a Jasco V-530 at a wavelength of 405 nm to determine their absorbance. The calibration curve generated through this procedure is depicted in Figure 15, and the value of R^2 was found to be 0.9994, which shows a good fit for the linear regression.

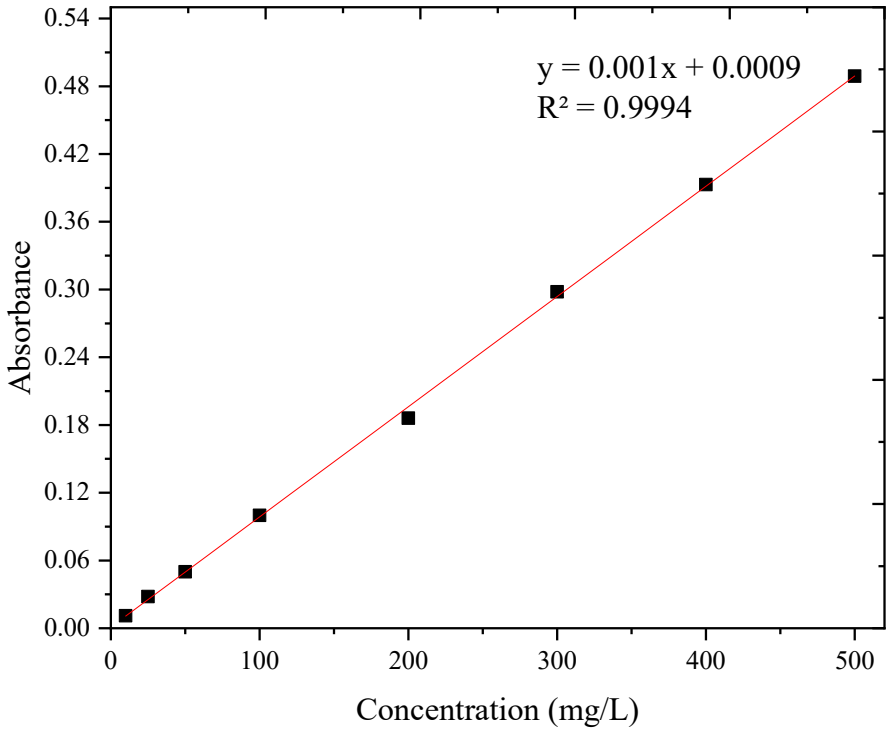

Figure 15. Calibration curve for H_2O_2 determination.

The determination of hydrogen peroxide concentration in the samples taken from the CWPO reaction medium was performed by collecting 1 mL and storing it in an Eppendorf tube. Then, the sample was centrifuged, and 0.2 mL of the supernatant was added to a 5 mL volumetric flask containing 1 mL of H_2SO_4 (0.5 M) and 0.1 mL of $TiOSO_4$ in distilled water. The absorbance obtained by UV-VIS analysis of these final samples provided the concentrations of H_2O_2 over time in the CWPO procedure.

The system used for HPLC measurements consisted of Jasco equipment with a UV-VIS detector (UV-2075 Plus), a quaternary gradient pump (PU-2089 Plus) for solvent delivery (0.3 mL min^{-1}), and a Biphenyl 5 µm column (150 mm x 4.6 mm). The mobile phases used for this purpose were a mixture of acetonitrile (A) and acidified water (0.1 *v/v*% formic acid) with a proportion of 60:40 (isocratic). This setup enabled the

analysis of the model pollutant (bisphenol-A). A wavelength of 280 nm was used to measure the absorbance peaks of the compounds. The quantification of bisphenol-A in the remaining solution of the CWPO process was conducted to determine the leached bisphenol-A from the materials prepared for the reaction medium. Figure 16 shows the representation of the calibration curve obtained for the analysis.

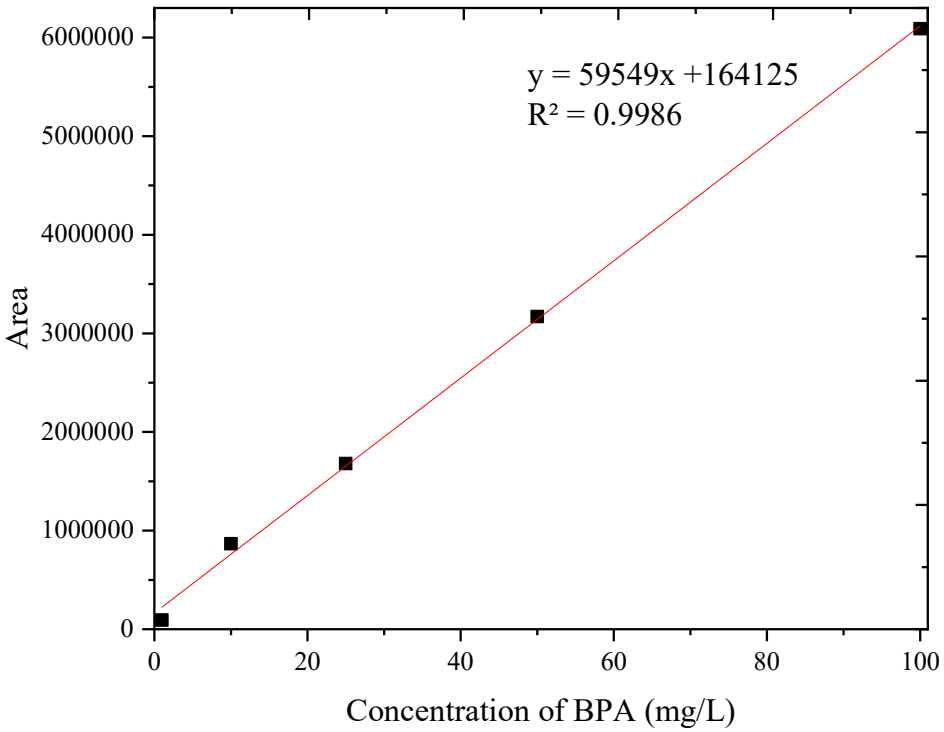

Figure 16. Calibration curve for pollutant leached measurements.

The value of R^2 was found to be 0.9986, which shows a good fit for the linear regression. After the CWPO runs, the residues were subjected to filtration through a PTFE filter 45 micrometers, and the supernatant liquid was preserved in a container and then analysed in the equipment to measure its absorbance and, consequently, determine the concentration of bisphenol-A.

RESULTS AND DISCUSSION

5 RESULTS AND DISCUSSION

5.1. CHARACTERIZATION OF MATERIALS

5.1.1. Textural properties and morphology

The adsorption-desorption isotherms of N_2 at -196.15 °C on prepared samples are depicted in Figure 17. In this analysis, the materials with the highest adsorption capacity are those doped with silver and functionalized with HNO_3, compared to those that are not functionalized or both non-functionalized and doped. CNT-COOH/Ag2-10% exhibited the highest adsorptive capacity, with approximately 455 cm^3/g of adsorbed volume under relative pressure p/p_0, followed by CNT-COOH/Ag1-10% (443 cm^3/g), CNT-COOH/Ag2-5% (388 cm^3/g), CNT-COOH/Ag1-5% (370 cm^3/g), CNT-COOH (378 cm^3/g), NiFe/CoFe@Al_2O_3 (241 cm^3/g) and finally, CNT (175 cm^3/g). This result is expected as COOH groups increase the surface area of the nanotubes. Additionally, silver nanoparticles have been investigated in the literature for their adsorptive properties, as shown in a study [110], where silver nanoparticles exhibited a surface composed of spherical particles and deep pores capable of adsorbing a significant amount of Cu^{2+} ions.

The adsorption isotherm graphs indicate that the materials fall into Type IV according to the IUPAC guidelines, suggesting mesoporous characteristics. This means that adsorption initially occurs in monolayer and multilayer on the walls of the mesopores, followed by pore condensation. Specifically, the materials are of Type IVa, where capillary condensation is accompanied by hysteresis, which arises when the pore width exceeds a critical limit, depending on the adsorption system and temperature, and hysteresis occurs in pores with a width greater than approximately 4 nm. Regarding the hysteresis curves, the material exhibits characteristics of type H3, which are observed in non-rigid aggregates of plate-shaped particles, or if the pore network consists of macropores that are not filled with pore condensate [105].

The results of S_{BET} obtained from the adsorption isotherms are shown in Table 8, demonstrating that the materials with the highest BET surface area are the silver-doped CNTs through wet impregnation (CNT-COOH/Ag2-5% and CNT-COOH/Ag2-10%). This can be explained because of the preparation method, increasing their surface area.

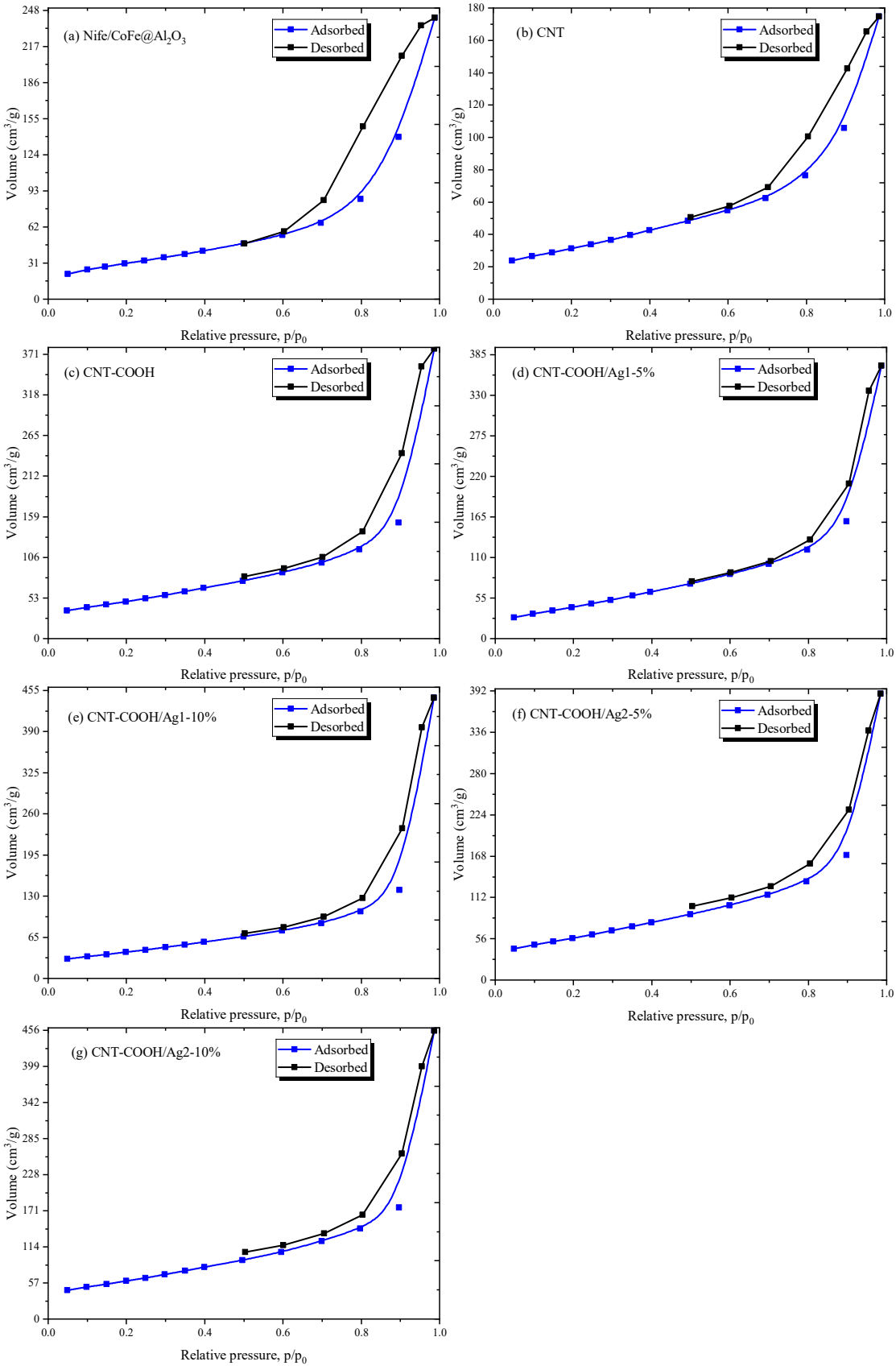

Figure 17. Adsorption-desorption isotherms for (a) NiFe/CoFe@Al_2O_3, (b) CNT, (c) CNT-COOH, (d) CNT-COOH/Ag1-5%, (e) CNT-COOH/Ag1-10%, (f) CNT-COOH/Ag2-5% and (g) CNT-COOH/Ag2-

10%.

Table 8. S_{BET} from the materials.

Material	S_{BET} (m^2/g)	Total pore volume, V_T (cm^3/g)
NiFe/CoFe@Al_2O_3	113	0.36176
CNT	113	0.27108
CNT-COOH	177	0.58662
CNT-COOH/Ag1-5%	172	0.61258
CNT-COOH/Ag1-10%	154	0.68747
CNT-COOH/Ag2-5%	209	0.60242
CNT-COOH/Ag2-10%	219	0.70599

TEM images were recorded from as-synthesized CNTs to confirm the formation of carbon nanotubes using the one-chamber reactor setup. The images confirm the formation of multi-walled CNTs. The resolution of the images recorded allowed graphene layer counting, returning values ranging from 17 to 28 layers on CNTs (17 layers shown in Figure 18(c) and 28 layers in Figure 18(b).

The CNTs formed during the synthesis procedure are mainly straight, representing one advance compared to the literature on the synthesis of CNTs using polymers as carbon feedstock. In previous work, the synthesized CNT samples presented several conformations (cup-stacked and bamboo-like, more notorious), which indicated poor control over the synthesis of CNTs [102]. Here, the metal catalyst used for the synthesis, being bimetallic and having a nickel phase, impacted positively over the synthesis of CNTs with one conformation mainly. The literature already discussed the influence of different metals on CNT structure, confirming that nickel yields straighter CNT structures compared to other transition metals [111].

The outer diameter was found to be 42 ± 3 nm, and the wall thickness was 9 ± 2 nm, which is in agreeance with the literature. The TEM images also revealed the presence of metal encapsulated on CNTs (red arrows show metals encapsulated in Figure 18(d)). Metal encapsulation was already observed in other studies using CNTs prepared in a similar reactor setup.

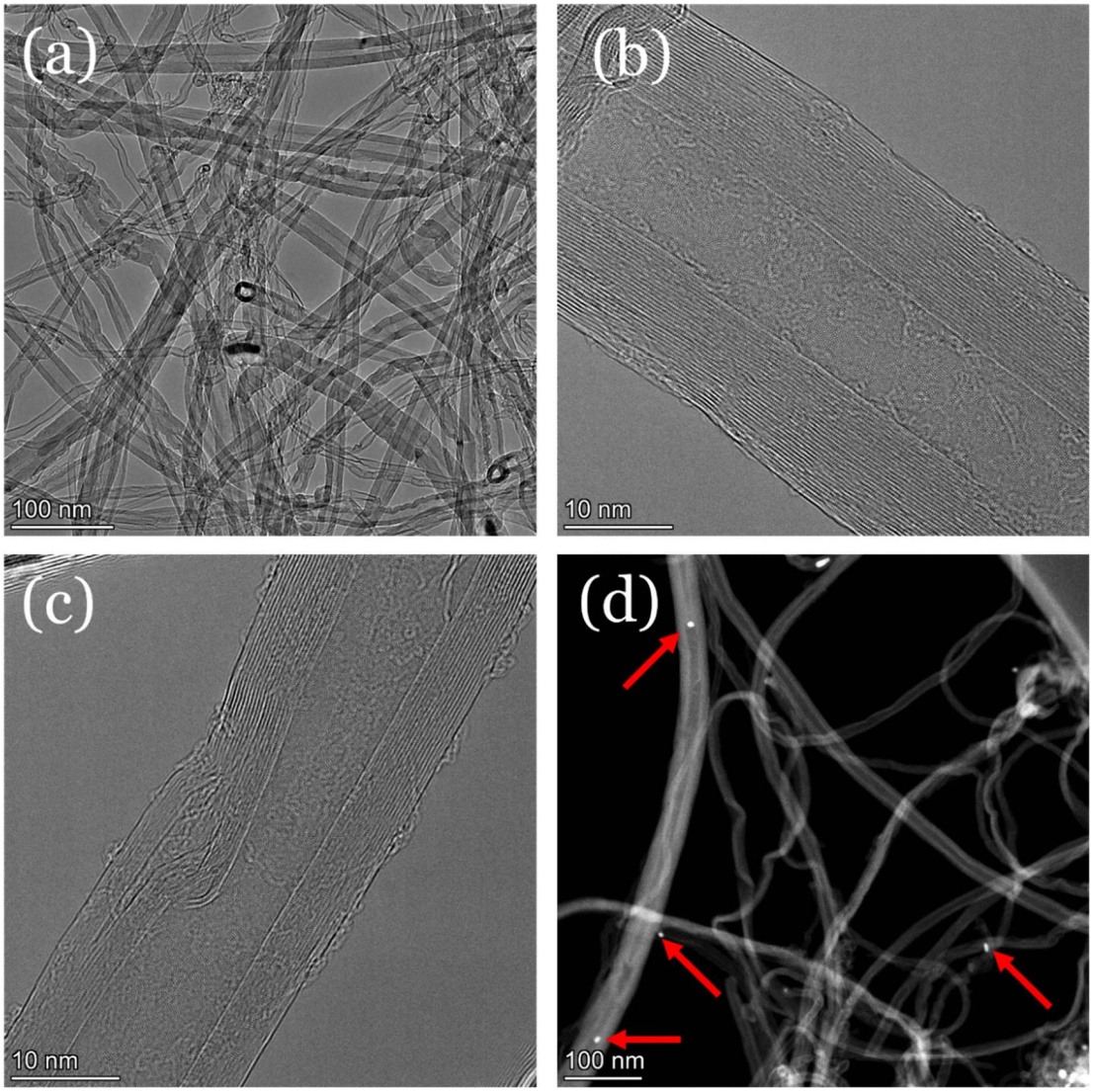

Figure 18. TEM images recorded for (a) CNT sample, (b) Image recorded showing 28 graphene layers, (c) Image recorded showing 17 graphene layers and (d) metals encapsulated on CNTs.

Figure 19 shows the images obtained with SEM analysis. The CNT conformation is present in all samples, confirming that carboxylation treatment did not modify the material structure. At first, the images did not reveal significant differences between the samples, apart from CNT-COOH/Ag2-5%, in which 2 clusters were soon identified. Other works have also reported no differences in samples doped with silver compared to pure CNT samples [104]. The luminous dots present in the results obtained here could either be ascribed to the presence of metals from CVD metal catalyst or silver. The latter is less likely due to the expected silver nanoparticle size, which is too small to be detected with SEM technique.

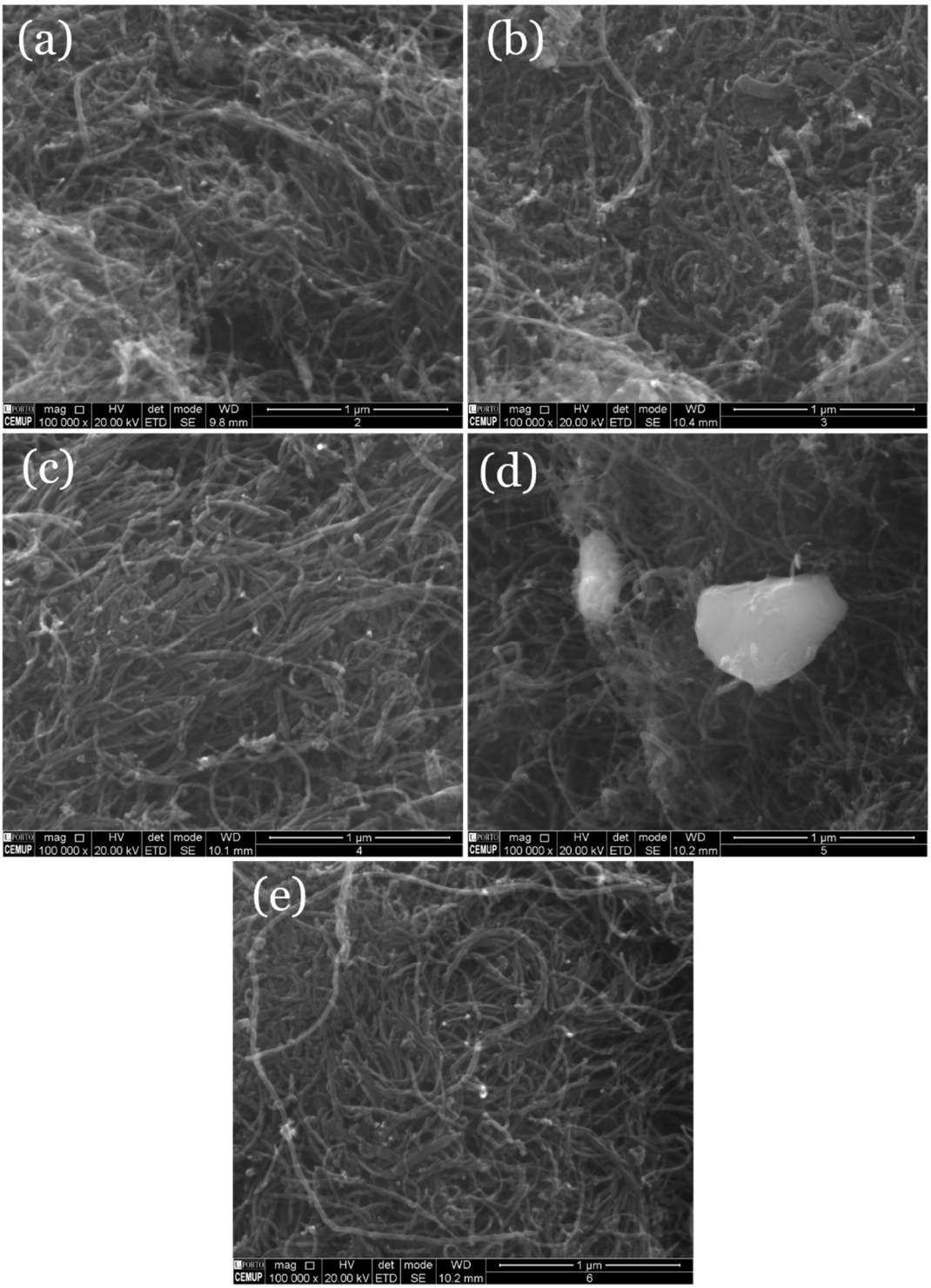

Figure 19. SEM images recorded for samples (a) CNT-COOH, (b) CNT-COOH@Ag1-5%, (c) CNT-COOH@Ag1-10%, (d) CNT-COOH@Ag2-5% and (e) CNT-COOH@Ag2-10%.

Figure 20 shows other SEM images recorded, along with EDS results. Silver was identified in EDS in samples CNT-COOHQAg1-5%, CNT-COOH/Ag1-10% and CNT-COOH/Ag2-5%.

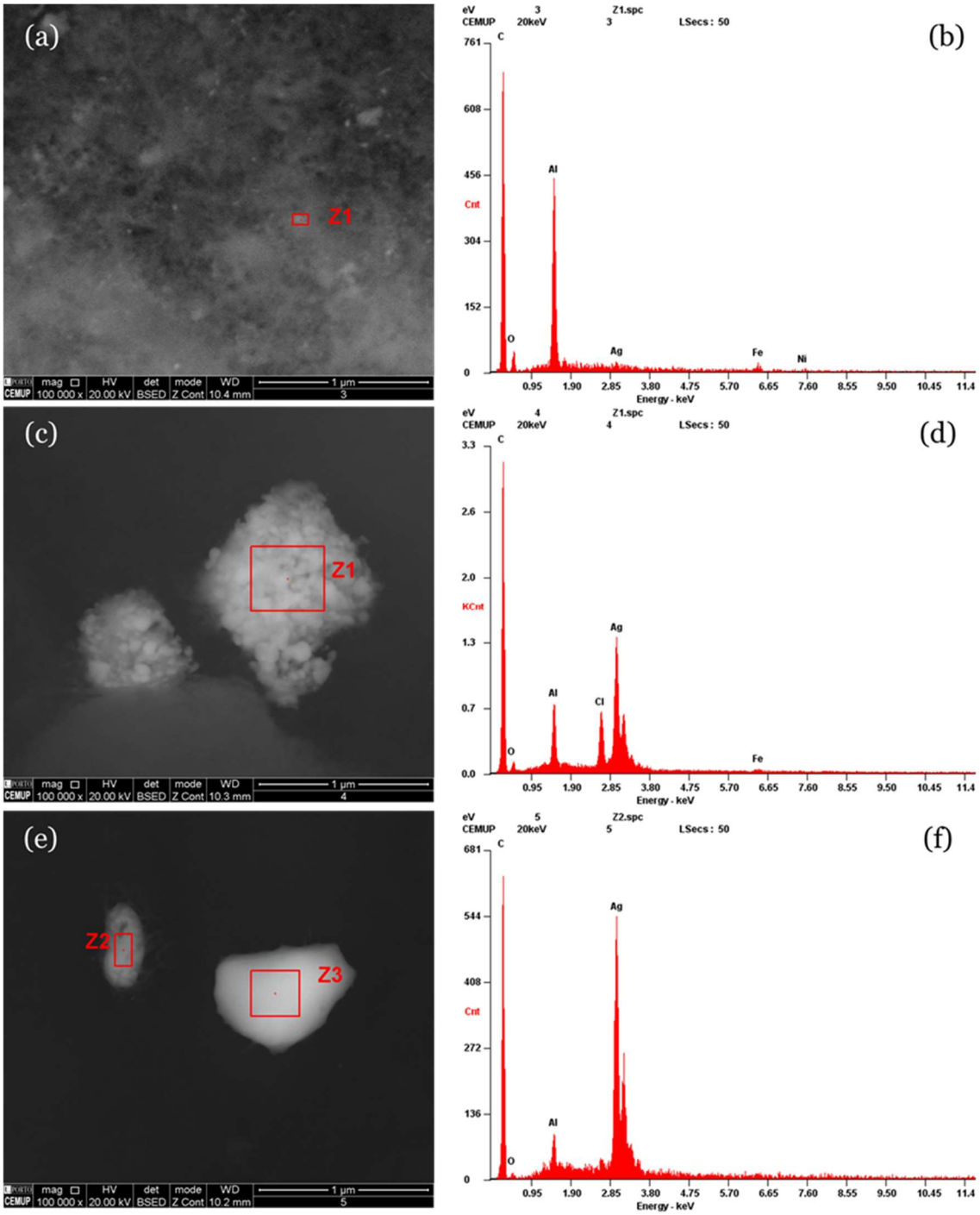

Figure 20. SEM and EDS results for sample (a,b) CNT-COOH/Ag1-5%, (c,d) CNT-COOH/Ag1-10%, and (e,f) CNT-COOH/Ag2-5%, respectively.

In the samples prepared using the co-precipitation method with sodium borohydride (CNT-COOH/Ag1-5% and CNT-COOH/Ag1-10%), the presence of silver nanoparticles was small, and sample CNT-COOH/Ag1-10% showed an anomaly. The cluster shown in Figure 20(c) revealed the presence of AgCl salt in the sample, which can be pointed out

as a limitation of the synthesis procedure using co-precipitation. The reaction can occur due to chloride ions remaining from CVD metal catalyst, which can react with silver and decrease the doping efficiency. In contrast, the cluster observed in sample prepared with wet impregnation method (CNT-COOH/Ag2-5%) comprises silver, and its formation can be associated with the high surface energy of silver that might accumulate on the CNT surface [112]. The absence of silver in the last sample, CNT-COOH/Ag2-10% could be associated with the silver nanoparticle size doped in CNT walls, which could block the signal obtained in SEM analysis.

5.1.2. Thermogravimetric analysis (TGA)

The TGA profile of the CNT samples is shown in Figure 21. The temperatures of main mass loss varied among the different materials analysed: for CNT and CNT-COOH, this loss occurred at 615 ºC; for CNT-COOH/Ag1-5% and CNT-COOH/Ag1-10%, it happened at higher temperatures, around 620 ºC and 617 ºC, respectively, indicating greater thermal stability compared to the others. On the other hand, for CNT-COOH/Ag2-5% and CNT-COOH/Ag2-10%, the mass loss occurred at lower temperatures, approximately 600 ºC and 610 ºC, respectively, demonstrating lower thermal stability compared to the other materials.

These results suggest a remarkable resistance to oxidation, a characteristic that demonstrates the materials are ideal for application in CWPO processes, which operate at temperatures of approximately 80 ºC. The samples (b), (c), and (d) show a slight mass loss in the initial thermogravimetric phase. This occurred due to the presence of oxygenated groups introduced during carboxylation; however, it does not occur with samples (e) and (f) due to the wet impregnation technique and the elimination of these groups during silver doping. Mass losses became noticeable around 450 - 470 ºC, and the CNTs were completely burned at around 680 ºC, regardless of the synthesis stage or doping technique used in the materials.

The different temperatures of main mass loss reflect variations in the thermal properties and thermal stability of the materials. The presence of additional materials, such as silver and functionalizing agents (CNT-COOH), can influence the thermal decomposition characteristics of carbon nanotubes, as silver does not corrode easily like other transition metals and achieves high thermal stability [113].

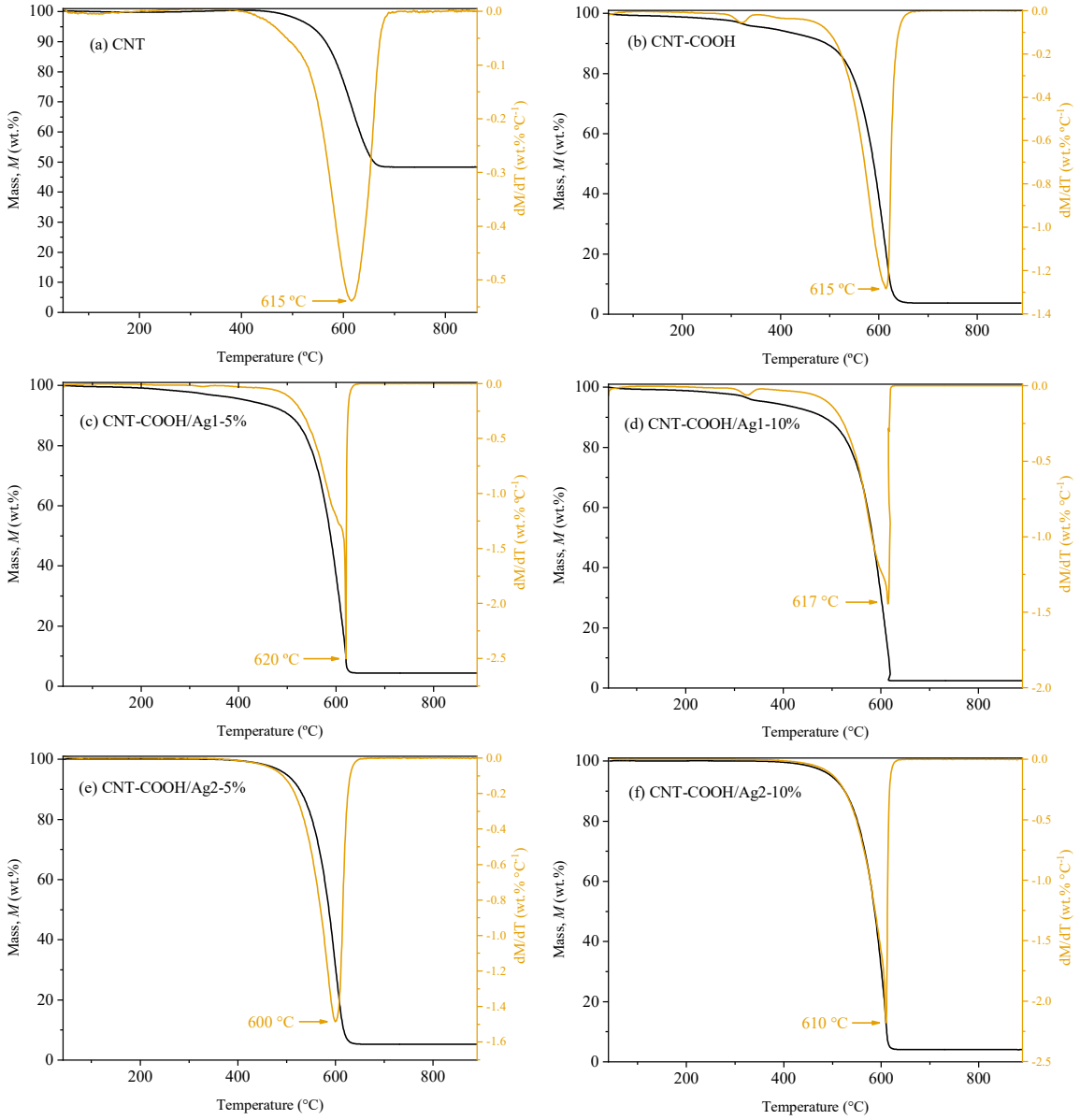

Figure 21. Mass losses (left Y-axis) and their corresponding derivatives (right Y-axis) of different CNTs.

The ash content in the samples varied according to the synthesis stage of the materials. For example, in the pure CNT sample, the ash content was considerably higher, reaching 50%, while in the other samples where the CNTs were carboxylated and/or carboxylated and silver-functionalized, the ash contents were lower, ranging between approximately 2% and 5%. This difference can be attributed to the presence of impurities and inorganic residues in the materials. Pure CNTs are primarily composed of carbon, but there are impurities or inorganic residues that were not completely removed from the catalyst used in the CVD process, such as alumina and other metals. On the other hand, carboxylated CNTs with HNO_3 and/or carboxylated and silver-doped underwent

purification processes, resulting in the removal or reduction of these inorganic impurities.

5.1.3. Elemental analysis (EA)

Table 9 summarizes the nitrogen (N), carbon (C), hydrogen (H), sulfur (S), and oxygen (O) contents for the six prepared CNT samples. Compared with the raw CNTs (61.3% by weight and 0.18% by weight of C and H, respectively), it is possible to observe that the carbon content increases (87.1–92.8% by weight) and the hydrogen composition decreases (0.06–0.21% by weight) for all prepared materials, increasing the C/H ratio (from 340.6 in raw CNTs to 414.8–1546.7 in carboxylated and/or carboxylated and silver-doped CNTs).

Table 9. Elemental composition of the different CNTs.

Sample	C/H	C (wt.%)	H (wt.%)	N (wt.%)	S (wt.%)	O (wt.%)	Remaining* (wt.%)
CNT	340.6	61.3 ± 0.05	0.18 ± 0.02	0.00 ± 0.00	0.00	1.36 ± 0.13	37.2
CNT-COOH	594.0	89.1 ± 0.33	0.15 ± 0.04	0.14 ± 0.01	0.00	5.00 ± 0.18	5.5
CNT-COOH/Ag1-5%	425.2	89.3 ± 0.26	0.21 ± 0.00	0.14 ± 0.00	0.00	4.22 ± 0.14	6.1
CNT-COOH/Ag1-10%	414.8	87.1 ± 4.62	0.21 ± 0.01	0.12 ± 0.02	0.00	5.22 ± 0.18	7.3
CNT-COOH/Ag2-5%	1143.7	91.5 ± 0.87	0.08 ± 0.00	0.09 ± 0.00	0.00	1.83 ± 0.05	6.5
CNT-COOH/Ag2-10%	1546.7	92.8 ± 0.57	0.06 ± 0.01	0.11 ± 0.01	0.00	1.98 ± 0.02	5.0

* Obtained by the difference: 100%-N(%)-C(%)-H(%)-S(%)-O(%).

These results indicate that variations in carbon and hydrogen contents, as well as in the C/H ratio among different CNT samples, are linked to purification and doping processes. The CNT sample did not undergo purification to remove inorganic compounds and impurities, resulting in a carbon content of 61.3% by weight and a C/H ratio of 340.6, indicating that these impurities influenced a lower carbon content relative to hydrogen proportion. Conversely, in the CNT-COOH sample, carboxylation with HNO_3 removed impurities and introduced carboxyl groups on the surface of CNTs, resulting in oxidative functionalization and an increase in carbon content to 89.1% by weight and a C/H ratio of 594.

The C/H ratio varied among doped CNT samples depending on the method employed. Co-precipitation of silver nanoparticles yielded a C/H ratio of 425.2 for

CNT-COOH/Ag1-5% and 414.8 for CNT-COOH/Ag1-10%, suggesting an influence on the CNTs chemical composition, although less pronounced than carboxylation. Conversely, silver nanoparticle formation through wet impregnation resulted in the highest C/H ratios (1143.7 for CNT-COOH/Ag2-5% and 1546.7 for CNT-COOH/Ag2-10%). This is attributed to a more intense interaction between silver nanoparticles and CNTs during the doping process, facilitated by the diffusion of carbon atoms into CNTs and/or the formation of chemical bonds between silver and the nanotube structure, resulting in greater carbon atom incorporation into the nanotubes.

The CNT sample did not present nitrogen atoms. In contrast, the functionalized and doped samples showed varying contributions of this element, with the CNT-COOH and CNT-COOH/Ag1-5% samples exhibiting the highest presence of nitrogen. Nitrogen on the carbon nanotube walls has significant implications for the adsorption capacity of CNTs. The incorporation of nitrogen atoms can cause deformations and curvatures in the sp^2 layers, leading to a more complex structure [114].

Oxygen was the second most abundant element observed in the samples. The CNT sample showed the lowest contribution of oxygen, as it is not purified using oxidants such as HNO_3, suggesting that these samples do not contain a high degree of oxygen functional groups. Therefore, it is more likely that the observed oxygen is associated with salts and impurities of metallic oxides present in the CVD catalyst [115]. In the case of wet impregnation doped CNTs, namely CNT-COOH/Ag2-5% and CNT-COOH/Ag2-10%, low oxygen contributions were also observed in the final samples, suggesting that, in general, there was a successful reaction of COOH groups with silver, demonstrating efficient doping [116].

Ash content in the pure CNT sample is the highest for all materials (37.2%) because of the inorganic matter, as reported on the TGA analysis. The other samples follow the same perspective, and the ash content typically indicates the quantity of oxidized metal catalyst left in CNT samples after synthesis. Metal content in CNTs is regarded as an impurity [117].

5.1.4. X-ray diffraction (XRD)

The metal CVD catalyst was analyzed by XRD to identify the crystal composition,

and the result is shown in Figure 22.

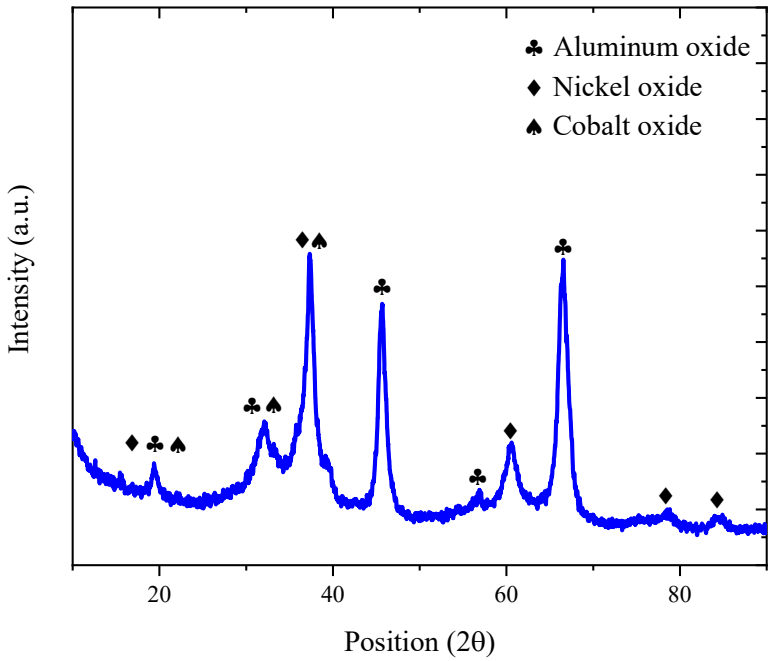

Figure 22. X-ray diffractogram of NiFe/CoFe@Al_2O_3.

The analysis of the NiFe/CoFe@Al_2O_3 sample with the software X'Pert HighScore Plus allowed phase identification of nickel and cobalt oxides mixed with alumina based on reference cards 96-152-2026 (nickel oxide), 96-451-2476 (cobalt oxide), 96-154-1583 (aluminum oxide) from Crystallography Open Database. The semi-quantitative analysis revealed a composition of 88% aluminum oxide phase, 9% nickel oxide phase, and 3% cobalt ferrite phase. The result is consistent with the synthesis procedure, in which the stoichiometric amount of reagents was calculated to achieve a 15% metal phase supported on 85% alumina, with a predominance of nickel on the metal phase. The choice of nickel and cobalt was related to the effect of the metal catalyst on CNT synthesis and activity during CWPO reactions of cobalt. For instance, nickel is recognized as a good precursor for ordered CNTs compared to cobalt [111]. On the other hand, cobalt possesses higher activity for hydroxyl radical formation in Fenton reactions [118]. Despite the CNT purification required to apply the materials as catalysts, some studies reported the presence of stable metals encapsulated in CNTs. In this work, it was also noted the presence of metals encapsulated in CNTs, as discussed in another section. In this regard, the remaining cobalt on CNT structure could enhance the catalytic activity towards the process studied.

5.2. MICROBIOLOGICAL CHARACTERIZATION OF LANDFILL LEACHATE

In the microbiological characterization, a concentration of yeast and fungi of 3,200 ± 4 CFU/mL of leachate was identified. As for the bacterial characterization, a concentration of 41,000 ± 4.5 CFU/mL of leachate was recorded. The results of the cultivation of bacteria, yeast, and fungi are presented in Figure 23.

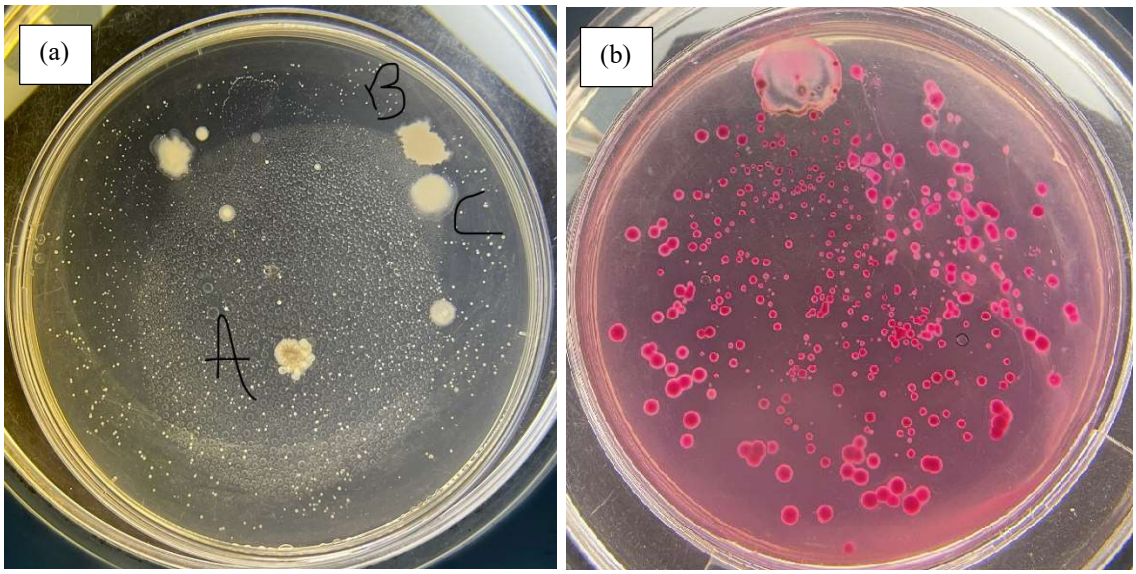

Figure 23. Plate (a) Growth of bacteria, (b) Growth of yeasts and fungi.

These findings suggest favourable conditions for microbiological growth in the leachate environment. However, it is important to note that the presence and concentration of microorganisms may vary over time and in different leachate samples, depending on factors such as chemical composition, pH, and temperature [66].

5.3. EXPERIMENTAL REACTIONS

5.3.1. Adsorption

The purpose of the adsorption test was to assess whether the pollutant removal is occurring through the oxidation process or if the pollutant is merely being adsorbed onto the materials. The result obtained for BPA removal after 8 hours in the adsorption tests compared with the oxidation process after 8 hours is shown in Figure 24.

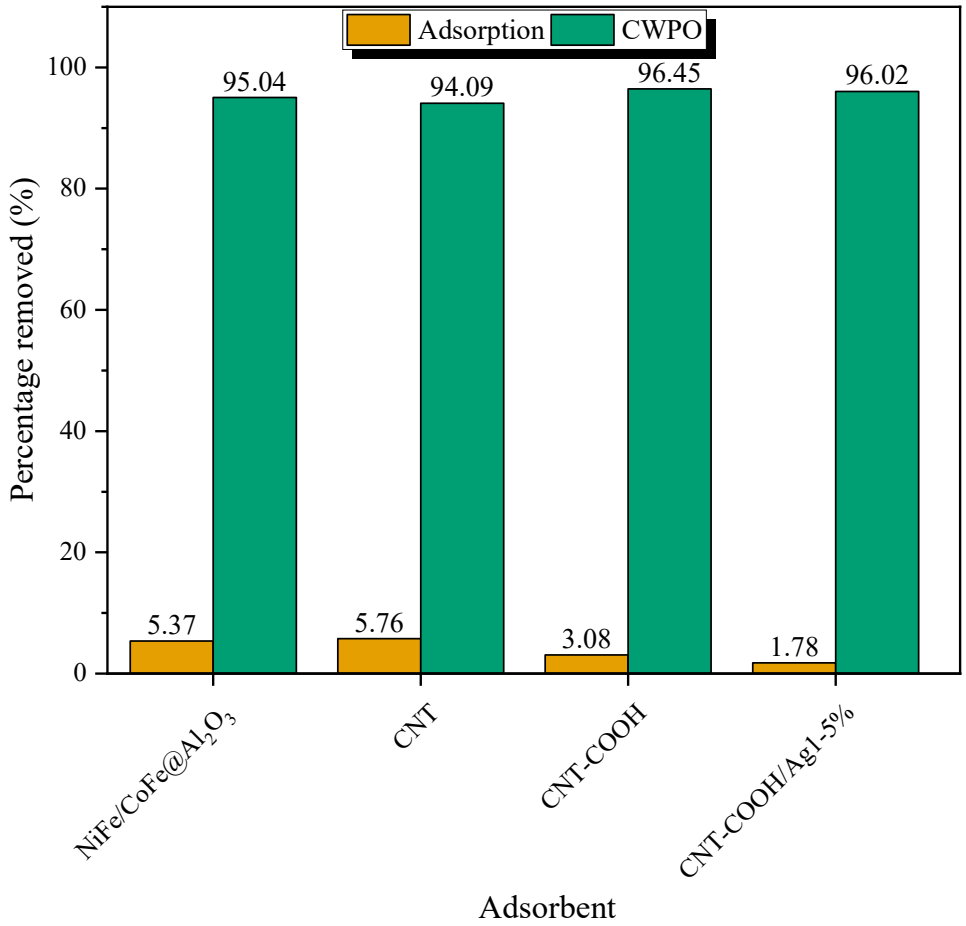

Figure 24. Comparison between removal of BPA with adsorption after 8 h and CWPO after 8 h.

The results of BPA adsorption using the synthesized materials indicated that, after 8 hours, the amount of adsorbed pollutant varied from 1.78 to 5.76%. However, the conversion of BPA in CWPO after 8 hours was observed to be higher than its removal by adsorption. Therefore, it is possible to discard the possibility that BPA is primarily being adsorbed and not oxidized. Materials not shown on the graph did not undergo adsorption.

5.3.2. H_2O_2 catalytic decomposition

The tests carried out to verify the catalytic activity of the different synthesized materials showed that all of them have significant activity for the decomposition of H_2O_2, and the results can be observed in Figure 25.

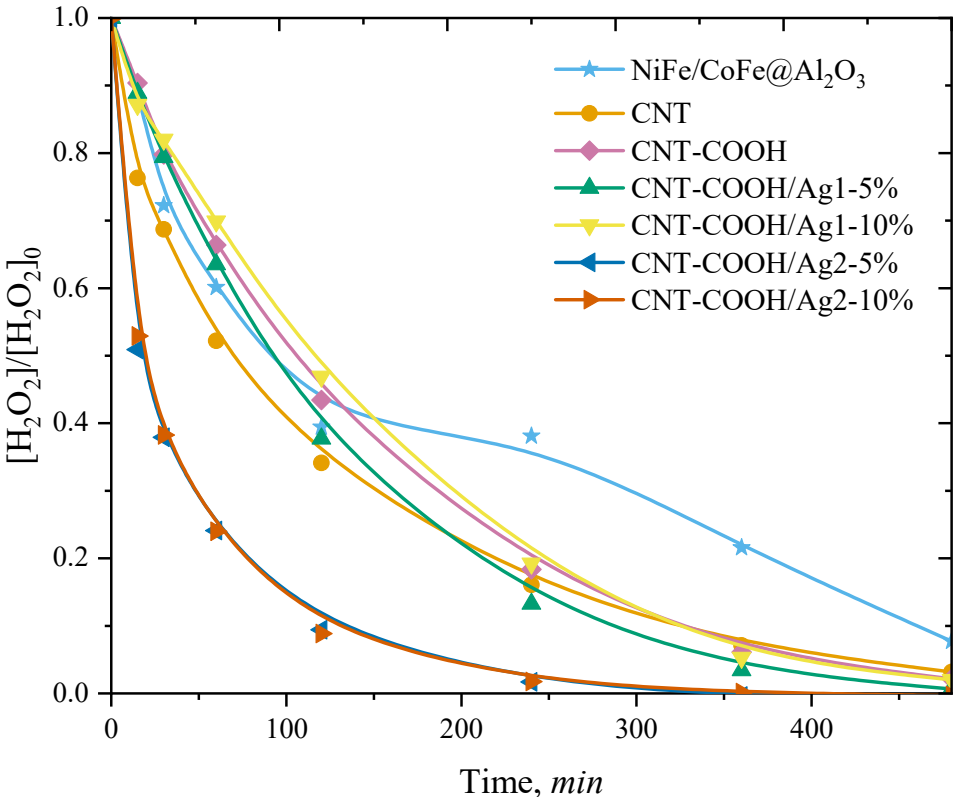

Figure 25. Catalytic efficiency of synthesized materials for H_2O_2 decomposition.

The test results indicated that CNT-COOH/Ag2-5% and CNT-COOH/Ag2-10% demonstrated the highest catalytic activity. The catalytic activity showed silver-doped CNTs by co-precipitation (CNT-COOH/Ag1-5% and CNT-COOH/Ag1-10%), and CNTs functionalized with nitric acid (CNT-COOH) can be explained by the fact that the functionalization of CNTs with nitric acid introduces a large number of defects in their structure. The oxygen functional groups and internal or external defects of carbon materials play a crucial part during the catalytic process. Carbon materials with such characteristics can serve as electron donors or chelators to enhance Fenton/Fenton-like oxidation [119]. However, when doping with silver occurs, these introduced COOH groups are replaced by Ag, which has better catalytic properties as a metal. Therefore, it can be concluded that, in the case of doping with wet impregnation, there was efficient doping, confirmed by the results of Elemental Analysis (EA), where the presence of oxygen in the sample is approximately 2%, while in the sample only functionalized with HNO_3 it is approximately 5%. However, co-precipitation doping was also efficient, albeit to a lesser extent than wet impregnation doping.

5.3.3. Catalytic wet peroxide oxidation (CWPO)

Figure 26 illustrates the concentration profiles of BPA and H_2O_2 obtained in the CWPO of BPA using all the prepared materials.

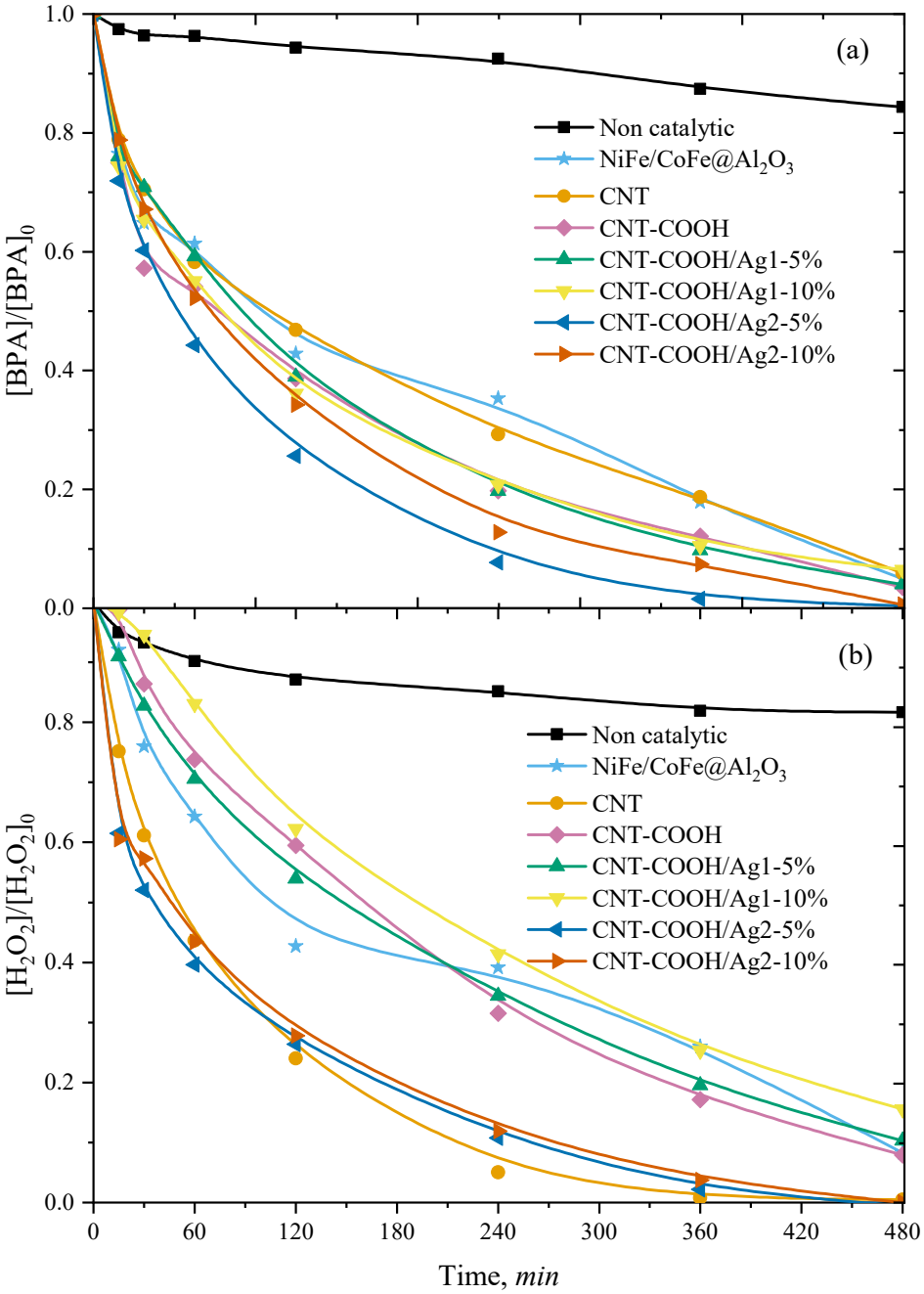

Figure 26. The concentration of (a) BPA and (b) H_2O_2 upon reaction time during CWPO experiences.

Compared to the non-catalytic run (XBPA = 16% and XH_2O_2 = 18%), all materials demonstrated catalytic activity towards the decomposition of H_2O_2 and reduction of BPA.

Thermal decomposition is responsible for the H_2O_2 degradation observed in the non-catalytic run performed at 80 ºC. This amount of decomposed H_2O_2 was sufficient to promote the degradation of 18% of the pollutant's initial concentration in the system.

Figure 26(a) illustrates the reduction of BPA. With the NiFe/CoFe@Al_2O_3 metallic catalyst, a 50% reduction in BPA was observed after two hours of reaction, increasing to 80% after 6 hours, and reaching a reduction of approximately 95% at the end of 8 hours of reaction. Despite presenting sifnificant activity towards the BPA removal by CWPO, the CVD catalyst does not present metal stability to ensure a sustainable utilization. The CNT catalyst showed a remarkable performance in reducing BPA by approximately 95% at the end of the reaction period. The BPA was rapidly reduced by over 40% in the presence of the CNT-COOH catalyst after just 30 minutes of reaction, thus facilitating a reduction of 96% by the end of 8 hours. The silver-doped CNTs through co-precipitation, namely CNT-COOH/Ag1-5% and CNT-COOH/Ag1-10%, demonstrated good catalytic performance. However, there was not a complete reduction of BPA after 8 hours, reaching a reduction of 96% and 93%, respectively, by the end of this period. On the other hand, silver-doped CNTs through wet impregnation, specifically CNT-COOH/Ag2-5% and CNT-COOH/Ag2-10%, managed to completely reduce the pollutant, achieving 100% reduction of BPA after 8 hours of reaction, with emphasis on the CNT-COOH/Ag2-5% catalyst, which showed the best performance among the materials, achieving a 90% reduction of BPA in just 4 hours of CWPO.

Both the incorporation of metals and carbon in the catalysts justify their efficiency in the CWPO process for BPA [120]. It is noteworthy that the simultaneous presence of carbon layers and metallic phases in the materials results in a synergistic effect. Regardless of the preparation approach, hybrid materials have demonstrated superior activity compared to pure cores (NiFe/CoFe@Al_2O_3). Both the metallic phase and the carbon layer exhibit electron-donating properties. Thus, a hybrid material containing both phases enhances electron transfer compared to a pure core. Electron transfer is a crucial condition for catalyzing the degradation of H_2O_2, resulting in the formation of hydroxyl radicals and, ultimately, the removal of pollutants from the system. Both metallic phases, such as iron and cobalt, and carbon layers facilitate this electron transfer; additionally, the more hydrophobic properties and larger surface area due to the carbon layer increase the adsorptive interactions between the pollutant and the catalysts surface [121].

Figure 26(b) illustrates the decomposition of H_2O_2 during the CWPO of BPA, showing that the CNT-COOH/Ag1-10% catalyst leads to slower and lower quantity degradation of H_2O_2, reaching only 82% decomposition by the end of the reaction. The CNT-COOH and CNT-COOH/Ag1-5% catalysts exhibit similar behaviors, decomposing approximately 60% of H_2O_2 in 4 hours and achieving a total efficiency of 96% at the end of the CWPO reaction. The CNT-COOH/Ag2-5% and CNT-COOH/Ag2-10% catalysts were able to completely decompose H_2O_2 by the end of the CWPO process, with CNT-COOH/Ag2-5% showing a slightly faster and higher proportion rate than CNT-COOH/Ag2-10%. Regarding the CNT catalyst, despite demonstrating a 100% H_2O_2 decomposition rate at the end of CWPO, no corresponding efficiency was observed in BPA degradation. As for the NiFe/CoFe@Al_2O_3 metallic catalyst, an initial rapid decomposition is observed, reaching 50% within 2 hours of reaction. However, the decomposition slows down until 4 hours of reaction, followed by an increase in the decomposition rate until 8 hours, resulting in a total efficiency of 96% in H_2O_2 decomposition.

In summary, the H_2O_2 decomposition rate and BPA reduction rate during CWPO is correlated for the NiFe/CoFe@Al_2O_3, CNT-COOH, CNT-COOH/Ag1-5%, CNT-COOH/Ag2-5%, and CNT-COOH/Ag1-10% catalysts due to hydroxyl radical ($HO^{\bullet}$) formation. On the other hand, the CNT and CNT-COOH/Ag1-10% catalysts did not reduce BPA in the same proportion as they decomposed H_2O_2, indicating a lack of correspondence and, consequently, inefficient performance [108,122]. Thus, the activity order of the catalyst for both activities is: CNT-COOH/Ag2-5% > CNT-COOH/Ag2-10% > CNT-COOH/Ag1-5% > CNT-COOH > NiFe/CoFe@Al_2O_3 > CNT-COOH/Ag1-10% > CNT.

The additional experiments conducted on the samples recovered from the adsorption tests to evaluate the desorption of physically adsorbed molecules, aiming to determine whether pollutant removal is primarily driven by adsorption or oxidation, have their results presented in Figure 27. According to the presented results, approximately 94% of BPA was recovered from NiFe/CoFe@Al_2O_3 and CNT materials, while the CNT-COOH/Ag1-5% sample exhibited around 95% recovery, and the CNT-COOH/Ag1-10% sample showed approximately 97% recovery, with no desorption observed for the other materials.

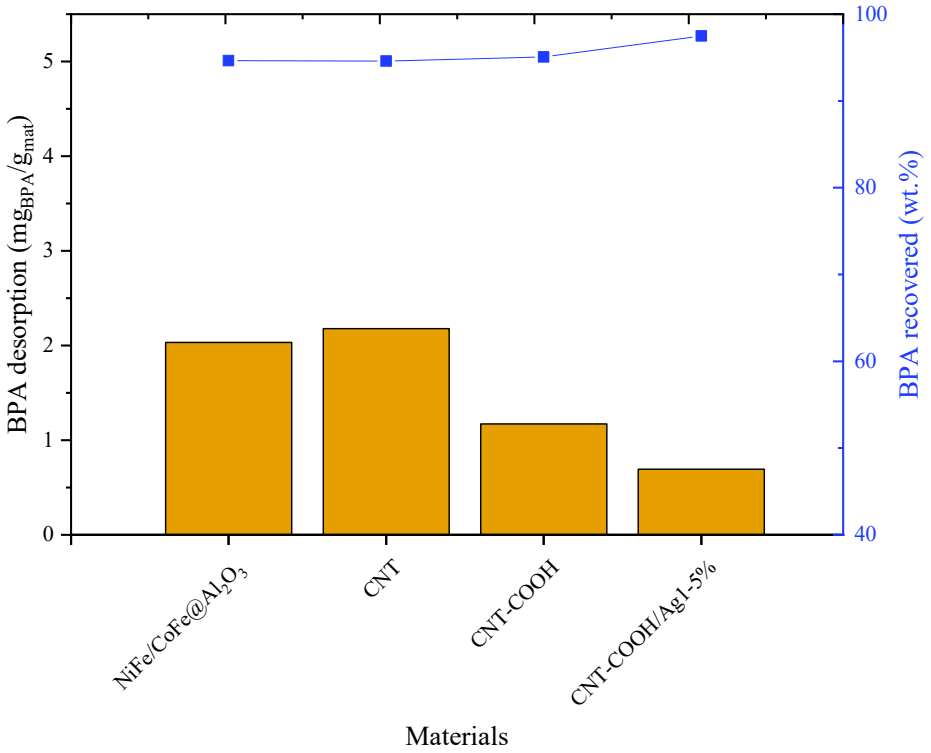

Figure 27. BPA desorption results obtained using materials recovered from pure adsorption experiments.

The higher efficiency in BPA recovery in these materials may be attributed to mass transfer mechanisms. Overall, the method proved effective in BPA desorption from carbonaceous materials, suggesting that physisorption is the main adsorption mechanism for BPA removal by adsorption using these samples. The desorption experiments using catalysts recovered from CWPO reactions indicated no BPA desorption in all materials. Therefore, while these materials have adsorption capacity, the results showed the complete degradation of the pollutant during the reaction [102,123].

5.3.4. Coupled disinfection and CWPO

The kinetics of BPA reduction and catalytic decomposition of H_2O_2 during coupled disinfection and CWPO is presented in Figure 28. These results demonstrate that the CWPO process occurs even under conditions optimized for microorganisms during the experiment (pH 5 to 45 °C), for the material showing the best efficiency demonstrated in CWPO runs (CNT-COOH/Ag2-5%). In this case, an improvement in activity is observed after 1440 minutes of reaction, resulting in a total reduction of 90% of BPA and decomposition of 70% of H_2O_2 by the catalyst.

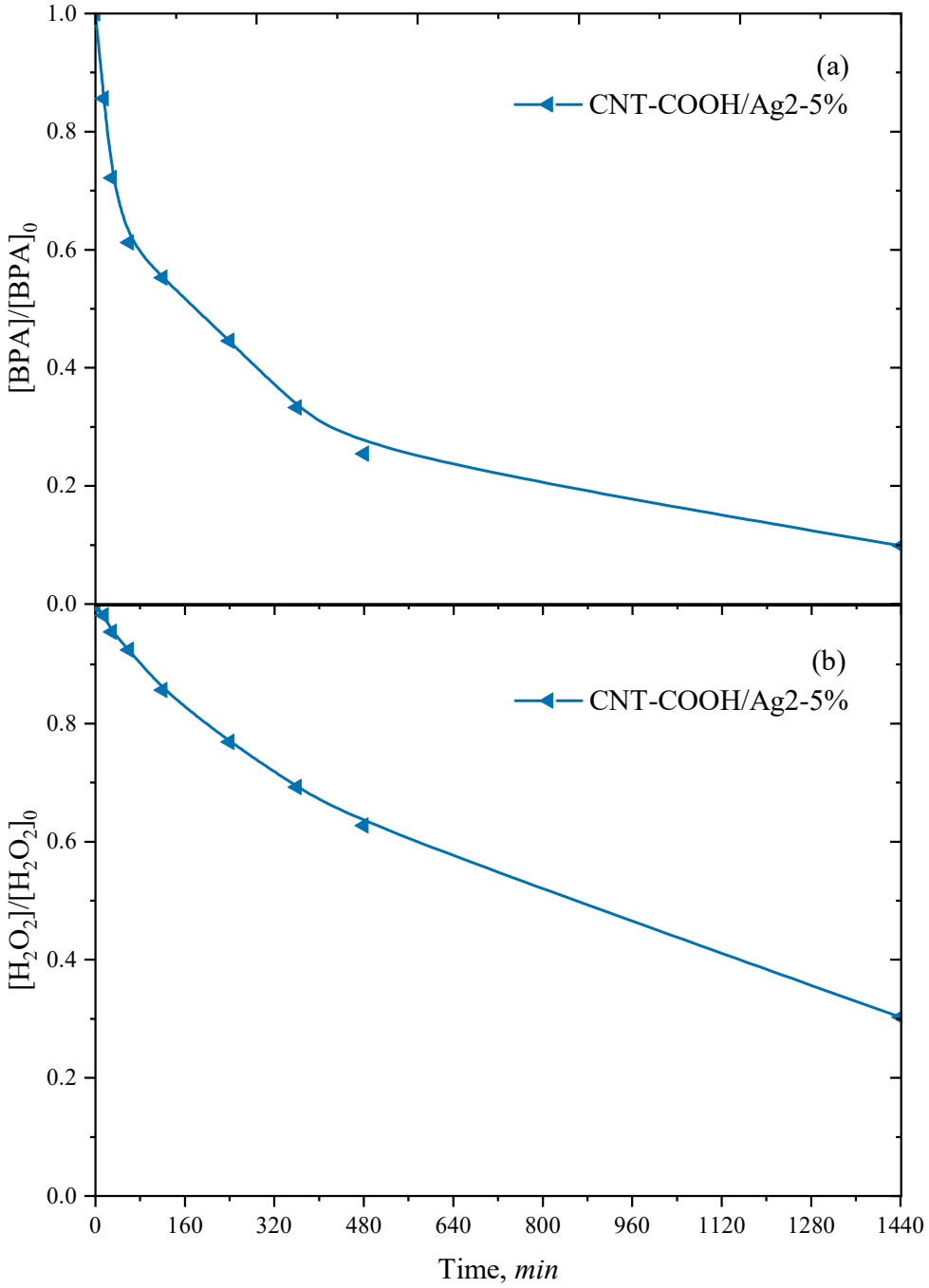

Figure 28. The concentration of (a) BPA and (b) H_2O_2 upon reaction time during coupled disinfection and CWPO experiences.

The results of the biological treatment conducted for *Escherichia coli* disinfection are presented in Table 10. In the case of the sample with BPA, a 92% reduction in the microbial load indicates that the agent is bacteriostatic, meaning it inhibits bacterial growth (keeping them in the stationary phase of growth). Therefore, it cannot be stated that BPA has the ability to eliminate microorganisms. However, in the case of the H_2O_2

and CWPO samples, the elimination of 99.99% of the microorganisms indicates that the agents have bactericidal properties, meaning they are capable of killing bacteria [124].

Table 10. Results of disinfection experiment.

Sample	0 minutes (CFU/mL)	1440 minutes (CFU/mL)	Reduction (%)
BPA	$8.5x10^6 \pm 0.5$	$6.7x10^5 \pm 20.5$	92
H_2O_2	$1.4x10^6 \pm 1.5$	0	99.99
CWPO	$1.5x10^6 \pm 0.5$	0	99.99

The standard deviations observed in the samples, particularly in the triplicate sample, which showed a standard deviation of σ=20.5 after 1440 minutes, may be attributed to several factors. These variations may result from discrepancies in the agitation methods employed, heterogeneities in the distribution of bacteria in the sample, or possibly the presence of microbiological contaminants.

CONCLUSIONS AND FUTURE WORK

6 CONCLUSIONS AND FUTURE WORK

6.1. CONCLUSIONS

This research aimed to assess the antimicrobial and catalytic activity of silver-doped carbon nanotubes in the removal of organic pollutants through catalytic wet oxidation with hydrogen peroxide and disinfection of wastewater. Texture and morphology analysis revealed that doping carbon nanotubes with silver and functionalization with HNO_3 significantly enhance their adsorption capacity, as evidenced by N_2 adsorption isotherms. The 10% silver-doped materials exhibit the highest adsorptive capacities, and all materials display mesoporous characteristics and a high specific surface area. TEM analysis confirmed the formation of MWCNTs during synthesis, primarily with a straight conformation, indicating improved process control. SEM images showed that doping efficiency in the co-precipitation method was affected by the formation of AgCl salt, and the wet impregnation method resulted in higher doping efficiency. The increased efficiency observed in wet impregnation doped samples compared to co-precipitation ones can be explained by the presence of AgCl impurities.

The TGA analysis revealed that all analyzed materials exhibit high thermal resistance, with combustion occurring above 600 ºC, a characteristic that makes them suitable for application in AOPs. Through EA, the efficiency of doping techniques in replacing these COOH groups with silver ions was evidenced, revealing to be higher for the wet impregnation method than for the co-precipitation method. The analysis of leachates reveals high levels of COD and TOC, typical of young leachates. The microbiological characterization indicates favorable environmental conditions in the leachate for the growth of yeasts, fungi, and bacteria.

The CWPO runs revealed in the adsorption analysis that BPA was primarily oxidized rather than adsorbed, a fact confirmed by the desorption analysis, where no materials were recovered from CWPO, indicating complete oxidation of the pollutant. The catalytic decomposition test of H_2O_2 showed that nitric acid-functionalized and silver-doped CNTs exhibited higher catalytic activity due to the presence of oxygen functional groups and internal or external structural defects, contributing to enhanced oxidation. Moreover, silver doping resulted in superior catalytic properties. Both wet impregnation and co-precipitation methods were effective, with wet impregnation doping

proving slightly more efficient. The CWPO test revealed that wet impregnation method catalysts achieved complete BPA reduction after 8 hours, with 5% doping showing better performance. However, pure CNT and carboxylated CNT doped with 10% by co-precipitation method showed a lack of correspondence between H_2O_2 decomposition and BPA reduction, indicating inefficient performance in the process.

As the wet impregnation method with 5% silver-doped CNT exhibited the best structural properties and performance in CWPO experiments, it was then applied in the coupled disinfection and CWPO experiment. This demonstrated that the CWPO process was effective in reducing BPA and decomposing H_2O_2, even under optimized temperature and pH conditions for microorganisms. After 1440 minutes of reaction, there was a 90% reduction in BPA and a 70% decomposition of H_2O_2. While BPA exhibited bacteriostatic properties by inhibiting bacterial growth, H_2O_2 and CWPO samples showed bactericidal properties by eliminating 99.99% of microorganisms. This indicates that the materials prepared and applied in the CWPO process possess both antimicrobial and catalytic activity.

6.2. FUTURE WORK

Based on everything explored in this study, a possible direction for future research would be to investigate the stability and long-term performance of Ag-doped CNTs in real wastewater treatment scenarios. Additionally, studying the stability of silver nanoparticles on carbon nanotubes would contribute to a comprehensive understanding of the sustainability and overall safety of the applications. Another relevant issue is the enhancement of the disinfection experiment, as experimental limitations necessitate the use of BPA doses much higher than those found in real systems. This, in turn, increases the required amount of H_2O_2. Therefore, it would be pertinent to conduct additional investigations to assess microbial resistance to lower doses of H_2O_2. Additionally, the current test was conducted only with the *Escherichia coli* strain. However, it would be interesting to expand the study to include a variety of microorganisms present in wastewater. Those showing resistance to H_2O_2 could then be subjected to the CWPO process, allowing for a more specific evaluation of the antimicrobial activity of Ag-doped CNTs.

REFERENCES

7 REFERENCES

[1] H.H. Shah, M. Amin, F. Pepe, Maximizing resource efficiency: opportunities for energy recovery from municipal solid waste in Europe, J Mater Cycles Waste Manag 25 (2023) 2766–2782. https://doi.org/10.1007/s10163-023-01733-5.

[2] A. Maalouf, A. Mavropoulos, Re-assessing global municipal solid waste generation, Waste Management and Research 41 (2023) 936–947. https://doi.org/10.1177/0734242X221074116.

[3] Agência Portuguesa do Ambiente, Relatório Anual - Resíduos Urbanos 2022, (2023). https://apambiente.pt/sites/default/files/_Residuos/Producao_Gest%C3%A3o_Residuos/Dados%20RU/RARU_2022_V1.1.pdf (accessed December 10, 2023).

[4] European Commission, Waste Framework Directive, (2008). https://eur-lex.europa.eu/legal-content/EN/TXT/?uri=CELEX%3A02008L0098-20180705 (accessed December 29, 2023).

[5] European Commission, Commission Decision (EU) 2019/1004, (2019). https://eur-lex.europa.eu/eli/dec_impl/2019/1004/oj#:~:text=Commission%20Implementing%20Decision%20(EU)%202019,2384%20(notified%20under%20document%20C((accessed November 10, 2023).

[6] Presidência do Conselho de Ministros de Portugal, Decreto-Lei n.º 102-D/2020, de 10 de dezembro, (2020). https://diariodarepublica.pt/dr/detalhe/decreto-lei/102-d-2020-150908012 (accessed October 30, 2023).

[7] S. Huang, H. Wang, W. Ahmad, A. Ahmad, N.I. Vatin, A.M. Mohamed, A.F. Deifalla, I. Mehmood, Plastic Waste Management Strategies and Their Environmental Aspects: A Scientometric Analysis and Comprehensive Review, Int J Environ Res Public Health 19 (2022) 1–31. https://doi.org/10.3390/ijerph19084556.

[8] M.S.S.R. Tejaswini, P. Pathak, S. Ramkrishna, P.S. Ganesh, A comprehensive review on integrative approach for sustainable management of plastic waste and its associated externalities, Science of the Total Environment 825 (2022) 1–14. https://doi.org/10.1016/j.scitotenv.2022.153973.

[9] Parlamento Europeu, Resíduos de plástico e reciclagem na UE: factos e números, (2023). https://www.europarl.europa.eu/topics/pt/article/20181212STO21610/residuos-de-plastico-e-reciclagem-na-ue-factos-e-numeros (accessed January 10, 2024).

[10] A. Chamas, H. Moon, J. Zheng, Y. Qiu, T. Tabassum, J.H. Jang, M. Abu-Omar, S.L. Scott, S. Suh, Degradation Rates of Plastics in the Environment, ACS Sustain Chem Eng 8 (2020) 3494–3511. https://doi.org/10.1021/acssuschemeng.9b06635.

[11] I.C.B.L.S.A. Santos, Estratégia de desenvolvimento de uma solução circular de embalagem alimentar: um estudo do mercado e do consumidor, 2020. https://www.google.com/url?sa=t&rct=j&q=&esrc=s&source=web&cd=&ved=2ahUKEwjq3obasLKDAxUcVaQEHePwCxcQFnoECCgQAQ&url=https%3A%2F%2Fsigarra.up.pt%2Ffep%2Fpt%2Fpub_geral.show_file%3Fpi_doc_id%3D260249&usg=AOvVaw2VDLykF9OlSLeiUxcO5zR1&opi=89978449 (accessed December 28, 2023).

[12] Plastics Europe, Plastics-the Facts 2022, (2022).

[13] L.O. Mark, M.C. Cendejas, I. Hermans, The Use of Heterogeneous Catalysis in the Chemical Valorization of Plastic Waste, ChemSusChem 13 (2020) 5808–5836. https://doi.org/10.1002/cssc.202001905.

[14] I. Tsuchimoto, Y. Kajikawa, Recycling of Plastic Waste: A Systematic Review Using Bibliometric Analysis, Sustainability (Switzerland) 14 (2022) 1–2. https://doi.org/10.3390/su142416340.

[15] Y. Wu, B. Wang, G. Chen, Sustainable landfill leachate treatment, Waste Management and Research 38 (2020) 1093–1100. https://doi.org/10.1177/0734242X20931937.

[16] H.I. Abdel-Shafy, A.M. Ibrahim, A.M. Al-Sulaiman, R.A. Okasha, Landfill leachate: Sources, nature, organic composition, and treatment: An environmental overview, Ain Shams Engineering Journal 15 (2024) 1–11. https://doi.org/10.1016/j.asej.2023.102293.

[17] S.M. Medina, A. Rey, C. Durán-Valle, A. Bahamonde, M. Faraldos, Performance of iron-functionalized activated carbon catalysts (Fe/Ac-F) on cwpo wastewater treatment, Catalysts 11 (2021) 1–17. https://doi.org/10.3390/catal11030337.

[18] A. Veksha, W. Chen, L. Liang, G. Lisak, Converting polyolefin plastics into few-walled carbon nanotubes via a tandem catalytic process: Importance of gas composition and system configuration, J Hazard Mater 435 (2022) 1–2. https://doi.org/10.1016/j.jhazmat.2022.128949.

[19] A.K. Shukla, J. Alam, M.A. Ansari, M. Alhoshan, M. Alam, A. Kaushik, Selective ion removal and antibacterial activity of silver-doped multi-walled carbon nanotube / polyphenylsulfone nanocomposite membranes, Mater Chem Phys 233 (2019) 102–112. https://doi.org/10.1016/j.matchemphys.2019.05.054.

[20] S. Kaza, L. Yao, P. Bhada-Tata, F. Van Woerden, What a Waste 2.0 - A Global Snapshot of Solid Waste Management to 2050, Washington, DC, 2018. https://doi.org/10.1596/978-1-4648-1329-0.

[21] D.P. Lozano Lazo, C. Bojanic Helbingen, A. Gasparatos, Household waste generation, composition and determining factors in rapidly urbanizing developing cities: case study of Santa Cruz de la Sierra, Bolivia, J Mater Cycles Waste Manag 25 (2023) 565–581. https://doi.org/10.1007/s10163-022-01535-1.

[22] A. Minelgaitė, G. Liobikienė, Waste problem in European Union and its influence on waste management behaviours, Science of the Total Environment 667 (2019) 86–93. https://doi.org/10.1016/j.scitotenv.2019.02.313.

[23] K.D. Sharma, S. Jain, Municipal solid waste generation, composition, and management: the global scenario, Social Responsibility Journal 16 (2020) 917–948. https://doi.org/10.1108/SRJ-06-2019-0210.

[24] V.A. Ferraz de Campos, V.B. Silva, J.S. Cardoso, P.S. Brito, C.E. Tuna, J.L. Silveira, A review of waste management in Brazil and Portugal: Waste-to-energy as pathway for sustainable development, Renew Energy 178 (2021) 802–820. https://doi.org/10.1016/j.renene.2021.06.107.

[25] M.P. López-Portillo, G. Martínez-Jiménez, E. Ropero-Moriones, M.C. Saavedra-Serrano, Waste treatments in the European Union: A comparative analysis across its member states, Heliyon 7 (2021) 1–11. https://doi.org/10.1016/j.heliyon.2021.e08645.

[26] Eurostat, Recycling rate of municipal waste, (2022). https://ec.europa.eu/eurostat/databrowser/view/sdg_11_60/default/table?lang=en (accessed February 10, 2024).

[27] Eurostat, Municipal waste statistics, (2021). https://ec.europa.eu/eurostat/statistics-explained/index.php?title=Municipal_waste_statistics (accessed December 29, 2023).

[28] S. Wu, L. Montalvo, Repurposing waste plastics into cleaner asphalt pavement materials: A critical literature review, J Clean Prod 280 (2021) 2–4. https://doi.org/10.1016/j.jclepro.2020.124355.

[29] T. Thiounn, R.C. Smith, Advances and approaches for chemical recycling of plastic waste, Journal of Polymer Science 58 (2020) 1347–1364. https://doi.org/10.1002/pol.20190261.

[30] H. Li, H.A. Aguirre-Villegas, R.D. Allen, X. Bai, C.H. Benson, G.T. Beckham, S.L. Bradshaw, J.L. Brown, R.C. Brown, V.S. Cecon, J.B. Curley, G.W. Curtzwiler, S. Dong, S. Gaddameedi, J.E. García, I. Hermans, M.S. Kim, J. Ma, L.O. Mark, M. Mavrikakis, O.O. Olafasakin, T.A. Osswald, K.G. Papanikolaou, H. Radhakrishnan, M.A. Sanchez Castillo, K.L. Sánchez-Rivera, K.N. Tumu, R.C. Van Lehn, K.L. Vorst, M.M. Wright, J. Wu, V.M. Zavala, P. Zhou, G.W. Huber, Expanding plastics recycling technologies: chemical aspects, technology status and challenges, Green Chemistry 24 (2022) 8899–9002. https://doi.org/10.1039/d2gc02588d.

[31] M. Goyal, R.K. Goyal, Confirming Antecedents of Green Consumption Intention: A Sustainable Model for Food Aggregators, IETE J Res 67 (2021) 634–645. https://doi.org/10.1080/03772063.2021.1906336.

[32] E.P. da Silva, V.H. Fragal, E.H. Fragal, T. Sequinel, L.F. Gorup, R. Silva, E.C. Muniz, Sustainable energy and waste management: How to transform plastic waste into carbon nanostructures for electrochemical supercapacitors, Waste Management 171 (2023) 71–85. https://doi.org/10.1016/j.wasman.2023.08.028.

[33] S. Huysveld, K. Ragaert, R. Demets, T.T. Nhu, D. Civancik-Uslu, M. Kusenberg, K.M. Van Geem, S. De Meester, J. Dewulf, Technical and market substitutability of recycled materials: Calculating the environmental benefits of mechanical and chemical recycling of plastic packaging waste, Waste Management 152 (2022) 69–79. https://doi.org/10.1016/j.wasman.2022.08.006.

[34] M. Larrain, S. Van Passel, G. Thomassen, B. Van Gorp, T.T. Nhu, S. Huysveld, K.M. Van Geem, S. De Meester, P. Billen, Techno-economic assessment of mechanical recycling of challenging post-consumer plastic packaging waste, Resour Conserv Recycl 170 (2021) 1–13. https://doi.org/10.1016/j.resconrec.2021.105607.

[35] D. Civancik-Uslu, T.T. Nhu, B. Van Gorp, U. Kresovic, M. Larrain, P. Billen, K. Ragaert, S. De Meester, J. Dewulf, S. Huysveld, Moving from linear to circular household plastic packaging in Belgium: Prospective life cycle assessment of mechanical and thermochemical recycling, Resour Conserv Recycl 171 (2021) 1–12. https://doi.org/10.1016/j.resconrec.2021.105633.

[36] S. Huysveld, K. Ragaert, R. Demets, T.T. Nhu, D. Civancik-Uslu, M. Kusenberg, K.M. Van Geem, S. De Meester, J. Dewulf, Technical and market substitutability of recycled materials: Calculating the environmental benefits of mechanical and chemical recycling of plastic packaging waste, Waste Management 152 (2022) 69–79. https://doi.org/10.1016/j.wasman.2022.08.006.

[37] M. Solis, S. Silveira, Technologies for chemical recycling of household plastics – A technical review and TRL assessment, Waste Management 105 (2020) 128–138. https://doi.org/10.1016/j.wasman.2020.01.038.

[38] K. Ragaert, S. Huysveld, G. Vyncke, S. Hubo, L. Veelaert, J. Dewulf, E. Du Bois, Design from recycling: A complex mixed plastic waste case study, Resour Conserv Recycl 155 (2020) 1–9. https://doi.org/10.1016/j.resconrec.2019.104646.

[39] D.N. Luu, M. Barbaroux, G. Dorez, K. Mignot, E. Doger, A. Laurent, J.M. Brossard, C.J. Maier, Recycling of Post-Use Bioprocessing Plastic Containers—Mechanical Recycling Technical Feasibility, Sustainability (Switzerland) 14 (2022) 1–18. https://doi.org/10.3390/su142315557.

[40] L. Yu, D. Zhao, W. Wang, Mechanical properties and long-term durability of recycled polysulfone plastic, Waste Management 84 (2019) 402–412. https://doi.org/10.1016/j.wasman.2018.11.025.

[41] I.S. Lase, A. Bashirgonbadi, F. van Rhijn, J. Dewulf, K. Ragaert, L. Delva, M. Roosen, M. Brandsma, M. Langen, S. De Meester, Material flow analysis and recycling performance of an improved mechanical recycling process for post-

consumer flexible plastics, Waste Management 153 (2022) 249–263. https://doi.org/10.1016/j.wasman.2022.09.002.

[42] A. Bashirgonbadi, I. Saputra Lase, L. Delva, K.M. Van Geem, S. De Meester, K. Ragaert, Quality evaluation and economic assessment of an improved mechanical recycling process for post-consumer flexible plastics, Waste Management 153 (2022) 41–51. https://doi.org/10.1016/j.wasman.2022.08.018.

[43] M.C. Mulakkal, A. Castillo Castillo, A.C. Taylor, B.R.K. Blackman, D.S. Balint, S. Pimenta, M.N. Charalambides, Advancing mechanical recycling of multilayer plastics through finite element modelling and environmental policy, Resour Conserv Recycl 166 (2021) 1–13. https://doi.org/10.1016/j.resconrec.2020.105371.

[44] M. Bustos Seibert, G.A. Mazzei Capote, M. Gruber, W. Volk, T.A. Osswald, Manufacturing of a PET Filament from Recycled Material for Material Extrusion (MEX), Recycling 7 (2022) 1–20. https://doi.org/10.3390/recycling7050069.

[45] T. Ramos-Hernández, J.R. Robledo-Ortíz, M.E. González-López, A.S.M. del Campo, R. González-Núñez, D. Rodrigue, A.A. Pérez Fonseca, Mechanical recycling of PLA: Effect of weathering, extrusion cycles, and chain extender, J Appl Polym Sci 140 (2023) 1–15. https://doi.org/10.1002/app.53759.

[46] J.K. Park, M.O. Kim, Mechanical properties of cement-based materials with recycled plastic: A review, Sustainability (Switzerland) 12 (2020) 1–21. https://doi.org/10.3390/su12219060.

[47] M.Y. Khalid, Z.U. Arif, W. Ahmed, H. Arshad, Recent trends in recycling and reusing techniques of different plastic polymers and their composite materials, Sustainable Materials and Technologies 31 (2022) 1–21. https://doi.org/10.1016/j.susmat.2021.e00382.

[48] H. Raghuram, J. Roitner, M.P. Jones, V.M. Archodoulaki, Recycling of polyethylene: Tribology assessment, Resour Conserv Recycl 192 (2023) 1–7. https://doi.org/10.1016/j.resconrec.2023.106925.

[49] C. Shan, A.H. Pandyaswargo, H. Onoda, Environmental Impact of Plastic Recycling in Terms of Energy Consumption: A Comparison of Japan's Mechanical and Chemical Recycling Technologies, Energies (Basel) 16 (2023) 1–6. https://doi.org/10.3390/en16052199.

[50] D.P. Ghumra, O. Rathi, T.A. Mule, V.S. Khadye, A. Chavan, F.C. Barba, S. Main, A. Odaneth, B.N. Thorat, Technologies for valorization of municipal solid wastes, Biofuels, Bioproducts and Biorefining 16 (2022) 877–890. https://doi.org/10.1002/bbb.2340.

[51] M. Selina, B. Markus, S. Daniel, S. Renato, Wet-mechanical processing of a plastic-rich two-dimensional-fraction from mixed wastes for chemical recycling, Waste Management and Research 39 (2021) 731–743.

https://doi.org/10.1177/0734242X21996435.

[52] I. s. Sani, N.R. Demarquette, E. David, Investigation and characterization of dielectric, thermal, and chemical properties of recycled high-density polyethylene blended with virgin polyethylene, Polym Eng Sci 63 (2023) 3254–3267. https://doi.org/10.1002/pen.26441.

[53] D. dos Santos Luiz, C. Saron, Catalytic effect of natural clays on properties and chemical structure of recycled polyethylene, J Mater Cycles Waste Manag 24 (2022) 2545–2554. https://doi.org/10.1007/s10163-022-01502-w.

[54] P. Quicker, M. Seitz, J. Vogel, Chemical recycling: A critical assessment of potential process approaches, Waste Management and Research 40 (2022) 1494–1504. https://doi.org/10.1177/0734242X221084044.

[55] S.M. Al-Salem, H.J. Karam, M.H. Al-Wadi, S. Alsamaq, G. Jiang, J. Wang, G.A. Leeke, Thermal degradation kinetics of real-life reclaimed plastic solid waste (PSW) from an active landfill site: The mining of an unsanitary arid landfill, Ain Shams Engineering Journal 12 (2021) 983–993. https://doi.org/10.1016/j.asej.2020.05.011.

[56] F. Weiland, L. Lundin, M. Celebi, K. van der Vlist, F. Moradian, Aspects of chemical recycling of complex plastic waste via the gasification route, Waste Management 126 (2021) 65–77. https://doi.org/10.1016/j.wasman.2021.02.054.

[57] J. González-Arias, R. Forero-Franco, C. Mandviwala, M. Seemann, Steam gasification as a viable solution for converting single-use medical items into chemical building blocks with high yields for the plastic industry, Resour Conserv Recycl 201 (2024) 1–10. https://doi.org/10.1016/j.resconrec.2023.107342.

[58] M. Zeller, N. Netsch, F. Richter, H. Leibold, D. Stapf, Chemical Recycling of Mixed Plastic Wastes by Pyrolysis – Pilot Scale Investigations, Chem Ing Tech 93 (2021) 1763–1770. https://doi.org/10.1002/cite.202100102.

[59] S. Musivand, M.P. Bracciale, M. Damizia, P. De Filippis, B. de Caprariis, Viable Recycling of Polystyrene via Hydrothermal Liquefaction and Pyrolysis, Energies (Basel) 16 (2023) 1–13. https://doi.org/10.3390/en16134917.

[60] H. Jiang, W. Liu, X. Zhang, J. Qiao, Chemical Recycling of Plastics by Microwave-Assisted High-Temperature Pyrolysis, Global Challenges 4 (2020) 1–4. https://doi.org/10.1002/gch2.201900074.

[61] D. Almeida Streitwieser, A. Arteaga, A. Gallo-Cordova, A. Hidrobo, S. Ponce, Chemical Recycling of Used Motor Oil by Catalytic Cracking with Metal-Doped Aluminum Silicate Catalysts, Sustainability (Switzerland) 15 (2023) 1–13. https://doi.org/10.3390/su151310522.

[62] E. Tito, J.S. dos Passos, S. Bensaid, R. Pirone, P. Biller, Multilayer plastic film chemical recycling via sequential hydrothermal liquefaction, Resour Conserv Recycl 197 (2023) 1–9. https://doi.org/10.1016/j.resconrec.2023.107067.

[63] F. Akhmetova, Y. Aubakirov, Z. Tashmukhambetova, L. Sassykova, H. Arbag, A. Kurmangaliyeva, Recycling of waste plastics to liquid fuel mixture over composite zeolites catalysts, Chemical Bulletin of Kazakh National University (2021) 12–18. https://doi.org/10.15328/cb1117.

[64] C. Santagata, G. Iaquaniello, A. Salladini, E. Agostini, M. Capocelli, M. De Falco, Production of low-density poly-ethylene (LDPE) from chemical recycling of plastic waste: Process analysis, J Clean Prod 253 (2020) 1–11. https://doi.org/10.1016/j.jclepro.2019.119837.

[65] C. Gorre, T.P. Tumolva, Solvent and non-solvent selection for the chemical recycling of waste Polyethylene (PE) and Polypropylene (PP) metallized film packaging materials, in: IOP Conf Ser Earth Environ Sci, Institute of Physics Publishing, 2020: pp. 1–8. https://doi.org/10.1088/1755-1315/463/1/012070.

[66] A. Rani, S. Negi, A. Hussain, S. Kumar, Treatment of urban municipal landfill leachate utilizing garbage enzyme, Bioresour Technol 297 (2020) 1–2. https://doi.org/10.1016/j.biortech.2019.122437.

[67] A.R. Adaryani, O. Keen, Occurrence of pharmaceuticals and plasticizers in leachate from municipal landfills of different age, Waste Management 141 (2022) 1–7. https://doi.org/10.1016/j.wasman.2022.01.023.

[68] M.D. Vaverková, D. Adamcová, J. Winkler, E. Koda, L. Petrželová, A. Maxianová, Alternative method of composting on a reclaimed municipal waste landfill in accordance with the circular economy: Benefits and risks, Science of the Total Environment 723 (2020) 1–2. https://doi.org/10.1016/j.scitotenv.2020.137971.

[69] N.F.B. Ahamad Sanadi, N. Ibrahim, P.Y. Ong, J.J. Klemeš, C. Li, C.T. Lee, Dilution rate of compost leachate from different biowaste for the fertigation of vegetables, J Environ Manage 295 (2021) 1–9. https://doi.org/10.1016/j.jenvman.2021.113010.

[70] H. Chen, H. Xu, C. Zhong, M. Liu, L. Yang, J. He, Y. Sun, C. Zhao, D. Wang, Treatment of landfill leachate by coagulation: A review, Science of the Total Environment 912 (2024) 9–10. https://doi.org/10.1016/j.scitotenv.2023.169294.

[71] G. Chen, G. Wu, N. Li, X. Lu, J. Zhao, M. He, B. Yan, H. Zhang, X. Duan, S. Wang, Landfill leachate treatment by persulphate related advanced oxidation technologies, J Hazard Mater 418 (2021) 1–11. https://doi.org/10.1016/j.jhazmat.2021.126355.

[72] Y. Li, F. Tang, D. Xu, B. Xie, Advances in biological nitrogen removal of landfill leachate, Sustainability (Switzerland) 13 (2021) 1–18. https://doi.org/10.3390/su13116236.

[73] N. Remmas, N. Manfe, I. Zerva, P. Melidis, R. Raga, S. Ntougias, A Critical Review on the Microbial Ecology of Landfill Leachate Treatment Systems,

Sustainability (Switzerland) 15 (2023) 1–20. https://doi.org/10.3390/su15020949.

[74] M.S. Kabir, H. Wang, S. Luster-Teasley, L. Zhang, R. Zhao, Microplastics in landfill leachate: Sources, detection, occurrence, and removal, Environmental Science and Ecotechnology 16 (2023) 1–12. https://doi.org/10.1016/j.ese.2023.100256.

[75] M.H. Samsudin, M.A. Hassan, M.Z. Mohd Yusoff, J. Idris, M.A. Ahmad Farid, A.B.A. Lawal, M.N.F. Norrrahim, Y. Shirai, Production of nanopore structure bio-adsorbent from wood waste through a self-sustained carbonization process for landfill leachate treatment, Biochem Eng J 189 (2022) 1–10. https://doi.org/10.1016/j.bej.2022.108740.

[76] A. Nalladiyil, P. Sughosh, G.L.S. Babu, S. Ramaswami, Landfill leachate treatment using fungi and fungal enzymes: a review, Biodegradation (2023) 1–23. https://doi.org/10.1007/s10532-023-10052-3.

[77] S. Kanmani, A.G.B. Dileepan, Treatment of landfill leachate using photocatalytic based advanced oxidation process – a critical review, J Environ Manage 345 (2023) 1–17. https://doi.org/10.1016/j.jenvman.2023.118794.

[78] Z. Guo, Y. Zhang, H. Jia, J. Guo, X. Meng, J. Wang, Electrochemical methods for landfill leachate treatment: A review on electrocoagulation and electrooxidation, Science of the Total Environment 806 (2022) 1–19. https://doi.org/10.1016/j.scitotenv.2021.150529.

[79] V.E. Silva, S.L. Rollemberg, S.G. Santos, T.F. Silva, V.J. Vilar, A.B. Santos, Landfill leachate biological treatment: perspective for the aerobic granular sludge technology, Environmental Science and Pollution Research 29 (2022) 45150–45170. https://doi.org/10.1007/s11356-022-20451-3.

[80] Y. Li, F. Tang, D. Xu, B. Xie, Advances in biological nitrogen removal of landfill leachate, Sustainability (Switzerland) 13 (2021) 1–18. https://doi.org/10.3390/su13116236.

[81] Y. Lei, J. Hou, C. Fang, Y. Tian, R. Naidu, J. Zhang, X. Zhang, Z. Zeng, Z. Cheng, J. He, D. Tian, S. Deng, F. Shen, Ultrasound-based advanced oxidation processes for landfill leachate treatment: Energy consumption, influences, mechanisms and perspectives, Ecotoxicol Environ Saf 263 (2023) 1–18. https://doi.org/10.1016/j.ecoenv.2023.115366.

[82] A.M.H. Shadi, M.A. Kamaruddin, N.M. Niza, M.I. Emmanuel, M.S. Hossain, N. Ismail, Electroflotation treatment of stabilized landfill leachate using titanium-based electrode, International Journal of Environmental Science and Technology 18 (2021) 2425–2440. https://doi.org/10.1007/s13762-020-03005-3.

[83] H. Zineb, M. Latifa, S. Salah, S. Laila, Removal of Pollution by Intensive Aeration Technology for Landfill Leachate Treatment, J Health Pollut 10 (2020) 1–13. https://doi.org/https://doi.org/10.5696/2156-9614-10.28.201212.

[84] I. Schneider, I. Yotinov, N. Dinova, B. Geneva, E. Daskalova, S. Lincheva, Y. Topalova, Assessment of Denitrification and Nitrification Processes during Landfill Leachate Treatment, Processes 11 (2023) 1–18. https://doi.org/10.3390/pr11102960.

[85] Y. Yuan, J. Liu, B. Gao, J. Hao, Ozone direct oxidation pretreatment and catalytic oxidation post-treatment coupled with ABMBR for landfill leachate treatment, Science of the Total Environment 794 (2021) 1–11. https://doi.org/10.1016/j.scitotenv.2021.148557.

[86] D. Revelo-Romo, M. Guerrero-Flórez, A. Ordóñez, I.A. Sánchez-Ortiz, N. Pusapaz-Villota, O.C. Yela, L.A. Galeano, Bacterial diversity of leachates retained in adsorbents regenerated by wet catalytic peroxide oxidation: potential driving bioelectrochemical systems, International Journal of Environmental Science and Technology 18 (2021) 2913–2924. https://doi.org/10.1007/s13762-020-03058-4.

[87] A. Thakur, R. Bharti, R. Sharma, Carbon nanotubes: Types, synthesis, cytotoxicity and applications in biomedical, in: Mater Today Proc, Elsevier Ltd, 2021: pp. 2256–2268. https://doi.org/10.1016/j.matpr.2021.10.002.

[88] F. Robert, Power Withstanding Capability and Transient Temperature of Carbon Nanotube-Based Nano Electrical Interconnects, Res Sq (2021) 1–27. https://doi.org/10.21203/rs.3.rs-188713/v1.

[89] S.K. Prajapati, A. Malaiya, P. Kesharwani, D. Soni, A. Jain, Biomedical applications and toxicities of carbon nanotubes, Drug Chem Toxicol 45 (2022) 435–450. https://doi.org/10.1080/01480545.2019.1709492.

[90] B.K. Mishra, B. Ashok, Coaxial carbon nanotubes: From springs to ratchet wheels and nanobearings, Mater Res Express 5 (2018) 1–13. https://doi.org/10.1088/2053-1591/aad07a.

[91] I. Kotcioglu, M. Mustafaoglu, N. Dogan, Numerical thermal analysis of armchair (6,6) and zig-zag (12,0) carbon nano-tubes (CNTs), Mechanics of Advanced Materials and Structures (2023) 1–19. https://doi.org/10.1080/15376494.2023.2169794.

[92] I. Rafique, A. Kausar, Z. Anwar, B. Muhammad, Exploration of Epoxy Resins, Hardening Systems, and Epoxy/Carbon Nanotube Composite Designed for High Performance Materials: A Review, Polymer - Plastics Technology and Engineering 55 (2016) 312–333. https://doi.org/10.1080/03602559.2015.1070874.

[93] P. Wang, Q. Dong, C. Gao, W. Bai, D. Chu, Y. He, A comprehensive review of carbon nanotubes: growth mechanisms, preparation and applications, Fullerenes Nanotubes and Carbon Nanostructures (2023) 1–16. https://doi.org/10.1080/1536383X.2023.2292694.

[94] H. Ribeiro, M.C. Schnitzler, W.M. da Silva, A.P. Santos, Purification of carbon nanotubes produced by the electric arc-discharge method, Surfaces and Interfaces

26 (2021) 1–16. https://doi.org/10.1016/j.surfin.2021.101389.

[95] A.H. Hammadi, A.M. Jasim, F.H. Abdulrazzak, A.M.A. Al-Sammarraie, Y. Cherifi, R. Boukherroub, F.H. Hussein, Purification for carbon nanotubes synthesized by flame fragments deposition via hydrogen peroxide and acetone, Materials 13 (2020) 1–9. https://doi.org/10.3390/ma13102342.

[96] T. Bortolamiol, P. Lukanov, A.-M. Galibert, B. Soula, P. Lonchambon, L. Datas, E. Flahaut, Double-walled carbon nanotubes: Quantitative purification assessment, balance between purification and degradation and solution filling as an evidence of opening, Carbon N Y 78 (2014) 79–90. https://doi.org/10.1016/j.carbon.2014.06.051ï.

[97] M. V. Kharlamova, M. Paukov, M.G. Burdanova, Nanotube Functionalization: Investigation, Methods and Demonstrated Applications, Materials 15 (2022) 1–24. https://doi.org/10.3390/ma15155386.

[98] M.L. Del Prado-Audelo, I. García Kerdan, L. Escutia-Guadarrama, J.M. Reyna-González, J.J. Magaña, G. Leyva-Gómez, Nanoremediation: Nanomaterials and Nanotechnologies for Environmental Cleanup, Front Environ Sci 9 (2021) 1–7. https://doi.org/10.3389/fenvs.2021.793765.

[99] Z. Noorimotlagh, A.S. Silva, S.A. Mirzaee, S. Silva Martínez, H.T. Gomes, J.L. Diaz De Tuesta, FNPs based antimicrobial coating for environmental applications. Chapter 1: wastewater purification using advanced functionalized nanoparticles, (2023) 223–283. https://doi.org/10.1016/B978-0-323-91783-4.00002-4 (accessed March 4, 2024).

[100] H.I. Hamouda, H.M. Abdel-Ghafar, M.H.H. Mahmoud, Multi-walled carbon nanotubes decorated with silver nanoparticles for antimicrobial applications, J Environ Chem Eng 9 (2021) 1–9. https://doi.org/10.1016/j.jece.2021.105034.

[101] M.A. Saleemi, Y.L. Kong, P.V.C. Yong, E.H. Wong, An Overview of Antimicrobial Properties of Carbon Nanotubes-Based Nanocomposites, Adv Pharm Bull 12 (2022) 449–465. https://doi.org/10.34172/apb.2022.049.

[102] J.L. Diaz de Tuesta, A.S. Silva, F.F. Roman, L.F. Sanches, F.A. da Silva, A.I. Pereira, A.M.T. Silva, J.L. Faria, H.T. Gomes, Polyolefin-derived carbon nanotubes as magnetic catalysts for wet peroxide oxidation of paracetamol in aqueous solutions, Catal Today 419 (2023) 1–10. https://doi.org/10.1016/j.cattod.2023.114162.

[103] European Parliament and Council of the European Union, DIRECTIVE 98/37/EC, 1998.

[104] A. Khalid, A. Ibrahim, O.C.S. Al-Hamouz, T. Laoui, A. Benamor, M.A. Atieh, Fabrication of polysulfone nanocomposite membranes with silver-doped carbon nanotubes and their antifouling performance, J Appl Polym Sci 134 (2017) 1–12. https://doi.org/10.1002/app.44688.

[105] M. Thommes, K. Kaneko, A. V. Neimark, J.P. Olivier, F. Rodriguez-Reinoso, J. Rouquerol, K.S.W. Sing, Physisorption of gases, with special reference to the evaluation of surface area and pore size distribution (IUPAC Technical Report), Pure and Applied Chemistry 87 (2015) 1051–1069. https://doi.org/10.1515/pac-2014-1117.

[106] J.L. Diaz De Tuesta, F.F. Roman, V.C. Marques, A.S. Silva, A.P.F. Silva, T.C. Bosco, A.A. Shinibekova, S. Aknur, M.S. Kalmakhanova, B.K. Massalimova, M. Arrobas, A.M.T. Silva, H.T. Gomes, Performance and modeling of Ni(II) adsorption from low concentrated wastewater on carbon microspheres prepared from tangerine peels by FeCl3-assisted hydrothermal carbonization, J Environ Chem Eng 10 (2022) 1–15. https://doi.org/10.1016/j.jece.2022.108143.

[107] B.D. Cardoso, A.R.O. Rodrigues, M. Bañobre-López, B.G. Almeida, C.O. Amorim, V.S. Amaral, P.J.G. Coutinho, E.M.S. Castanheira, Magnetoliposomes based on shape anisotropic calcium/magnesium ferrite nanoparticles as nanocarriers for doxorubicin, Pharmaceutics 13 (2021) 1–27. https://doi.org/10.3390/pharmaceutics13081248.

[108] N. Yue, L. Wang, X. He, H. Liu, W. Zhang, Optimizing the SEM specimen preparation method for accurate microanalysis of carbon nanotube/nanocluster hybrids, J Microsc 282 (2021) 267–273. https://doi.org/10.1111/jmi.13008.

[109] International Standard, ISO 7218:2007/Amd.1:2013(E). Microbiology of food and animal feeding stuffs-General requirements and guidance for microbiological examinations, 2013. www.iso.org/patents.

[110] G.M. Al-Senani, N. Al-Kadhi, The synthesis and effect of silver nanoparticles on the adsorption of Cu2+ from aqueous solutions, Applied Sciences (Switzerland) 10 (2020) 1–13. https://doi.org/10.3390/app10144840.

[111] Z.P. Huang, D.Z. Wang, J.G. Wen, M. Sennett, H. Gibson, Z.F. Ren, Effect of nickel, iron and cobalt on growth of aligned carbon nanotubes, Appl Phys A Mater Sci Process 74 (2002) 387–391. https://doi.org/10.1007/s003390101186.

[112] F.L. Tchinda Taghu, B. Pone Kamdem, V. Ngouana, Z. Yajeh Tanka, V.L. Yimgang, J. Nsami Ndi, P. Keilah Lunga, F. Fekam Boyom, Biological Synthesis and Characterization of Silver-Doped Nanocomposites: Antibacterial and Mechanistic Studies, Drugs and Drug Candidates 3 (2023) 13–32. https://doi.org/10.3390/ddc3010002.

[113] Y.S. Itas, C.E. Ndikilar, T. Zangina, H.Y. Hafeez, A.A. Safana, M.U. Khandaker, P. Ahmad, I. Abdullahi, B.K. Olawumi, M.A. Babaji, H. Osman, S. Alamri, Synthesis of thermally stable h-BN-CNT hetero-structures via microwave heating of ethylene under nickel, iron, and silver catalysts, Crystals (Basel) 11 (2021) 1–13. https://doi.org/10.3390/cryst11091097.

[114] S. Boncel, S.W. Pattinson, V. Geiser, M.S.P. Shaffer, K.K.K. Koziol, En route to controlled catalytic CVD synthesis of densely packed and vertically aligned

nitrogen-doped carbon nanotube arrays, Beilstein Journal of Nanotechnology 5 (2014) 219–233. https://doi.org/10.3762/bjnano.5.24.

[115] E.I. Braun, P. Pantano, The importance of an extensive elemental analysis of single-walled carbon nanotube soot, Carbon N Y 77 (2014) 912–919. https://doi.org/10.1016/j.carbon.2014.06.005.

[116] S. Acosta, A. Sierra-Castillo, J.-F. Colomer, R. Snyders, M. Quintana, C. Ewels, C. Bittencourt, Thermal stability of oxygen functionalization in v-CNTs by low kinetic energy ion irradiation, Vacuum (2021) 1–18. https://doi.org/10.1016/j.vacuum.2021.110423ï.

[117] M. V. Ivanova, C. Lamprecht, M. Jimena Loureiro, J. Torin Huzil, M. Foldvari, Pharmaceutical characterization of solid and dispersed carbon nanotubes as nanoexcipients, Int J Nanomedicine 7 (2012) 403–415. https://doi.org/10.2147/ijn.s27442.

[118] X. Lin, Y. Xia, G. Wei, J. Zhou, X. Liang, H. Xian, J. Zhu, H. He, Distinct effects of transition metal (cobalt, manganese and nickel) ion substitutions on the abiotic oxidation of pyrite: In view of hydroxyl radical production, Geochim Cosmochim Acta 321 (2022) 170–183. https://doi.org/10.1016/j.gca.2022.01.026.

[119] A. Zamudio, A.L. Elías, J.A. Rodríguez-Manzo, F. López-Urías, G. Rodríguez-Gattorno, F. Lupo, M. Rühle, D.J. Smith, H. Terrones, D. Díaz, M. Terrones, Efficient anchoring of silver nanoparticles on n-doped carbon nanotubes, Small 2 (2006) 346–350. https://doi.org/10.1002/smll.200500348.

[120] M. Hachemaoui, C.B. Molina, C. Belver, J. Bedia, A. Mokhtar, R. Hamacha, B. Boukoussa, Metal-loaded mesoporous mcm-41 for the catalytic wet peroxide oxidation (Cwpo) of acetaminophen, Catalysts 11 (2021) 1–17. https://doi.org/10.3390/catal11020219.

[121] A.S. Silva, F.F. Roman, A. V. Dias, J.L. Diaz de Tuesta, A. Narcizo, A.P.F. da Silva, I. Çaha, F.L. Deepak, M. Bañobre-López, A.M.C. Ferrari, H.T. Gomes, Hybrid multi-core shell magnetic nanoparticles for wet peroxide oxidation of paracetamol: Application in synthetic and real matrices, J Environ Chem Eng 11 (2023) 1–11. https://doi.org/10.1016/j.jece.2023.110806.

[122] J. Jiang, Z. An, M. Li, Y. Huo, Y. Zhou, J. Xie, M. He, Comparison of ribavirin degradation in the UV/H2O2and UV/PDS systems: Reaction mechanism, operational parameter and toxicity evaluation, J Environ Chem Eng 11 (2023) 1–9. https://doi.org/10.1016/j.jece.2022.109193.

[123] A.S. Silva, M.S. Kalmakhanova, B.K. Massalimova, J.L.D. de Tuesta, H.T. Gomes, Wet peroxide oxidation of paracetamol using acid activated and Fe/Co-pillared clay catalysts prepared from natural clays, Catalysts 9 (2019) 1–16. https://doi.org/10.3390/catal9090705.

[124] G.A. Pankey, L.D. Sabath, Clinical Relevance of Bacteriostatic versus Bactericidal

Mechanisms of Action in the Treatment of Gram-Positive Bacterial Infections, (2004) 864–870. https://academic.oup.com/cid/article/38/6/864/320723.